

– An international journal for New Concepts in Global Tectonics –

NCGT



JOURNAL

Volume 9, Number 2, June 2021. ISSN 2202-0039.

Editor-in-Chief: Louis HISSINK (louis.hissink@bigpond.com)

EDITORIAL BOARD

Bruce LEYBOURNE, USA (leybourneb@iascc.org);
Giovanni P. GREGORI, Italy (giovanni.gregori@idasc.cnr.it);
Yoshihiro KUBOTA, Japan (yokbt@icloud.com);
Per MICHAELSEN, Mongolia (perm@must.edu.mn);

CONTENTS

From the Editor In this issue.....	57
Obituary – Professor Michihei HOSHINO (1923 -2021).....	58
Articles	
Distribution of island endemic animals and the late Middle Pleistocene land bridges as evidence of sea level rise of 1,000 m since 430 ka: Masahiro Shiba	60
Space Weather and geomagnetic activity related to Ecuadorean M7.5 earthquake recorded on February 22, 2019: Gabriele Cataldi, Daniele Cataldi, Valentino Straser.....	79
Solar Activity and geomagnetic activity related to M6+ global seismic activity recorded on March 20, 2021: Gabriele Cataldi, Daniele Cataldi, Valentino Straser.....	87
Space weather and geomagnetic activity related to M6+ global seismic activity recorded on 3-4 March 2021: Gabriele Cataldi, Daniele Cataldi, Valentino Straser.....	94
Solar activity and geomagnetic activity related to M6.0 South Sandwich Islands region earthquake recorded March 14, 2021, Gabriele Cataldi, Daniele Cataldi, Valentino Straser.....	99
Space weather and geomagnetic activity related to the Vanuatu M6.5 earthquake recorded on March 20, 2019: Gabriele Cataldi, Daniele Cataldi, Valentino Straser.....	106
Possible quake-related, pre-seismic impulses near 10 and 15 Hz that were not recorded by a 1 Hz seismometer: John Ricken Wright.....	112
About the NCGT Journal	120

Please feel free to contact the CEO of the Geoplasma Research Institute, Mr. Bruce Leybourne, at (leybourneb@iascc.org). For contact, correspondence, or inclusion of material in the NCGT Journal please use the following methods: NCGT Journal: 1. E-mail: louis.hissink@bigpond.com; 2. Mail, air express, etc., 33 Fields Road, Tanja, NSW 2550, Australia (files in MS Word or ODT format, and figures in gif, bmp or tif format) as separate files; 3. Telephone, +61 419 283 775. **DISCLAIMER:** The opinions, observations and ideas published in this journal are the responsibility of the contributors and do not necessarily reflect those of the Editor and the Editorial Board. *NCGT Journal* is a refereed quarterly international on-line journal and appears in March, June, September and December. *ISSN number:* ISSN 2202-0039.

From the Editor

We sadly learn of the recent passing of Professor Michihei Hoshino in Japan and publish his obituary, by Masahiro Shiba, in this issue of the Journal. We are also witnessing the inevitable change of the guard which reminds me of the wise conclusion stated by Max Planck who noted that "a scientific truth does not triumph by convincing its opponents and making them see the light, but rather because its opponents eventually die and a new generation grows up that is familiar with it" Where is the new generation?

In this issue Masahiro Shiba also presents us with another thought provoking paper, this time on a significant (1,000 m) inferred rise in sea-level 430 ka ago. Our Italian colleagues continue their reporting with five reports of recent space weather and geomagnetic activity related to earthquake activity, and finally John Ricken Wright comments about monitoring EM earthquake precursors using the existing electrical utility infrastructure.

It seems the political scene is undergoing unprecedented changes and there also seems to be no change in the climate change situation. There are some interesting changes occurring in the scientific approach to weather phenomena, however, with NASA now using lightning to help predict hurricane intensity. Interestingly there is now a greater emphasis on cosmic plasma phenomena with a technical book, "Electric Currents in Geospace and Beyond" edited by Andreas Keiling. It is AGU Geophysical Monograph 235, first published in 2018 by John Wiley and Sons, Inc, and the American Geophysical Union. A quote from its introduction:

(Geospace is the term used for the space between the Sun and the Earth) "*Solar wind plasma is streaming through geospace and due to the omnipresent magnetic field, electrons and positive ions blowing with the wind are forced to move in different directions with electric currents as an outcome. These electric currents forming in the magnetosphere are connected to the ionosphere of the Earth by field-aligned currents that are closed by horizontal currents in the upper atmosphere. **The effects on ground caused by these currents have been a challenge for humankind for generations***". (My emphasis).

The application of plasma physics to geology has recently been proposed linked to Expanding Earth theory by Dr. James Maxlow in order to explain the inferred increase in mass needed for earth expansion, (<https://www.expansiontectonics.com/index1.html>). This theory proposes that solar ionized particles, electrons and protons, enter the Earth and recombine to new matter in the "D" region of the mantle. The main theoretical difficulty is explaining how solar electrons and protons can pass through physical matter to reach the mantle since empirically these sub-atomic particles are easily stopped by water and the crystalline crust, with an increased penetration depth possible if the particles are of a higher energy types.

The principal problem applying plasma physics to geology/geophysics involves plasma's inherently catastrophic nature. Catastrophism, however, remains a strong cultural taboo, first codified as Geological Uniformitarianism during the early 19th century during the heyday of British Imperialism and which has since become established globally as geological orthodoxy. But as the historian George Grinnell wrote in 1975, on the political implications of early 19th century geology, its gestalt-shift and the setting up of the London Geological Society in 1807 CE:

"In 1807, Humphrey Davy wrote to his friend William Pepys: "We are forming a little talking geological dinner club, of which I hope you will be a member." Of the original thirteen members, four were doctors, one was an ex-Unitarian minister. Two were booksellers; another, Comte Jacques-Louis, had fled the French Revolution. Four were Quakers, and two - William Allen and Humphrey Davy - were independently wealthy amateur chemists. Only one, George Greenough, had any training in geology or mineralogy. He had paid a visit to the Academy at Freiburg some years earlier along with Goethe, but did not by any stretch of the imagination pursue the subject for a living. He was a Member of Parliament. Indeed, what is extraordinary about the London Geological Society is that none of the original members were geologists. "The little talking dinner club" as Davy put it was a club for gentlemen given to talk, not to hammering rock." (http://www.grazian-archive.com/quantavolution/QUANTAVOL/rfs_docs/rfs_4.pdf).

Are we seeing a repeat of the 19th century troubles, when politics intruded into the workings of science, during our times?

OBITUARY

Professor Michihei HOSHINO (1923-2021)



We have lost a great geologist. Dr. Michihei Hoshino, Professor Emeritus of Tokai University, Japan, passed away at the age of 98 on April 29, 2021. He was born on January 11, 1923, at the western foot of Mount Akagi in Gunma Prefecture, Japan. He graduated from the Department of Geology and Mineralogy, Tokyo University of Literature and Science in 1947, and worked in the Hydrographic Department of the Japan Coast Guard from 1950 to 1964 and was a professor at the School of Marine Science and Technology, Tokai University from 1964 to 1993.

In the Hydrographic Department, he studied the sediments on the continental shelf in the seas around Japan, and received his degree with a thesis on “The Shelf Sediments in the Adjacent Seas of Japan” (1958). At the same time, he wrote several popular books and text books in Japanese on oceanography and marine geology, “The Pacific Ocean” (1962); “World under the Sea” (1965); “Science of the Pacific Ocean” (1969); “Continental Slope” (1970); “Continental Shelf” (1972). He has also translated Hans Petterson's “Westward to with the Albatross” (1957) and “The Ocean Floor” (1959) into Japanese.

Since 1964, he has been teaching students as a professor, running the department, and conducting his own research at School of Marine Science and Technology, Tokai University, which had just been established in 1962. He was a great contributor to develop oceanography and marine geology in Japan. In his own research, he verified the hypothesis proposed in “The Pacific Ocean” that the sea level rose by 2,000 m after the Pliocene, i.e., the sea level was 2,000 m lower than the present level at the end of the Miocene, because the terminal depth of submarine canyons is always 2,000 m deep and the youngest stratum comprising the eroded valley floor is the Upper Miocene. In the latest Miocene, the sea level was 2,000 m lower than the present level, and the subsequent uplift of the landward side and the sea floor caused the sea level to rise in stages. He wrote “EUSTACY IN RELATION TO OROGENIC STAGE” (1975), in which his hypothesis was tested.

In the 1970s, it was argued that the trenches extending deep into the deep sea floor were not areas of crustal subsidence, but areas left behind by the uplift of the ocean floor outside the trenches, and that the sea level during the Middle Cretaceous was 4,000 m lower than present. Based on the discovery of the Middle Cretaceous coral reef fossils at the summit of Elimo seamount in the northern end of the Japan Trench (at a depth of about 4,000 m), he estimated that the Middle Cretaceous coral reef fossils could be found at the similarly deep summit of Daiichi Kashima seamount in the southern end of the Japan Trench. He then conducted a survey using the Tokai University research vessel and found the Middle Cretaceous coral reef fossils from the summit of Daiichi Kashima seamount (Daiichi Kashima seamount Survey Team of School of Marine Science and Technology, Tokai University, 1976, 1985).

In 1982, he wrote “MARINE GEOLOGY” in Japanese as a summary of his own research through the 1970s. His research plan for the 1980s was to study structural geology and petrology, including the terms “Unconformity” and “Peneplain” as they relate to sea level change, and he studied the geology and structural and igneous history of “Residual Basins” or “Plateaus” around the world. This was summarized in 1991 in his book, “THE BASALTIC STAGE: Basic Concepts of Geological Science” in Japanese with English abstract. In this book, he divided the Earth's history into the Granitic Stage (the Archean Era), the Transitional Stage (Proterozoic and Palaeozoic Eras), and the Basaltic Stage (Mesozoic and Cenozoic Eras). The driving force for the formation of the present topography during the Basaltic Stage was the ascent of basaltic magma dissolved and expanded in the asthenosphere, resulting in igneous activity and tilting movements of the block active with high-angle faulting. It is believed that the earth has undergone slight expansion due to igneous and uplifting activities, which have raised the sea level by 6,000 m since the Triassic. He assumed that the earth had micro-expanded.

After retiring from Tokai University in 1993, he continued to explore the Earth's micro-expansion hypothesis and wrote “THE EXPANDING EARTH: evidence, causes and effects” in 1998, “CRUSTAL DEVELOPMENT AND SEA LEVEL: with special reference to the geological development of Southwest Japan and adjacent” in 2008, “A PLATE TECTONICS CONTROVERSY” in 2010 in Japanese, “THE HISTORY OF MICRO-EXPANDING EARTH: History of the Earth from viewpoint of Sea Level Rise” in 2014. He was in good health even after turning 90 years old, but suddenly collapsed due to aortic dissection in 2017 when he turned 94 years old. Fortunately, after two operations, he was able to get well in 2019, and at the age of 96, he wrote the last book titled “UPLIFT OF THE

EARTH'S CRUST: Why mountains are high?" in Japanese.

He spent 98 years of his life reading through a vast amount of the world's geological literature, examining various categories of geology, and putting them together to formulate a grand and original hypothesis. While he working very closely with his students. Many of his students respect and admire him, and he cared for them closely even after they graduated.

Professor Hoshino, thank you very much, please rest in peace.

Masahiro Shiba

Distribution of island endemic animals and the late Middle Pleistocene land bridges as evidence of sea level rise of 1,000 m since 430 ka

Masahiro Shiba

Museum of Natural and Environmental History, Shizuoka, Japan

shiba@dino.or.jp

Abstract. Many endemic animals from the Pleistocene to the present are found on some islands around the world. In this paper, the distribution of endemic faunas and their transition in the islands of the world are examined. As a result, it became clear that many endemic faunas of the islands were converted after the late Middle Pleistocene and became unique. All islands with endemic fauna since the late Middle Pleistocene are connected to the nearest continent only at isobaths of 1,000 m or more. Because terrestrial animal migration occurs in their habitat environment, it is thought that these animals migrated through the land bridge that was formed in the late Middle Pleistocene, then an endemic fauna was formed after that was isolated to the island by the sea level rise of 1,000 m. In other words, the sea level in the late Middle Pleistocene was 1,000 m lower than the present, and the subsequent rise in sea level is thought to have led to the formation of endemic faunas on islands separated from the continent by the sea since the late Middle Pleistocene.

Keywords: land bridge, Pleistocene, insular mammals, sea level rise, Wallacea, Mediterranean

Introduction

It is known that many insular endemic mammals including proboscideans, artiodactyls, carnivores, rodents, insectivores, bats and lagomorphs inhabited the world's islands from the Pleistocene to the present (Van der Geer et al., 2010). However, it is still unclear how these animals migrated to the islands and how these endemic species were formed.

Van der Geer et al. (2010), who summarized the distribution of fossil mammals and their faunal evolution on islands around the world, showed that there were faunal transformations during the Pleistocene on each island, that the timing of faunal transformations coincided in some cases, and that many of these last transformations occurred in the late Middle Pleistocene or the Late Pleistocene.

The author postulated that island arcs and the continental slopes were formed by crustal uplift and sea level rise of up to 1,000 m since the late Middle Pleistocene, about 430 ka (Shiba, 2017a, 2017b, 2021). In other words, during the late Middle Pleistocene, the sea level was about 1,000 m lower than at the present level, and the subsequent large-scale uplift of island arcs and continents, and together with the simultaneous uplift of the seafloor, is thought to have raised the sea level by 1,000 m by the present time, forming the present land and seafloor topography (Shiba, 2017a, 2017b).

If we assume that the coastline in the late Middle Pleistocene was 1,000 m lower than the present sea level, many of the islands would be connected to the continent. In this paper, the author summarizes the evolution of the Pleistocene mammalian faunas of islands and the timing of their conversion, based mainly on the data on the world's islands mammals compiled by Van der Geer et al. (2010). Then, assuming that the shallower than 1,000 m depth areas around these islands were terrestrial at some time in the past, the author examines the causes of the endemic fauna of the islands. This paper is a remake of Shiba (2020) and has been translated into English.

In Van der Geer et al. (2010), the base of the Pleistocene is the Calabrian base based on the pre-2009 chronology as 1.806 Ma, which is cited directly in this paper. The terms "pygmy" and "dwarf" are also used according to Van der Geer et al. (2010), with "pygmy" used for particularly small forms, half or less than the size of the ancestor, "dwarf" for 60-80% of the size, and "small" for 90% of the size.

Faunal Changes in the Honshu region of the Japanese Archipelago

The Japanese Archipelago, excluding the Ryukyu Islands, consists mainly of the Honshu region and Hokkaido. The Honshu region includes Honshu, Kyushu and Shikoku islands. The Tsugaru Strait, the Korean Strait, and the Tsushima Strait, which are the peripheral boundaries of the Honshu region, did not become land during the Last Glacial period, suggesting that the Honshu region was isolated from the continent for hundreds of thousands of years before that. For this reason, these straits are considered as biogeographic boundaries (Fig. 1).

According to the paleontological study of small mammals in Japanese Archipelago by Kawamura et al. (1989), about half of



Fig. 1 Bathymetric chart around the Japanese Archipelago showing the biogeographic boundaries (white thick dotted lines). St.: Strait. Thin dotted line is shown depth of 100 m. The seafloor shallower than depth of 1,000 m shows the land area in the late Middle Pleistocene. The seafloor topography is based on NOAA bathymetric data.

the extant mammals, such as Shinto shrew (*Sorex shinto*), Japanese shrew-mole (*Urotrichus talpoides*), Japanese mountain mole (*Euroscaptor mizura*), large Japanese field mouse (*Apodemus speciosus*), raccoon dog (*Nyctereutes procyonoides*), and ermine (*Mustela erminea*), appeared as fossils during the Middle Pleistocene, and they had already become endemic during this period. In particular, the genera *Dymecodon*, *Urotrichus*, and *Glirulus* are endemic even at the genus level, and they are considered to be the basis of the mammalian fauna of the Honshu region as survivors of the Neogene period (Kamei et al., 1988).

In the Early Miocene, about 20 Ma, the Japanese Archipelago was located at the eastern margin of the Chinese continent, and most of the southern part of the Sea of Japan was still land. However, in the Middle Miocene, about 16 Ma, the region of the Sea of Japan submerged due to sea level rise, and the Japanese Archipelago appeared as an island arc. In the Late Miocene, about 10 Ma, the spine of the present-day Japanese Archipelago was uplifted to form the prototype, and the present-day Japanese Archipelago was formed by the uplift of island arc and sea level rise, especially during the Pleistocene (Shiba, 2017a, 2017b). In the Pleistocene, the Japanese Archipelago was temporarily connected to the continent for several times, and the phylogeny of organisms distributed around the continent is thought to have migrated to the Japanese Archipelago.

Based on the study of fossil proboscideans by Kawamura (1998, 2014) and Konishi and Yoshikawa (1999) concluded that *Mammuthus trogontheri* arrived in the Honshu region from China about 1.2 Ma (Marine oxygen isotope stage: MIS 36), *Stegodon orientalis* from the south via the East China Sea about 630 ka (MIS 16), and *Paleoloxodon naumanni* from the northern China via the Korean Peninsula about 430 ka (MIS 12). Kawamura (2014) argued that the arrival of each of these faunas from the continent was not a mass transfer, but rather a limited arrival due to the short span of time and unstable existence of the land bridge.

These proboscideans are thought to have been introduced to the Japanese Archipelago at different times, and to have become endemic soon afterwards as they inhabited the Japanese Archipelago in isolation, separated from the continent by the sea. According to Saegusa (2005), *Paleoloxodon naumanni* is closely related to the Stuttgart type of *Elephas antiquus*, whose skull type is older than that of *Elephas namadicus* found in China, and that the Stuttgart type, which was migrated to Japan at MIS 10 (about 350 ka) or shortly before, evolved as an isolated continental survivor.

In other words, most of the mammals currently inhabiting the Honshu region of the Japanese Archipelago are composed of



Fig. 2 Bathymetric chart around the Ryukyu Islands showing the biogeographic boundaries (white thick dotted lines). St.: Strait. Thin dotted line is shown depth of 100 m. The seafloor shallower than depth of 1,000 m shows the land area in the late Middle Pleistocene. The seafloor topography is based on NOAA bathymetric data.

species that were migrated to the Honshu region when it was connected to the continent several times since the Late Miocene, and were isolated and endemic. The last of these migrations is thought to be the time when the ancestors of the *Paleoloxodon naumanni* arrived from the continent in the late Middle Pleistocene, 430 ka.

The terrestrial herpetofauna and land bridge in the Ryukyu Islands

The boundary between the Palearctic and the Oriental Districts of zoogeography in Japan is the Watase's Line between the Japanese Archipelago and Ryukyu Islands, which corresponds to a deep fissure (the Tokara Gap) of more than 1,000 m depth between Akuseki and Kotakara Islands in the southern Tokara Islands between Amami-Oshima and Kyushu. (Fig. 2). On the western side of the Tokara Gap, a 1,000 m depth line connects the Ryukyu Islands with Kyushu to the north, but this area is shallow because it is buried by Pliocene and Pleistocene volcanic sediments (Aiba and Sekiya, 1979), and was separated by the sea during the Pliocene and Pleistocene (Hoshino, 1983).

In terms of herpetofauna, most of the reptiles in the Amami/Okinawa Islands consist of the Habu (genus *Protobothrops*), the Ryukyu green snake (*Cycophiops semicarinatus*) and the blue viper (*Takydromus smaragdinus*), with the northern limit south of Kodakara Island, while the northern reptiles in the Tokara Gap consist of the Japanese common species of the genus *Elaphe*, such as the Japanese striped snake and rat snake, which are not distributed in the Amami/Okinawa Islands even at the genus level (Hikita, 2002).

There are three more distributional boundaries between the Ryukyu Islands, Taiwan and the mainland. The Hachisuka's Line is located between the Okinawa and Miyako Islands, the Southern Sakishima Line is located between the Yaeyama Islands and Taiwan, and the Taiwan Strait Line is located between Taiwan and the mainland. Among these distribution boundaries, the Hachisuka's Line corresponds to the Kerama Gap, which is the deepest with a depth of over 1,000 m. In addition, the Yonaguni Strait, which separates Taiwan from the Yaeyama Islands and is deeper than 500 m, corresponds to the Southern Sakishima Islands Line. In contrast, the continental shelf connects the continent with Taiwan.

Hikita (2002) made a comparison of the terrestrial herpetofauna among these regions in the Ryukyu Islands, and found that most of the closely related species between the Okinawa/Amami Islands and the Yaeyama/Miyako Islands were differentiated at the species level, while most of the species between the Yaeyama/Miyako Islands and Taiwan were differentiated only at the subspecies level. Hikita (2002) stated that the land bridge of the Ryukyu Islands first extended from the continent through Taiwan to the Tokara Gap, then was divided by the Kerama Gap, and finally by the Yonaguni Strait. In other words, the Pleistocene land bridge extended only from Taiwan to the Miyako Islands, and the Okinawa/Amami Islands were isolated from the rest of the world by the Tokara and Kerama Gaps.

The terrestrial mammals on the islands of the Wallacea District

Wallace (1863) distinguished between the fauna of the regions east and west of the boundary of biological distribution (Wallace's Line), which runs from the Lombok Strait between the Indonesian islands of Bali and Lombok through the western side of Sulawesi, the Makassar Strait, to the south of Mindanao in the Philippine Archipelago. Huxley (1968) extended the boundary through the Sulu Sea and then west of the Philippines between Borneo and Sulu (Fig. 3). The Huxley's Line, which is the eastern margin of the Oriental District, is roughly at the eastern edge of the outer continental shelf and corresponds to the eastern coastline of Southeast Asia during the Last Glacial Maximum.

The area between the Wallace's or Huxley's Lines and the Weber's or Lydecker's Lines, which marks the western edge of the Australian District, is called Wallacea District, the boundary area between the Oriental and Australian Districts. The islands of the Wallacea District include the Philippine Archipelago, Sulawesi, and Flores, which are still rich in endemic animal species, and fossil endemics such as stegodons and other proboscideans, rhinoceros, water buffalos, wild boars, and deer have been discovered in the Pleistocene series.

Java

Java, an island west of the Wallace's Line, is important in considering the distribution of animals on the islands of the Wallacea District, so here is summary of its biostratigraphy according to Van der Geer et al. (2010).

The island arc of Java started to rise due to volcanic activity in the Late Pliocene, and the western and central parts of Java became land due to gradual uplift since 1.8 Ma. During the Early Pleistocene, the mammals inhabiting Java are characterized by small hippopotamuses and deer, and small mastodons, but during the Middle Pleistocene, elements of mainland Southeast Asia continued to arrive on Java, and this fauna is characterized by *Homo erectus* and endemic small stegodons. At the end of the Middle Pleistocene, animals from the rainforest elements of mainland Southeast Asia migrated to the Indonesian Archipelago.

From Java, seven consecutive faunas have been recognized (De Vos et al., 1982; Sondaar, 1984), and Van der Geer et al.

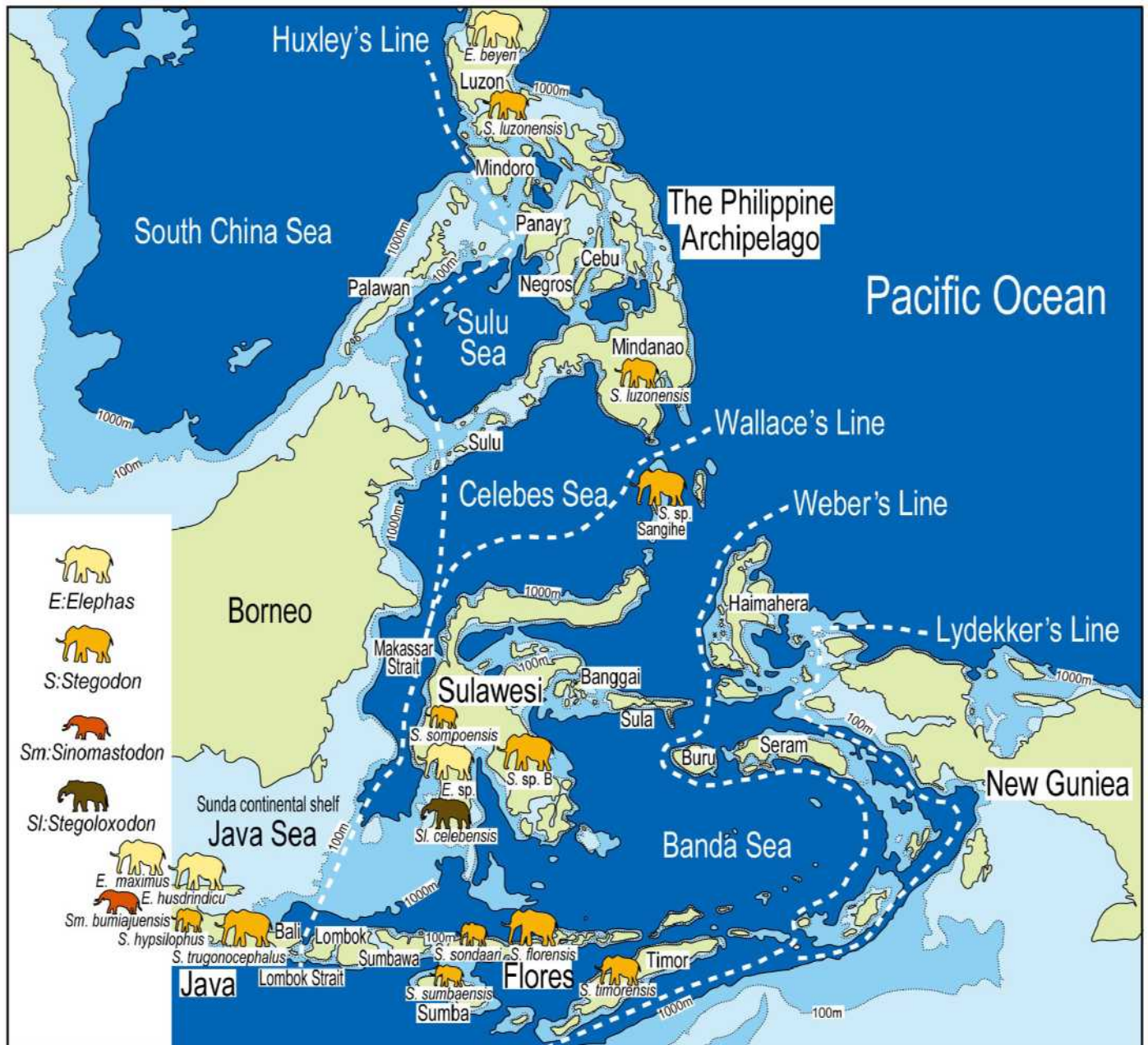


Fig. 3 Bathymetric chart around the Wallacea District showing biogeographic boundaries (white thick dotted lines) and the distribution of insular proboscideans. Thin dotted line is shown depth of 100 m. The seafloor shallower than depth of 1,000 m shows the land area in the late Middle Pleistocene. The seafloor topography is based on NOAA bathymetric data.

(2010) divided them into four major periods: (1) the Late Pliocene to Early Pleistocene (the Satir fauna), (2) the Middle Pleistocene (the Ci Saat fauna, the Trinil H. K. fauna, the Kedung Brubus fauna, and the Ngandong fauna), (3) Late Pleistocene (the Punung fauna), and (4) Holocene (the Wajak fauna). A summary of these faunas is given below, following Van der Geer et al. (2010).

(1) The Late Pliocene to Early Pleistocene fauna is represented by a mastodon (*Sinomastodon bumiajuensis*), a small hippopotamus (*Hexaprotodon sivajavanicus*), unidentified cervids, a giant tortoise *Geochelone* and perhaps pygmy stegodons.

(2) The fauna of the Middle Pleistocene is closely related to that of the Siwalik fauna of India, and is represented by *Homo electus*, the short-faced hyena (*Pachyrocute brevirostris*), the Javanese stegodon (*Stegodon trigonocephalus*), the Javanese elephant (*Elephas husdrindicus*), the Kendeng rhinoceros (*Rhinoceros unicornis kendengindicus*), the antelope (*Duboisia santeng*), and the Lydekker's deer (*Cervus (Axis) lydekkeri*).

(3) The fauna of the Late Pleistocene was formed by the arrival in the Indonesian Archipelago of new elements of the tropical rainforest fauna of the mainland at the end of the Middle Pleistocene. These are represented by the India elephant (*Elephas maximus*), orang-utan (*Pongo pygmaeus*), gibbon (*Hylobates syndactylus*), the pig-tailed macaque (*Macaca nemestrina*), the Sunda

tiger (*Panthera tigris sondaica*), the Sumatran rhino (*Dicerorhinus sumatrensis*), the Malayan bear (*Ursus malayanus*), serow (*Nemorhaedus sumatraensis*), water buffalo (*Bubalus bubalis*), and wild boar (*Sus scrofa vittatus*).

(4) The fauna of the Holocene is thought to have been recently replaced by present-day species or to have evolved from earlier Pleistocene inhabitants.

Flores

Flores is one of the Lesser Sunda Islands east of Java (Bali, Lombok, Sumba, Sumbawa, Flores, and Timor), and is not connected to Java and Bali on the Sunda continental shelf by the Lombok Strait west of Lombok. The Lombok Strait is 18 km wide at its narrowest point, contiguous at the isobath at a depth of 250 m or more, it was not contiguous at the low sea level during the Last Glacial Maximum.

Flores emerged above the sea surface between about 15 and 21 Ma during the Early to Middle Miocene (Nishimura et al., 1981) and has been rising since the end of the Pliocene (Van den Bergh, 1999). The southern half is composed of Pliocene to Pleistocene volcanoes, while the southeastern and southwestern margins are composed of younger active volcanoes.

Flores was inhabited in the Middle and Late Pleistocene by pygmy and dwarf stegodons, giant rats, komodo dragons, and enigmatic species of dwarf human. According to Van der Geer et al. (2010), three faunas can be distinguished on Flores: (1) the Early Pleistocene (Fauna A), (2) the Middle Pleistocene (Fauna B), and (3) the Late Pleistocene.

(1) Fauna A of the Early Pleistocene is characterized by a pygmy stegodon (*Stegodon sondaari*), which is about half the size of Java stegodon (*Stegodon trigonocephalus*) and shows a mixture of primitive and advanced traits. The fission track age of the stratum in which the fauna was found is 0.9 Ma (Van der Geer et al., 2010).

(2) Fauna B of the Middle Pleistocene shows that mammals migrated to Flores approximately during the transition between the Early Pleistocene and Middle Pleistocene. The new mammalian elements are a middle-sized stegodon (*Stegodon florensis*), a middle-sized cave rat (*Hoijeromys nusatenggara*), and an early hominin (Van der Geer et al. 2010). Morwood et al. (1998) dated volcanic layers at about 0.88 and 0.68 Ma from this biozone. Fossils of early humans have not been found, and proof of their presence stems only from lithic artefacts. The primitive tools are found in association with fossils of the stegodon and in the same area where tektites belonging to the Australian strewnfield, dated to 0.8 Ma, are found (Van der Geer et al., 2010).

(3) The fauna of the Late Pleistocene is a variation of the fauna of the Middle Pleistocene, without major changes in the fauna of the Middle Pleistocene, characterized by a dwarf stegodon (*Stegodon florensis insularis*) (Van der Geer et al., 2010). The dwarf stegodon is smaller than its ancestor from the previous biozone (Van den Bergh et al, 2008). This fauna is also characterized by a dwarf human (*Homo floresiensis*) (Brown et al., 2004).

Sulawesi

Sulawesi, formerly known as Celebes, is the largest of the Sunda Archipelago to the east of Borneo. Sulawesi is separated from Borneo by the Makassar Strait, which is over 2,000 m deep, but is contiguous with the Java Sea to its south by a 1,000 m deep isobath.

Sulawesi is currently home to a number of endemic species and subspecies, including the babirusa (*Babyrousa babyrussa*), the anoa (*Bubalus depressicornis*), the marsupial (*Ailurops ursinus*), the Sulawesi black macaque (*Macaca nigra*), the Muna-Buton macaque (*M. brunnescens*), the Heck's macaque (*M. hecki*), the Gorontalo macaque (*M. nigrescens*), the Dian's tarsier (*Tarsius dentatus*), and the pygmy tarsier (*T. pumilus*).

In Sulawesi, Van den Bergh et al. (2001) and Van der Geer et al. (2010) distinguished three faunas: (1) the Late Pliocene to Early Pleistocene Walanae faunal unit, (2) the Middle or Late Pleistocene Tanrung faunal unit, and (3) the Late Pleistocene to present fauna (Fig. 4).

(1) The Walanae faunal unit consists mainly of the Sulawesi dwarf elephant (*Stegoloxodon celebensis*), the giant Sulawesi pig (*Celebochoerus heekereni*) and the dwarf stegodon (*Stegodon sompoensis*). The oldest occurrence of this fauna is at about 2.5 Ma (Van der Geer et al., 2010).

(2) The Tanrung faunal unit is poorly represented and therefore also poorly known. Recorded elements are a large elephant (*Elephas* sp.), a medium-sized stegodon (*Stegodon* sp. B), and a short-legged form of the Sulawesi pig (*Celebochoerus* sp.) (Van der Geer et al., 2010).

(3) The Late Pleistocene to present fauna is clearly distinguished from the earlier fauna by the absence of proboscideans and giant pigs, and is thought to have been established in South Sulawesi during the Late Pleistocene by the gradual replacement of endemic species with new ones introduced to Sulawesi towards the end of the Tanrung faunal unit in the Middle Pleistocene (Van den Bergh et al., 2001). This fauna seems to have undergone the effects of long-term isolation and evolved into endemic forms, as noted by Wallace (1863).

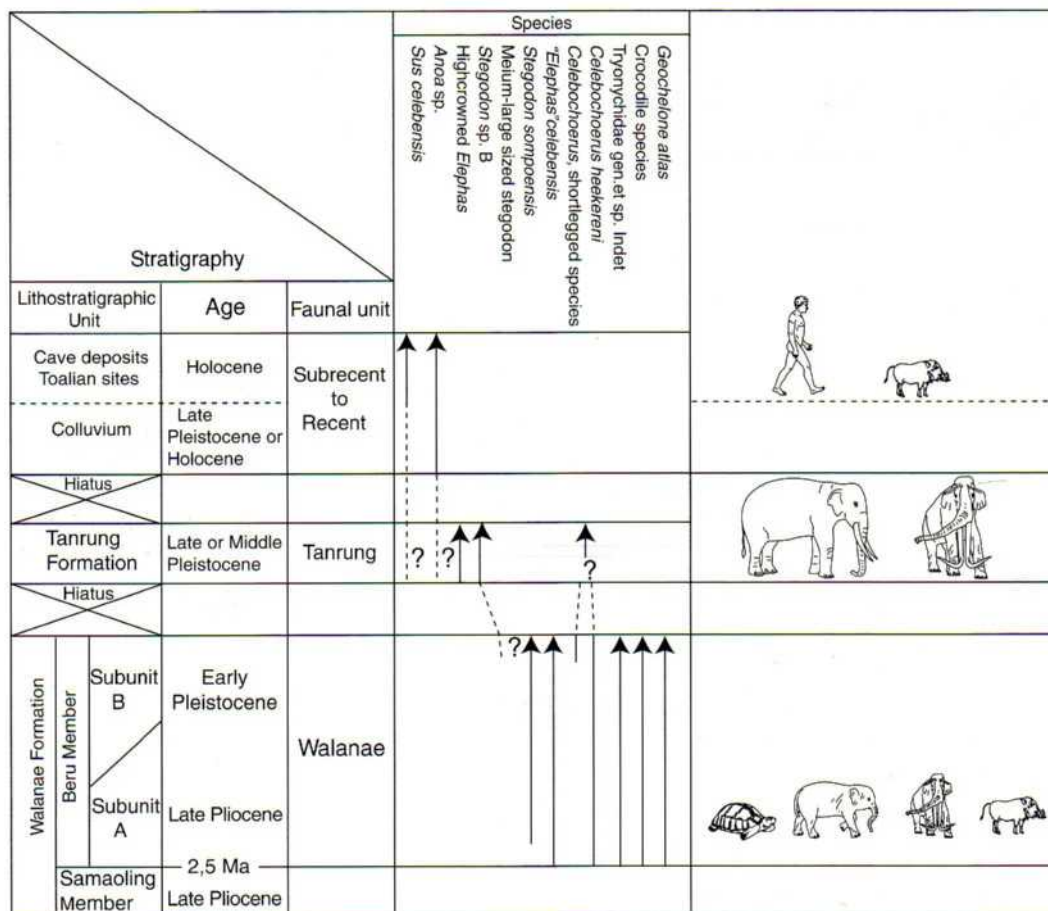


Fig. 4 Stratigraphic scheme, showing the land vertebrate faunal succession of Sulawesi (From Van der Geer et al., 2010). The subrecent to recent fauna is omitted.

The Philippine Archipelago

The Philippine Archipelago consists of more than 7,000 islands located between Borneo and Taiwan. Croft et al. (2006) reconstructed the paleogeography of the Philippine Archipelago during the Last Glacial Maximum by dividing it into isobaths of 120 m depth and showed that they consisted of six major paleo-islands: Greater Luzon, Mindoro, Greater Palawan, Greater Negros-Panay, Greater Mindanao, and Greater Sulu.

The northern end of the Philippine Archipelago is separated from Taiwan by a seafloor of more than 2,000 m in depth. On the southwest side, Palawan is contiguous with Borneo at a depth of 200 m. However, Greater Palawan and Mindoro are contiguous only at a depth of 500 m. Borneo and Mindanao are contiguous at the 500 m depth isobath, and the southern tip of Mindanao is contiguous with Sulawesi only at the 1,500 m depth isobath.

The Philippine Archipelago is currently home to a large number of endemic species, even surpassing Madagascar in their degree of endemism. The main endemic species are the Philippine sambar (*Cervus mariannus*), the Prince Alfred's deer (*Cervus alfredi*), the Philippine tarsier (*Tarsius syrichta*), the Philippine flying lemur (*Cynocephalus volans*), the Philippine long-tailed macaque (*Macaca fascicularis philippinensis*), and several bat species and many endemic rodents (Muridae) (Van der Geer et al., 2010).

A reliable biostratigraphy for the Philippine Archipelago has not yet been established due to the scarcity of fossil records and the unknown stratigraphic contrast between the different islands. However, Van der Geer et al. (2010) distinguished three faunas: (1) the Middle to Late Pleistocene, (2) the Late Pleistocene, and (3) the Late Pleistocene to Holocene.

(1) The Middle to Late Pleistocene fauna is distributed in Greater Luzon, Greater Negros-Panay, and Greater Mindanao. This fauna includes a large stegodon (*Stegodon luzonensis*), a large elephant (*Elephas* sp.), a rhinoceros (*Rhinoceros philippinensis*), a Luzon buffalo (*Bubalus* sp.), a Mindoro buffalo (*Bubalus mindorensis*), and a Cebu buffalo (*Bubalus cebus*), a Luzon wild boar (*Sus* sp.), and a deer (*Cervus* sp.) from Luzon and Palawan. Stegodon fossils are found together with tektites and stone tools that have been dated to 0.8 Ma (Van der Geer et al., 2010).

(2) The Late Pleistocene fauna includes a dwarf deer (*Cervus* spp.) and a giant rat (*Rattus* cf. *everetti*) from Masbate Island (Greater Negros-Panay) (Van der Geer et al., 2010).

(3) The fauna of the Late Pleistocene to Holocene is the ancestor of the present fauna, which arrived at the end of the Pleistocene or the beginning of the Holocene. These species underwent speciation under isolation, and as result developed one of the most unique faunas in the world with regard to the level of endemic species (Van der Geer et al., 2010).

Fauna of the Wallacea District since the Middle Pleistocene and its formation period

The fauna of Java, excluding the Holocene, consists of the Early, the Middle and the Late Pleistocene faunas (Van der Geer et al., 2010). The Late Pleistocene fauna (the Punung fauna) replaced the Middle Pleistocene fauna, which was closely related to the earlier Siwalik fauna, and was formed at the end of the Middle Pleistocene when a new component of the rainforest fauna typical of mainland Southeast Asia migrated to the Indonesian Archipelago (Van der Geer et al., 2010).

In Flores, there were faunal transformations during the Early and Middle Pleistocene, and the fauna of the Late Pleistocene is a variation of the fauna of the Middle Pleistocene (Van der Geer et al., 2010). The time of conversion between fauna A of the Early Pleistocene and fauna B of the Middle Pleistocene may be around 0.9 Ma, because the stratigraphic level of fauna A is 0.9 ka, and fauna B includes volcanic ash layer of 0.88 Ma and tektites of 0.8 Ma (Morwood et al., 1998; Van der Geer et al., 2010).

Sulawesi also underwent faunal transformations during the Early, the Middle and the Late Pleistocene, of which the Late Pleistocene to present fauna is thought to have been formed by the gradual replacement of newly introduced species with endemic species in the Tanrung fauna of the Middle Pleistocene (Van der Geer et al. 2010).

In the Philippine Archipelago, the conversion from the Middle to Late Pleistocene fauna to the Late Pleistocene fauna probably occurred in the late Middle Pleistocene. However, because the biostratigraphy of the Philippine Archipelago has not been established and the characteristics of the fauna in each region of the Philippines are not clear, the details of this process are unknown. It is estimated that new fauna arrived at the end of the Pleistocene or the beginning of the Holocene (Van der Geer et al., 2010).

The Early, the Middle, and the Late Pleistocene faunas are unique to Java, Flores, Sulawesi, and the Philippines in the Wallacea District. Of these, the period of conversion from the Middle Pleistocene fauna to the Late Pleistocene fauna is thought to fall in the latter part of the Middle Pleistocene, although the specific age value of the conversion period for each island is unknown.

The terrestrial mammals on the islands of the Mediterranean Sea

The Mediterranean Sea is surrounded by the Eurasian continent to the north and east, the African continent to the south, the Atlantic Ocean to the west through the Gibraltar Strait, and the Marmara Sea and the Black Sea to the east through the Dardanelles and Bosphorus Straits. There are many islands in the Mediterranean Sea. In the western and central Mediterranean Sea, the Balearic Islands of Spain in the western part, Sardinia and Corsica in the Tyrrhenian Sea of the west of the Italian Peninsula, and Sicily and Malta in the south of the Italian Peninsula. In the eastern Mediterranean Sea, there are many islands such as the Cyclades in the Aegean Sea between Greece and Turkey, and Crete and Rhodes bound the southern border of the Aegean Sea, Cyprus is further south of Turkey.

Most of these Mediterranean islands were not connected to the continent by land when the sea level dropped by about 100 m during the Last Glacial Maximum (Fig. 5). However, fossils of many species of endemic mammals such as proboscideans, hippopotamuses, deer, otters and shrews have been found in the Pleistocene series of many of these islands.

Cyprus

Cyprus, the third largest island in the Mediterranean Sea, emerged from the sea during the Miocene. Cyprus is separated from the Turkish mainland by a distance of about 80 km at the shortest point, where the seafloor extends to a depth of 500 m or more, and is connected by a 1,000 m deep isobath.

On Cyprus, two faunas are recognized: (1) the Late? Pleistocene and (2) the Holocene faunas (Van der Geer et al., 2010).

(1) The strata of the Late? Pleistocene yield fossils of a pygmy hippopotamus (*Phanourios minor*) and a dwarf elephant (*Elephas cypriotes*). The pygmy hippopotamus is the smallest hippopotamus of all known insular hippopotamuses and account for more than 90% of the mammal fossils found on Cyprus. This may be due to its lack of terrestrial predators or competitors, which allowed it to adapt well to all environments on the island (Van der Geer et al., 2010). *Elephas cypriotes* is thought to have been derived from *E. antiquus*. Elephants and pygmy hippopotamuses were introduced to this island in the late Middle Pleistocene and adapted to the island's area through subsequent isolation, becoming insular, or dwarfed, and endemic (Van der Geer et al., 2010).

(2) The Holocene fauna is in principle a mainland fauna, although rather impoverished, unbalanced and endemic on at most the subspecies level (Van der Geer et al. 2010). The Holocene fauna of Cyprus includes red fox (*Vulpes vulpes indutus*), Cypriot mouflon (*Ovis orientalis ohion*), small rats and bats. It is probable that these mammals, except for the bats, were introduced

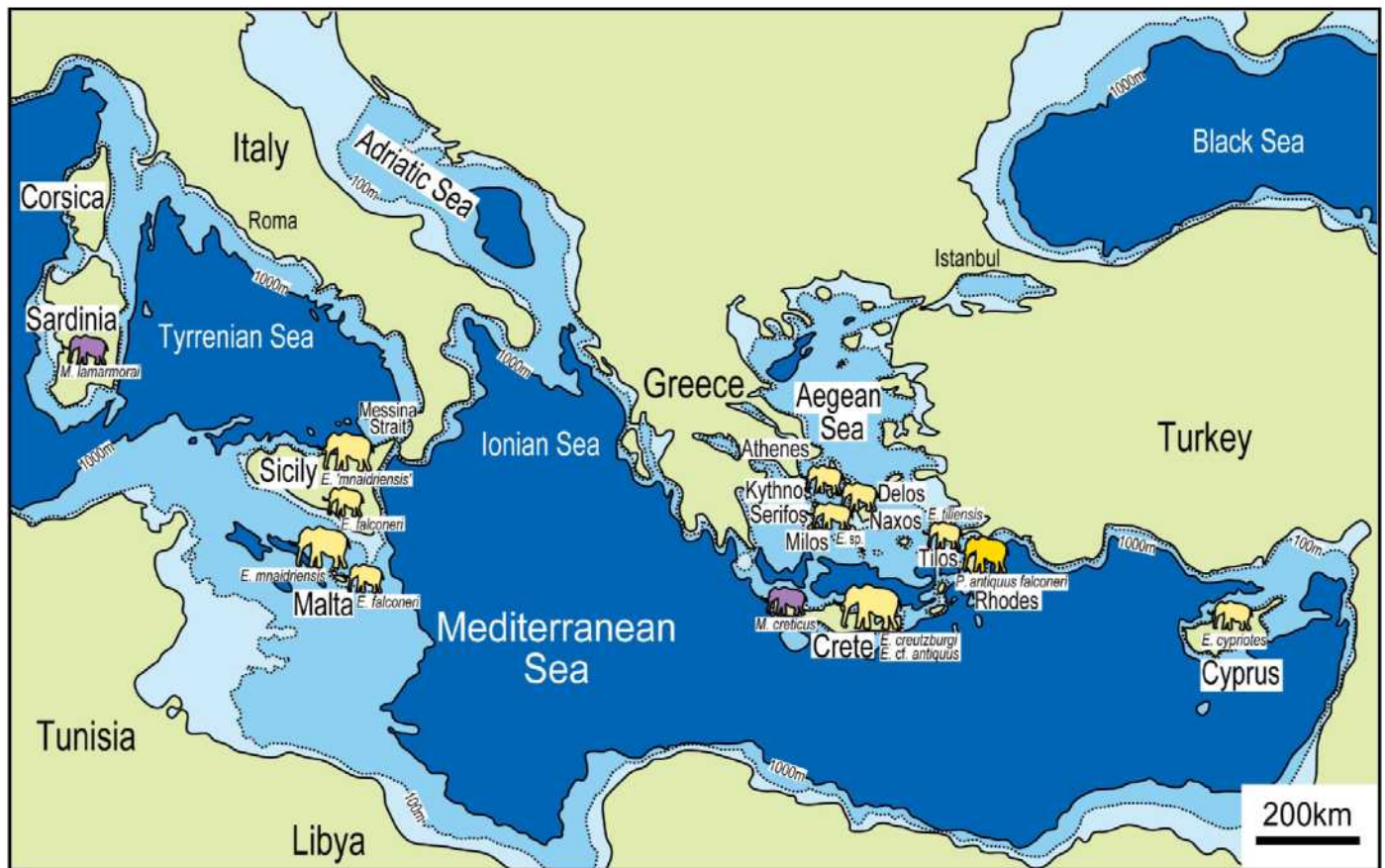


Fig. 5 Bathymetric chart around the Mediterranean Sea showing the distribution of insular proboscideans. Thin dotted line is shown depth of 100 m. The seafloor shallower than depth of 1,000 m shows the land area in the late Middle Pleistocene. The seafloor topography is based on NOAA bathymetric data.

through human agency.

Crete

Crete is the largest island in Greece, located in the Cretan Sea between Greece and Turkey, and is connected to the Peloponnese of Greece by a 1,000 m deep isobath.

An endemic Pleistocene mammalian fauna is known from Crete, including dwarf deer, dwarf proboscideans, dwarf hippopotamus, and large mice. The pre-Pleistocene mammal fossils are of the Late Miocene age and belong to a continental type, but two distinct major biotic zones were recognized in the Pleistocene, with major faunal transformations at the boundaries of these zones (Sondaar et al., 1986; Dermitzakis and De Vos, 1987).

Crete was connected to the mainland until the Late Miocene. Gradually, Crete became fragmented into small pieces during the Late Miocene and Early Pliocene. The region became largely submerged towards the end of Pliocene Period, during what is known as the Pliocene transgression (Dermitzakis and Sondaar, 1978) and forming the present landscape at the end of the Pliocene or Early Pleistocene (Van der Geer et al., 2010). According to Van der Geer et al. (2010), excluding the Late Miocene biozones, Crete is divided into two biozones: (1) the *Kritimys* zone (the Early Pleistocene to early Middle Pleistocene) and (2) the *Mus* zone (the late Middle Pleistocene to late Late Pleistocene) (Fig. 6).

(1) The *Kritimys* zone is represented by the Cretan rat (*Kritimys*), the Cretan pygmy mammoth (*Mammuthus creticus*) and the Creutzburg's dwarf hippopotamus (*Hippopotamus creutzburgi*). According to Van der Geer et al. (2010), the absolute ages obtained by AAR and ESR of hippopotamus molar fragments range between 850 ka and 375 ka. Mol et al. (1996) estimated that the mainland ancestor of the pygmy mammoth was probably the southern mammoth (*Mammuthus meridionalis*).

(2) The *Mus* zone is represented by two species of common mice (*Mus bateae*, *M. minotaurus*), the Creutzburg's elephant (*Elephas creutzburgi*, *E. antiquus creutzburgi* or *E. cf. antiquus*), the Cretan deer (seven species of the genus *Candiacervus*), the Cretan otter (*Lutrogale cretensis*), and the Cretan shrew (*Crociodura zimmermanni*), which were introduced and endemic before the late Middle Pleistocene (Van der Geer et al., 2010).

The Aegean Islands

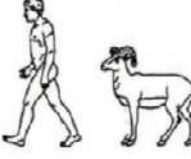
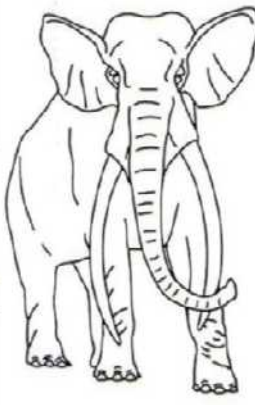
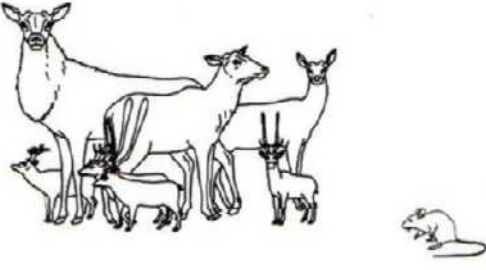
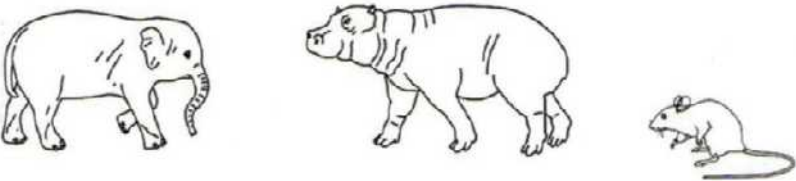
Zones	Subzones	Range-zones		
				Holocene
Mus	Mus minotaurus	Elephas creutzburgi		Pleistocene
		Elephas antiquus		
	Mus bateae			
Kritimys	Kritimys catraus	Hippopotamus creutzburgi parvus		
		Hippopotamus creutzburgi creutzburgi		
	Kritimys kiridus	Elephas creticus		
	K. aff. kindus			

Fig. 6 Stratigraphic scheme, showing the land vertebrate faunal succession of Crete (Simplified version of figure from Van der Geer et al., 2010).

Fossils of dwarf elephants during the Late Pleistocene have also been found on the Aegean islands of Tilos, Rhodes, Naxos, and Delos. These islands are not contiguous with the continent at the 100 m depth isobath, but are distributed on a plateau above the seafloor at depths of 500 m to 1,000 m.

On Tilos, 11,000 fossil proboscideans were found, with a large variation in their size, and they were identified to two different subspecies (*Palaeoloxodon antiquus falconeri* and *P. a. mnaidriensis*) (Symeonidis et al., 1973). Theodorou et al. (2007) described a new species (*Elephas tiliensis*) from among them, and the absolute age of this new elephant ranges from about 45 ka to 3.5 ka.

The fossils from Naxos and Delos belong to a dwarf elephant that has not yet been described, with an elephant's maxilla from Naxos, an elephant's molar from Delos, and elephant remains from Rhodes, Ross and Serifos, and Kythnos. In addition, there are reports of proboscidean fossils from Rhodes, Ross and Serifos, and Kinos, but few species have been described and the material is untraceable (Van der Geer et al., 2010).

Sicily

Sicily is a large island in the central Mediterranean, close to the southwestern tip of the Italian Peninsula by the Messina Strait, which is 3 km wide at its narrowest point. The Messina Strait is contiguous with the peninsula by isobaths at depth of 250 m.

Van der Geer et al. (2010) described the geological history and faunal evolution of Sicily since the Pliocene as follows. Sicily consisted of two islands in the Early Pliocene and Early Pleistocene, and the southern part of Calabria in the southern tip of the Italian Peninsula was also a series of islands with northern Sicily. The distance between Sicily and Calabria, the Messina Strait, varied in accordance with changing sea levels during the Pleistocene. Apart from this strait, the isthmus of Catanzaro between the north and south part of Calabria also played an important filter role in the colonization events of Sicily and Malta.

Sicily is characterized by a continuous mammalian endemic fauna that includes dwarf elephants and dwarf hippopotamuses

and giant dormice during the Pleistocene. Since then, Sicily has gradually lost its isolation and the number of mainland species inhabiting the island has increased. During the early Middle Pleistocene, Sicily was connected to Malta, sharing the same endemic fauna. This connection was lost before the end of the Pleistocene and both islands harboured their own endemic faunas.

The Pleistocene vertebrate assemblages of Sicily are generally known as Faunal Complexes. According to Van der Geer et al. (2010), it consists of excluding the Holocene fauna, (1) the Early Pleistocene fauna (the Monte Pellegrino Faunal Complex), (2) the early and middle Middle Pleistocene fauna (the *Elephas falconeri* Faunal Complex), (3) the late Middle Pleistocene to early Late Pleistocene fauna (the *Elephas 'mnaidriensis'* Faunal Complex), and (4) the Latest Pleistocene fauna (the Gotta San Teodoro-Contrada Pianetti Faunal Complex).

(1) The Early Pleistocene fauna is represented by a marten (*Mustelercta arzilla*), a large red-toothed shrew (*Asoriculus burgioi*), a large field mouse (*Apodemus maximus*), two large dormice (*Leithia* sp. *Maltamys* cf. *gollcheri*), a ctenodactylid (*Pellegrinia panormensis*), and a hare (*Hypolagus peregrinus*) (Van der Geer et al., 2010). The shrew evolved in parallel with the other Mediterranean insular red-toothed shrews, all of which are thought to have originated from a clade of common ancestors, and the dormouse genera *Leithia* and *Maltamys* are regarded as relics of an older fauna of the Messinian age (Late Miocene) by Daams and De Bruijn (1995).

(2) The early and middle Middle Pleistocene fauna is highly endemic and impoverished. Its only known elements are the pygmy elephant (*Elephas falconeri*), a shrew (*Crocidura esuae*), a giant dormice (*Leithia melitensis*), two large dormice (*Leithia cartei* and *Maltamys gollcheri*), the Sicilian otter (*Lutra trinacriae*), and bats (Van der Geer et al. 2010). Fossil pygmy elephants were dated to 455 ± 90 ka using amino-acid racemization by Bada et al. (1991). This fauna is almost identical to the fauna of Malta at this time, and provides evidence that Sicily and Malta were connected and became one island. The habitat of the pygmy elephants is thought to consist of an open environment with sparse tree cover, dominated by grasses, and was much like the habitat of the extant African elephant as indicated by pollen analysed by Bertoldi et al. (1989) and Suc et al. (1995). The Sicilian and Maltese extant shrew might in turn have descended from the Saharan shrew (*Crocidura tarfayaensis*), as ascertained by Dubey et al. (2007), based on DNA.

(3) The late Middle Pleistocene and early Late Pleistocene fauna is represented by an endemic small elephant (*Elephas 'mnaidriensis'*) and a small hippopotamus (*Hippopotamus pentlandi*). In this period, a new invasion of mainland species took place. Other new insular elements of this fauna are fallow deer (*Dama carburangelensis*), aurochs (*Bos primigenius*), red deer (*Cervus elaphus*), wild boar (*Sus scrofa*), brown bear (*Ursus arctos*), European bison (*Bison priscus*), grey wolf (*Canis lupus*), lions (*Panthera leo*), spotted hyenas (*Crocuta crocuta*), and European hedgehogs (*Erinaceus europaeus*), all typical for a warm period (Van der Geer et al. 2010). Dating by ESR on teeth enamel of *Elephas 'mnaidriensis'* and *Hippopotamus pentlandi* by Rhodes (1996), provided an age ranging between 146 ± 28.7 ka and 88.2 ± 19.5 ka.

(4) The Latest Pleistocene fauna includes the large mammals of the earlier *Elephas 'mnaidriensis'* fauna, but more mainland taxa, including the European ass (*Equus hydruntinus*) arrived on the island at the end of this stage. The new micromammals of this period are the common field mouse (*Apodemus silvaticus*), the pine vole (*Microtus savii*) and Sicilian shrew (*Crocidura sicula*), (Van der Geer et al., 2010).

Malta

Malta is a small island south of Sicily, which is not connected to Sicily by the 100 m depth isobath, but is connected by the 200 m depth isobath. Malta was connected to Sicily in the early Middle Pleistocene, but sea level rise by the end of the Pleistocene separated Malta from Sicily. Since that period, Malta has harboured its own endemic fauna, consisting mainly of dwarf proboscideans, dwarf deer and giant dormice. The fauna of Malta was divided by Van der Geer et al. (2010) into (1) the middle Middle Pleistocene, (2) the late Middle Pleistocene, and (3) the Late Pleistocene, excluding the Holocene fauna, as follows.

(1) The middle Middle Pleistocene fauna is characterized by the Sicilian dwarf elephant (*Elephas falconeri*) and a giant dormouse (*Leithia melitensis*), two large dormice (*Maltamys gollcheri* and *M. wiedincitensis*), the Maltese otter (*Lutra euxena*) and a white-toothed shrew (*Crocidura esuae*). Malta was connected by land with Sicily, based on the occurrence of the same species of dwarf elephant, dormice and shrew.

(2) The late Middle Pleistocene fauna is thought to have been formed by new arrivals, represented by the Maltese dwarf hippopotamus (*Hippopotamus melitensis*) and a small elephant (*Elephas mnaidriensis*). The main difference between the Sicilian fauna and the Maltese fauna of this period is the smaller size of the Maltese hippopotamus and elephant in combination with a larger degree of endemism of the Maltese fauna.

(3) The Late Pleistocene fauna consists mainly of the endemic short-limbed deer (*Cervus* sp.), a burrowing vole (*Microtus (Pitimus) melitensis*) and a white-toothed shrew (*Crocidura* sp.), all new immigrants. The Late Pleistocene fauna of Malta is more endemic than that of Sicily, and the fauna as a whole is much poorer than that from Sicily.

Sardinia and Corsica

Sardinia and Corsica are two large islands in the Tyrrhenian Sea on the western side of the Italian Peninsula. The two islands are contiguous at the 100 m depth isobath, so they were one island until the beginning of the Holocene. Therefore, the fauna of Sardinia and Corsica are practically the same. The Corsica Channel between Corsica and Elba Island on the west coast of the Italian Peninsula is about 50 km wide and deeper than 200 m. Corsica and Elba island are contiguous at an isobath of 500 m depth.

Sardinia and Corsica were a part of the adjacent continent during the Eocene, isolated from the continent at the beginning of the Miocene. At the onset of the Late Miocene Messinian salinity crisis (Hsü et al., 1977), Sardinia and Corsica became a part of the Italian region of Tuscany, forming the Tusco-Sardinian paleobioprovince. During the Middle Pliocene and Early Pleistocene, Sardinia and Corsica again were isolated from the mainland, but they were connected to the continent several times and new animal elements were introduced. It is thought to have been completely isolated from mainland Italy after the late Middle Pleistocene (Van der Geer et al., 2010).

The fauna of Sardinia and Corsica is divided into five groups by Van der Geer et al. (2010): (1) the Early to Middle Eocene, (2) the Early Miocene, (3) the Late Miocene, (4) the Middle Pliocene to Early Pleistocene, and (5) the late Early Pleistocene to Early Holocene. Here, the fauna groups of (1) to (3) omitted and start with (4), because this paper focuses mainly on the fauna of the Pleistocene.

(4) The fauna of the Middle Pliocene and the Early Pleistocene is balanced through impoverished, characterized by goral-like caprids (*Nesogoral melonii* and *Nesogoral cenisae*), a small pig (*Sus sondaari*), a macaque (*Macaca majori*), a hunting hyena (*Chasmaporthetes melei*), a small bovid (*Asoletragus gentryi*), an undetermined caprid, a mustelid (*Pannonictis* sp.), and several micromammals, including a large field mouse (*Apodemus mannu*), a small field mouse (*Rhagapodemus azzarolii*, *R. minor*), a dormouse (*Tyrrhenoglis*), a shrew (*Asoriculus* aff. *gibberodon*), a mole (*Talpa* sp.), a pika (*Prolagus* aff. *P. sorbinii*), and a rabbit (*Oryctolagus*). This fauna is generally characterized by small mammals. This fauna, generally referred to as the *Nesogoral* fauna after the goral-like caprid, was probably introduced by a land bridge that existed during the Late Miocene Messinian salinity crisis and formed as the result of a long period of subsequent isolation during the Pliocene (Van der Geer et al., 2010).

(5) The fauna of the late Early Pleistocene to early Holocene is dominated by a canid (*Cynotherium* sp.), a small vole (*Microtus* (*Tyrrhenicola*) *sondaari*), a large deer (*Megaloceros* sp.), red-toothed shrews (*Asoriculus similis* and *Asoriculus corsicanus*) and possibly human (*Homo sapiens*). Fossils of Sardinian large deer have been obtained from strata dated to 450 ka and 367 ka. And the ancestors of the dwarf mammoth (*Mammuthus lamarmorae*) arrived on the island during the late Middle Pleistocene. The fauna of this period was unbalanced, strongly endemic, and probably evolved here after a long period of isolation, but from the Middle Pleistocene onwards it developed a fauna that was slightly different from the earlier ones (Van der Geer et al., 2010).

Fauna of the late Middle Pleistocene of the Mediterranean Islands and its formation period

The Pleistocene mammalian faunas of the Mediterranean islands show that most of them underwent major transformations in the early and late Middle Pleistocene. In Crete, that is a typical example, two biological zones are recognized: the Early to Middle Pleistocene (*Kritimys* Zone), represented by Cretan pygmy mammoth and Creutzburg's dwarf hippopotamus, and the Middle to Late Pleistocene (*Mus* Zone), represented by Creutzburg's elephant and Cretan deer. The mammals of the *Mus* Zone were introduced and endemic in the late Middle Pleistocene (Van der Geer et al. 2010).

In Cyprus, there is a Late? Pleistocene pygmy or dwarf fauna, which are thought to have migrated to the island in the late Middle Pleistocene (Van der Geer et al. 2010). The Late Pleistocene elephant fossils have also been found on the Aegean islands, and Van der Geer et al. (2010) state that the Cyclades Islands probably formed one large island during the Late Pleistocene.

In Sicily and Malta, the early and middle Middle Pleistocene and the late Middle to early Late Pleistocene mammalian faunas are highly endemic, represented by a pygmy elephant. The latter is thought to have been formed in Sicily by new introductions of species from mainland Italy between 455 ± 90 ka (Bada et al. 1991) and 146.8 ± 28.7 ka (Rhodes 1996) in the late Middle Pleistocene. The Maltese fauna is more isolated than that of Sicily due to the small size of Malta compared to Sicily and the extremely restricted number of species that came to the island. The composition of the Maltese fauna is thought to have been unique and different from that of the Sicilian fauna, even in the same period. Sicily may have been connected to the Italian Peninsula during the Late Pleistocene.

The Pleistocene fauna of Sardinia and Corsica consists of the Middle Pliocene to Early Pleistocene and the late Early Pleistocene to early Holocene faunas. Since the Middle Pleistocene, the fauna has been slightly different from the earlier ones, and the ancestor of the dwarf mammoth (*Mammuthus lamarmorae*) arrived on the island during the late Middle Pleistocene (Van der Geer et al. 2010).

This suggests that there was a major shift in the mammalian fauna of many of the Mediterranean islands at some time in the late Middle Pleistocene, with the arrival of new animals to the islands, although precise age values are not available.

Foxes and mammoths of the Channel Islands of California

The Channel Islands form a group of eight isles along the coast of southern California in the Pacific Ocean, from Los Angeles to San Diego, across the Santa Barbara Channel. The six isles of the Islands are home to a small gray fox called the Island fox (*Urocyon littoralis*), which is found only in this Islands.

The Channel Islands consist of the northern and southern groups. The northern group is separated from the mainland by the Santa Barbara Channel, which is approximately 20 km wide and 300 m deep. The group consists of four isles aligned in an east-west direction: Anagapa, Santa Cruz, Santa Rosa, and San Miguel. The south group consists of four isles, from east to west: Santa Catalina, San Clemente, Santa Barbara and San Nicolas (Fig. 7).

In the northern group of the Islands, 145 of the plant and animal species observed today are endemic. Santa Rosa is home to more than 100 species of land birds, three species of mammals (fox, skunk, and rat), two species of amphibians, three species of reptiles, seabirds and sea lions, and six species of plants found only on the isle (Web site of National Park Service Channel Islands). And fossils of dwarf mammoth (*Mammuthus exilis*) and Columbian mammoth (*M. columbi*) have been excavated on the isles of Santa Cruz, Santa Rosa, and San Miguel in the northern group (Agenbroad 1998).

The Island fox (*U. littoralis*) is similar to, but distinct from, the Gray fox (*U. cinereoargenteus*), which is distributed from USA to Colombia, and is divided into different subspecies on each of the six isles where it occurs (Animal Diversity Web Univ.



Fig. 7 Bathymetric chart around the Channel Islands of California showing the distribution of insular fox and mammoth. Thin dotted line is shown depth of 100 m. The seafloor shallower than depth of 1,000 m shows the land area in the late Middle Pleistocene. The seafloor topography is based on NOAA bathymetric data.

Michigan Mus. Zoology). In other words, *U. littoralis santacruzae* inhabits on Santa Cruz, *U. l. santarosae* on Santa Rosa, and *U. l. littoralis* on San Miguel in the northern group, and *U. l. catalinae* on Santa Catalina, *U. l. clementae* on San Clemente, and *U. l. dickeyi* on San Nicolas in the southern group. No Island fox inhabits in the two remaining isles of the Islands: Anagapa and Santa Barbara. The reason for this is that these isles are so small compared to the isles where the foxes live that they could not live there due to lack of food.

The Late Pleistocene to Holocene fossil fauna of the northern group consists of dwarf mammoth (*Mammuthus exilis*), the Is-

land fox (*U. littoalis*), a sea otter (*Enhydra lutris*), a large deer mouse (*Peromyscus nesodytes*) and a small deer mouse (*P. an-yapahensis*). Apart from the dwarf mammoth, a mainland American mammoth (*M. columbi*) also occurs, and a single proboscidean tooth have been recovered from San Nicolas in the southern group (Van der Geer et al., 2010).

As to how the Island fox and the dwarf mammoth came to inhabit the Channel Islands, there are theories that the Island fox was transported as a pet by native Americans (Collins, 1991) and that the mammoth swam across (Johnson, 1978).

Wolves of the Falkland Islands

The Falkland Islands are located in the South Atlantic Ocean, 500 km from Patagonia, Argentina, and consists of two large islands, the East Falkland and the West Falkland, and 776 isles (Fig. 8). The Falkland Islands are cold and mostly barren, but the flat land of the East Falkland Island has been turned into sheep pastures by the British colonists. On these cold, isolated islands, there were wolves.

The Falkland wolf (*Dusicyon australis*) of the Falkland Islands was alive when Charles Darwin visited there in 1834 on the Beagle, and is mentioned in Darwin's *The Voyage of the Beagle* (Darwin, 1956). The Falkland wolf fed on birds such as geese and penguins and on marine animals such as seals that inhabited the islands. Phylogenetically, the Falkland wolf is closely relat-

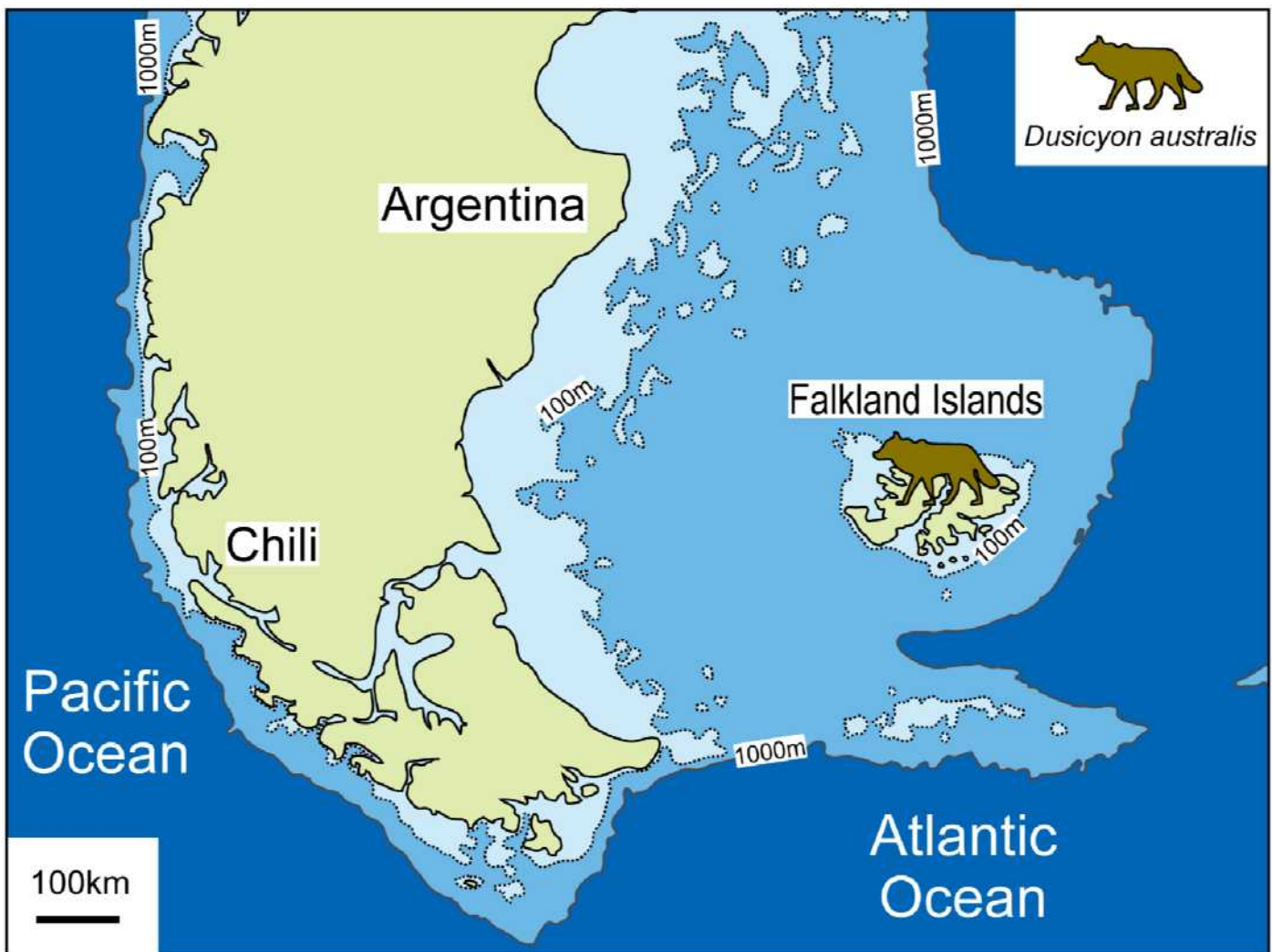


Fig. 8 Bathymetric chart around the Falkland Islands showing the distribution of insular wolf. Thin dotted line is shown depth of 100 m. The seafloor shallower than depth of 1,000 m shows the land area in the late Middle Pleistocene. The seafloor topography is based on NOAA bathymetric data.

ed to the South American fossil species *D. avus* (Van der Geer et al., 2010).

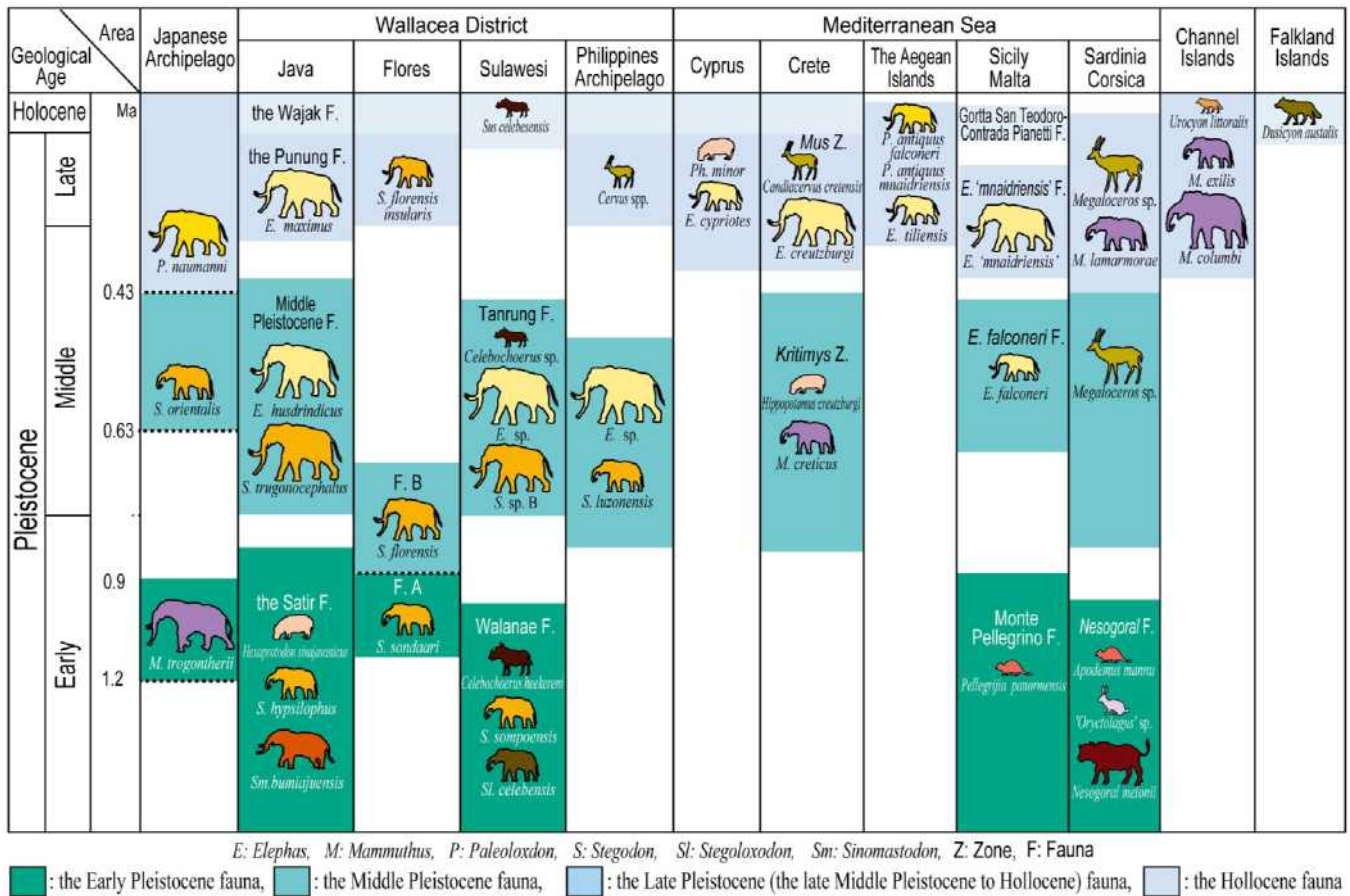


Fig. 9 Stratigraphic distribution of the insular mammalian faunas in each island of the world.

Distribution of endemic faunas on the islands and land bridges in the late Middle Pleistocene

In this paper, we have reviewed mainly the distribution and evolution of the endemic mammalian faunas of the world's islands, especially since the Pleistocene. The mammals that inhabited the world's islands since the Late Pleistocene, have been endemic to each island. Fig. 9 shows the stratigraphic distribution of the insular mammalian faunas in each island of the world.

Honshu region of the Japanese Archipelago

In the Honshu region of the Japanese Archipelago, Konishi and Yoshikawa (1999) and Kawamura (2014) have shown from proboscidean fossils that the *Paleoloxodon naumanni* was introduced from northern China via the Korean Peninsula 430 ka. This suggests that the most recent arrival of the fauna leading to the present occurred 430 ka, when the ancestors of the *P. naumanni* arrived in the late Middle Pleistocene. If the sea level 430 ka was 1,000 m lower than the present level, as described by Shiba (2017a, 2017b), the land bridge connecting the continent and the Japanese Archipelago would be as shown by the 1,000 m depth contour in Fig. 1. The land bridge in the late Middle Pleistocene was submerged due to the gradual rise of sea level, and the Honshu region was separated from the continent by the sea, and trapped animals evolved into endemic species.

The Ryukyu Islands

In the Ryukyu Islands, Hikita's interregional comparison (Hikita, 2002) of terrestrial herpetofauna showed that the land bridge initially extended from the continent through Taiwan to the Tokara Gap, but later in the Pleistocene it was divided by the Kerama Gap, and the Okinawa/Amami Islands were not connected to the continent and the Yaeyama/Miyako Islands. In the Ryukyu Islands, following the contour line at a depth of 1,000 m, the Okinawa/Amami Islands and the Taiwan/Yaeyama Islands are separated by the Kerama Gap, which well explains the Pleistocene Taiwan/Yaeyama Islands land bridge and the existence of the Okinawa/Amami Islands paleo-land shown by Hikita (2002) (See Fig. 2).

The Wallacea District

The Early Pleistocene, the Middle Pleistocene and the Late Pleistocene faunas are unique to Java, Flores, Sulawesi and the Philippine Archipelago in the Wallacea District. The last of these faunal transformations is thought to have occurred in the late Middle Pleistocene.

Audley-Charles (1981) proposed that the Banggai and Sula Islands, Seram, and Buru around Sulawesi were exposed as a vast land area (Stegoland) in the Late Pleistocene or earlier, and that the western part of Sulawesi was intermittently connected to Borneo through the partially exposed the Makassar Strait. In contrast, Van der Geer et al. (2010) argued that the sea around Sulawesi is a 1,000 m deep strait, making such a sea level drop unlikely. However, if the seafloor at depths of 1,000 m or less was once land, then Sulawesi would be connected to Borneo from the Sula Islands. Furthermore, Flores and the Philippines are also land-locked from the continent, which explains the distribution of endemic terrestrial animals on these islands (See Fig. 3).

Islands of the Mediterranean Sea

Islands of the Mediterranean Sea, i.e., Cyprus, Crete, the Aegean islands, Sicily and Malta, Sardinia and Corsica, have endemic faunas from the late Middle Pleistocene to Late Pleistocene Period, and their formation and conversion from earlier faunas are considered to be the late Middle Pleistocene. Fig. 5 shows the Mediterranean Sea at depths of 1,000 m or more in the sea and shallower depths on the land. If we assume that in the late Middle Pleistocene, the area shallower than the present depth of 1,000 m was a continental land area, new fauna migrated from the continent to these islands, which then became isolated from the continent and formed their own unique fauna.

The seafloor between the Italian Peninsula and Tunisia in Africa is shallower than 1,000 m deep and stretches from north to south, dividing the Mediterranean Sea into east and west. If this seafloor was once land, it would explain the analogous relationship with the African fauna in the Pleistocene fauna of Sicily shown by Dubey et al. (2007).

The Channel Islands and the Falkland Islands

In the Channel Islands, if we follow the 1,000 m depth isobath from California to the Channel Islands on the west coast of the Americas, all eight islands of the Channel Islands are a land area extending from California. If the seafloor shallower than today's depth of 1,000 m were once land, there would have been a vast land area along the present California coast (See Fig. 7). Probably in the late Middle Pleistocene, the common ancestor of the Gray fox and Island fox of present-day California may have lived in the natural environment of the west coast of the Americas, which is vastly larger than it is today.

The Falkland Islands are a contiguous land area from South America when divided by the 1,000 m depth contour line (See Fig. 8). In other words, if we assume that the sea level was 1,000 m lower than the present at some point in the past, the islands were part of the South American continent and was isolated by the subsequent rise in sea level, so that the Falkland wolf survived as an endemic species on the islands, feeding on marine animals.

Land bridges and terrestrial animal migration in the late Middle Pleistocene

The late Middle Pleistocene to Late Pleistocene faunas in the Honshu region of the Japanese Archipelago, the islands of the Wallacea District, the Mediterranean Sea, and the Channel Islands described in this paper can be considered to have been formed and converted from earlier faunas during the late Middle Pleistocene. This suggests that mainland animals migrated due to the connection between the islands and the continent caused by the expansion of the land area in the late Middle Pleistocene. It is also possible that this was the same time that the fauna of the late Middle Pleistocene was formed in the Honshu region of the Japanese Archipelago.

All islands with endemic fauna since the late Middle Pleistocene shown in this paper are connected to the nearest continent only at isobaths of 1,000 m or more. Assuming that the coastline existed at the present-day depth of 1,000 m the late Middle Pleistocene, the islands described in this paper would all be a part of the adjacent continent. In other words, the sea level in the late Middle Pleistocene was 1,000 m lower than the present, and the subsequent sea level rise is thought to have led to the formation of endemic faunas on islands separated from the continent by the sea since the late Middle Pleistocene.

The migration of terrestrial animals to ocean islands has been explained by Van der Geer et al. (2010) and many other researchers, especially biologists, by the swimming ability of elephants and deer and the dispersal of sweepstakes (Simpson, 1965) by natural rafts (Matthew, 1918). Sweepstake means horse races, lotteries, etc., with little chance of success due to the danger of crossing oceans, but great success if done well (Simpson, 1984).

However, in addition to elephants and deer, many other species are endemic to the islands, including grassland rodents and arboreal monkeys. In addition, the migration of terrestrial animals is limited to one-way traffic from continents to islands. The stratigraphic distribution of the faunas of the world's islands suggests that new faunas were formed in many islands almost since the late Middle Pleistocene (See Fig. 9). These results suggest that the migration of terrestrial animals to islands is mainly due to the expansion of their habitats, and that the formation or transformation of island fauna is not due to the accidental migration of animals across the sea.

Even if a few elephants or deer were to cross an island by chance, as in the case of the Sweepstake dispersal, it is unlikely that they would be able to reproduce and continue to live there. I also believe that if such coincidental events occur frequently

enough to allow animal exchange between islands and continents, then island endemism will not form.

Van der Geer et al. (2010) found that the fauna of the islands was characterized by imbalance and poverty, which had a strong filtering effect on migration to the islands. However, this may be due in part to the short time that land bridges have been able to cross to the island and the limited natural environment of these bridges. Furthermore, as the area of the island shrank due to isolation, the number of species that could adapt to changes in the natural environment was limited, and the composition of new niches may have caused the formation of endemic species within the island. In other words, the ancestors of the endemic species on the islands did not migrate by chance with their swimming ability or ability to ride on rafts with a rare chance of winning the lottery, but migrated within the same habitat of the continents and islands that were once connected by land.

It may be difficult to believe that the sea level has risen by almost 1,000 m since the late Middle Pleistocene. However, as mentioned by Shiba (2017a, 2017b), the formation of the Pleistocene around Suruga Bay involved uplift of the seafloor and sea level rise as well as land, and the formation of Suruga Bay and the continental slope (Inouchi et al. 1978) also occurred during this period. As for the sea level rise of 1,000 m during the Pleistocene, Hoshino (1975a, 1983) has already made a pioneering study that the sea level was 1,000 m lower during the Villafranchian period, and then rose by 1,000 m due to the Sicilian sea level rise based on the flat surface of the continental slope and the deltaic deposits distributed there. Hoshino (1962, 1975b, 1998) argued that the sea level at the latest Miocene was 2,000 m lower than the present level, and has since risen to the present level, because the terminal depth of the world's submarine valleys is at a depth of 2,000 m everywhere, and the youngest strata that make up the valley floor are the latest Miocene. Hoshino (1978) also attributes the distribution of Messinian evaporites on the seafloor at a depth of 2,000 m in the Mediterranean Sea (Hsü et al., 1977) to the 2,000 m lower sea level at the latest Miocene, and suggested that the sea level rose in stages with the uplift of the earth's crust.

If the sea level rises by 1,000 m in 430,000 years, the average rise in sea level will be 2.33 mm/year. If the sea level were to rise at such a rate, it would rise by 2.33 m in 1,000 years, and we would expect the land area to rise by the same amount or more. The rise of sea level is caused by the uplift of the ocean floor, ocean ridges, ocean rise, etc., or by volcanic activity on the sea floor, which raises the sea floor and pushes up the seawater above it (Hoshino, 1983, 1991, 1992). The cause is thought to be the large-scale uplift movement of the crust caused by the uplift of tholeiitic basaltic magmas from the upper mantle and their intrusive into the crust, as described by Hoshino (1998, 2014). Such crustal uplift was not confined to the sea floor, but was more pronounced on land, and land remained land because the uplift on land was greater than that on the sea floor.

The sea level in a region is the amount of crustal uplift in that region minus the amount of sea level rise. A positive value indicates uplift in relation to sea level, while a negative value indicates subsidence (submergence). In other words, the islands with endemic species since the late Middle Pleistocene are the areas of relative subsidence because they did not rise as much as land areas during the 1,000 m rise in sea level. The animals that inhabited these islands are not only valuable relics that evolved and survived while adapting to their isolated environment, but also are thought to be important in conveying the evolution of life and the history of the Earth.

Acknowledgments: In compiling this paper, I would like to thank the late Dr. Michihei Hoshino, who was a professor emeritus of Tokai University and had conducted pioneering research on the relationship between sea level rise and biological distribution, for guiding the author's research and interest in biogeography. In addition, I would like to thank the two reviewers who gave me appropriate advice to improve this paper.

References

- Agenbroad, L.D. (1998) Pygmy (Dwarf) Mammoths of the Channel Islands of California. *Mammoth Site of Hot Spring, SD, Inc.*, Hot Spring, SD, 27p.
- Aiba, J. and Sekiya, E. (1979) Distribution and characteristics of the Neogene sedimentary basins around the Nansei-Shoto (Ryukyu Islands). *Jour. Jap. Assoc. Petrol. Technol.*, 44, 90-103. (in Japanese with English abstract)
- Animal Diversity Web University of Michigan Museum of Zoology http://animaldiversity.org/accounts/Urocyon_littoralis/
- Audley-Charles, M.G. (1981) Geological history of the region of Wallace's line. In: Whitmore, T.C. (ed). *Wallace's Line and Plate Tectonics*, Gloucestershire, *Claredon Press*, 24-35.
- Bada J.L., Beloluomini, G., Bonfigglio L., Branca, M., Burgio, E. and Delitala, L. (1991) Isoleucine epimerization ages of Quaternary Mammals of Sicily. II *Quaternario*, 4, 5-11.
- Bertoldi R., Rio D. and Thunell, R. (1989) Pliocene-Pleistocene vegetational and climatic evolution of the southern-central Mediterranean. *Palaeogeography, Palaeoclimatology, Palaeoecology*, 72, 263-275.
- Brown, P., Sutikna, T., Morwood, M.J., Soejono, R.P., Saptomo, E.W. and Awe, D.R. (2004) A new small-bodied hominin from the Late Pleistocene of Flores, Indonesia. *Nature*, 431, 1055-1061.

- Collins, P.W. (1991) Interaction between island foxes (*Urocyon littoralis*) and native Americans on islands off the coast of southern California: II. Ethnographic, Archeological, and Historical Evidence. *Ethnobiol*, 11, 205-229.
- Croft, D.A., Heaney, L.R., Flynn, J.J. and Bautista, A. (2006) Fossil remains of a new, diminutive *Bubalus* (Artiodactyla: Bovidae: Bovini) from Cebu Island, Philippines. *Jour. Mammology*, 87, 1037-1051.
- Daams, R. and De Bruijn, H. (1995) A classification of the Gliridae (Rodentia) on the basis of dental morphology. *Hystrix*, 6 (1-2), 3-5.
- Darwin, C. (1956) The Voyage of the Beagle. v. I, Uchiyama, K. translated, *Shinchyo-shya*, Tokyo, 363p. (in Japanese)
- Dermitzakis, M.D. and Sondaar, P.Y. (1978) The importance of fossil mammals in reconstruction paleogeography with special reference to the Pleistocene Aegean Archipelago. *Annales Géologiques des Pays Helléniques*, 46, 808-840.
- Dermitzakis, M.D. and De Vos, J. (1987) Faunal succession and the evolution of mammals in Crete during the Pleistocene. *Neues Jahrbuch Geologische und Paläontologische Abhandlungen*, 173, 377-408.
- De Vos, J., Sartono, S., Hardja-Sasmita, H.S. and Sondaar, P.Y. (1982) The fauna from Trinil, type locality of *Homo erectus*; a reinterpretation. *Geologie en mijnbouw*, 61, 207-211.
- Dubey, S., Koyassua, K., Parapanoca, R., Ribic, M., Hutterere, R. and Vogela, P. (2007) Molecular phylogenetic reveals Messinian Pliocene, and Pleistocene colonization of islands by North Africa shrews. *Molecular Phylogenetics and Evolution*, 47, 877-882.
- Hikita, T. (2002) Evolution of Reptiles. *Tokyo Univ. Press*, Tokyo, 234p. (in Japanese)
- Hoshino, M. (1962) The Pacific Ocean. *Assoc. Geol. Collab. Japan*, Tokyo, 136p. (In Japanese)
- Hoshino, M. (1975a) Three transgression during the Quaternary orogenic period. *Chikyu-Kagaku (Earth Science)*, 29, 92-99. (in Japanese with English abstract)
- Hoshino, M. (1975b) Eustasy in Relation to Orogenic Stage, *Tokai Univ. Press*, Tokyo, 397p.
- Hoshino, M. (1978) Was there the high Gibraltar sill in the Messinian stage? *La mer*, 16, 111-123.
- Hoshino, M. (1983) Marine Geology. *Accoc. Geol. Collab. Japan*, Tokyo, 373 p. (in Japanese)
- Hoshino, M. (1991) The Basaltic Stage - Basic Concepts of Geological Science. *Tokai Univ. Press*, Tokyo, 456 p. (in Japanese with English abstract)
- Hoshino, M. (1992) The Way the Poisonous Snakes Came. *Tokai Univ. Press*, Tokyo, 150 p. (in Japanese)
- Hoshino, M. (1998) The Expanding Earth, Evidence, Causes and Effects. *E. G. Service Press*, Sapporo, 295p.
- Hoshino, M. (2014) The History of Micro-Expanding Earth - History of the Earth from viewpoint of Sea level Rise - . *E. G. Service Press*, Sapporo, 234p.
- Hsü K.J., Moutadertet, L., Bernoulli, D., Cita, M.B., Erickson, A., Carrison, R.E., Kide, R.B., Meliers, F. Muller, C. and Wright, R. (1977) History of the Mediterranean salinity crisis. *Nature*, 267. 399-403.
- Huxley, T. (1868) On the classification and distribution of the Allectormorphae and Heteromorphae. *Proc. Zool. Society London*, 294-319.
- Inouchi, Y., Okuda, Y. and Yoshida, F. (1978) On the age of formation of upper continental slope configuration in the south of the Kii Straits. *Jap. Jour. Geol.*, 84, 91-93. (in Japanese)
- Johnson, D.L. (1978) The origin of Island mammoths and the quaternary land bridge history of the Northern Channel Islands, California. *Quaternary Research*, 10, 204-225.
- Kamei, T., Taruno, H. and Kawamura, Y. (1988) Implication of Mammal Fauna for the Quaternary Geohistory of the Japanese Islands. *The Quaternary Research*, 26, 293-303. (in Japanese with English abstract)
- Kawamura, Y. (1998) Immigration of Mammals into the Japanese Islands during the Quaternary. *The Quaternary Research*, 37, 251-257. (in Japanese with English abstract)
- Kawamura, Y. (2014) Research on Quaternary mammal faunas in Japanese and adjacent East Asians: A review of my research. *The Quaternary Research*, 53, 119-142. (in Japanese with English abstract)
- Kawamura, Y., Kamei, T. and Taruno, H. (1989) Middle and Late Pleistocene Mammalian Faunas in Japan. *The Quaternary Research*, 28, 317-326. (in Japanese with English abstract)

- Konishi, S. and Yoshikawa, S. (1999) Immigration times of the two proboscidean species, *Stegodon orientalis* and *Paleoloxodon naumanni*, into the Japanese Islands and the formation of land bridge. *Chikyu-Kagaku (Earth Science)*, 53, 125-134. (in Japanese with English abstract)
- Matthews, W.D. (1918) Affinities and origin of the Antillean mammals. *Bull. Geol. Soc. America*, 29, 657-666.
- Mol, D., De Vos, J., Van den Bergh, G.D. and Sondaar, P.Y. (1996) The taxonomy and ancestry of the fossil elephants of Crete. Faunal turnover and comparison with proboscideans faunas of Indonesian islands. In Reese D.S. (ed). Pleistocene and Holocene Fauna of Crete and its First Settlers. Monographs in World Archaeology, 28, *Prehistory Press*, Madison, Wisconsin, 1-32.
- Morwood, M.J., O'Sullivan, P.B., Aziz, F. and Raza, A. (1998) Fission-Track ages of stone tools on the east Indonesian Island of Flores. *Nature*, 392, 173-176.
- Nishimura, S., Otofujii, Y., Ikeda T., Abe, E., Yokoyama, T., Kobayashi, Y., Hadiwisatra, S., Sopohaluwaken, J. and Hehuwat, F. (1981) Physical geology of the Sumba, Sumbawa and Flores Islands. In: Barber, A.J. and Wiryosujono, S. (eds). The Geology and Tectonics of Eastern Indonesia. *Geological Research Development Center Bandung*, Special Publication, 2, 105-113.
- NOAA bathymetry data: <https://maps.ngdc.noaa.gov/viewers/bathymetry/>
- Rhodes, E.J. (1996) ESR dating of tooth enamel. In: Basile B. and Chilardi S. (eds). Le ossa dei Giganti. Lo scavo paleontologico di Contrada Fusco, *Arnaldo Lombardi*, Siracusa, 39-44.
- Saegusa, H. (2005) Current issues on the systematics of Japanese fossil proboscideans. *Jour. Fossil Research*, 38, 78-89. (in Japanese with English abstract)
- Shiba, M. (2017a) Formation of Suruga Bay – Large-scale uplift and sea level rise -. *Tokai Univ. Press*, Hiratsuka, 406p. (in Japanese)
- Shiba, M. (2017b) Geology of the island arcs in the northwestern margin of the Pacific Ocean and their formation by a large-scale uplift and sea level rise - the formation of Suruga Bay. *New Concepts in Global Tectonics Journal*, 5, 532-548.
- Shiba, M. (2020) Distribution of island endemic animals and sea level rise of 1,000 m since the late Middle Pleistocene. *Jour. Fossil Research*, 53, 1-17. (in Japanese with English abstract)
- Shiba, M. (2021) Characteristics of crustal uplift since the Pliocene in central Honshu, Japan, and sea level rise. *Earth Science (Chikyu Kagaku)*, 75, 37-55. (in Japanese with English abstract)
- Simpson, G.G. (1965) The Geography of Evolution. *Capricorn Book*, New York, 249p.
- Simpson, G.G. (1984) Fossils and the History of Life. *Scientific American Books Inc.*, New York, 239p.
- Sondaar, P.Y. (1984) Faunal evolution and the mammalian biostratigraphy of Java. *Courier Forschungsinstitut Senckenberg*, 69, 210-235.
- Sondaar, P.Y., De Vos, J. and Dermitzakis, M.D. (1986) Late Cenozoic faunal evolution and Palaeogeography of the South Aegean Island arc. *Modern Geology*, 10, 249-259.
- Suc, J.P., Bertini, A., Combourieau-Nebout, N., Diniz, F., Russo-Ermolli, E., Zeheng, Z., Bessais, E. and Ferrier, J. (1995) Structure of West Mediterranean vegetation and climate since 5.3 Ma. *Acta Zoologica Cracoviensia*, 38, 3-16.
- Symeonidis, N., Bachmeyer, E. and Zapfe, H. (1973) Entdeckung von Zwergelafanten auf der Insel Rhodos (Ausgrabungen 1973). *Annalen des Naturhistorischen Museums in Wien*, 78, 193-202.
- Theodorou, G.E., Roussiakis, S.I., Athanassiou, A., Giaourtsakis, Z.I. and Panayides, I. (2007) A Late Pleistocene endemic genet (Carnivora, Viverridae) from Aghia Napa, Cyprus. Proceedings of the 11th International Congress, Athens, May, 2007. *Bull. Geol. Soc. Greece*, 40, 201-208.
- Van den Bergh, G.D. (1999) The Late Neogene elephantoid-bearing faunas of Indonesia and their palaeozoogeographic implications; a Java, including evidence for early hominid dispersal east of Wallace's line. *Scripta Geologica*, 117, 1-419.
- Van den Bergh, G.D., De Vos, J. and Sondaar, P.Y. (2001) The late quaternary palaeogeography of mammal evolution in Indonesian Archipelago. *Palaeontology, Palaeoclimatology, Palaeoecology*, 171, 385-408.
- Van den Bergh, G.D., Rokus, A.D., Morwood, M. J., Sutikna, T., Jatmiko, P. and Wahyu, S.E, (2008) The youngest *Stegodon* remains in south-east Asia from the Late Pleistocene archaeological site Liang Bua, Flores, Indonesia. *Quaternary International*, 181, 16-48.

Space weather and geomagnetic activity related to Ecuadorean M7.5 earthquake recorded on February 22, 2019

Gabriele Cataldi¹, Daniele Cataldi¹⁻², Valentino Straser³

- (1) Radio Emissions Project (I). ltpaobserverproject@gmail.com
 (2) Fondazione Permanente G. Giuliani - Onlus (I). danielle77c@hotmail.it
 (3) Department of Science and Environment UPKL Brussel (B). valentino.straser@gmail.com

Abstract

On February 22, 2019 at 10:17:23 UTC, an M7.5 earthquake was recorded in Ecuador. The authors, by monitoring in real time solar activity and terrestrial geomagnetic activity, identified a solar wind proton density increase and an increase in terrestrial geomagnetic activity that preceded the Ecuadorian seismic event of 72 hours (respect to solar wind ionic flux) and 48 hours (respect to geomagnetic perturbation). This type of correlation was first observed by the authors in 2011. To date, all destructive seismic events that are recorded on a global scale are always preceded by a solar wind proton density increase.

Keywords: proton density increase, seismic precursors, solar activity, geomagnetic activity, seismic prevision.

Introduction

Since the late 1800s, many studies have been conducted on the so-called seismic precursors of the electromagnetic type and much evidence has been collected (both from the ground and from space) on the existence of these natural radio emissions. Despite this, among researchers, there are still those who even claim that electromagnetic seismic precursors do not exist or that it is not worth spending economic and intellectual resources on a class of electromagnetic phenomena that will not produce any advancement in research. The authors of this work, on the other hand, think, because they have demonstrated it, that scientific research on

pre-seismic radiofrequency will represent the methodological substrate on which a new seismic forecasting methodology will be built, capable of freeing itself from historical seismometric data; but provided that the electromagnetic monitoring will also be accompanied by the monitoring of solar activity [19] [23].

There is no longer any doubt that there is a close correlation between solar activity and global seismic activity [1] [4] [5] [6] [7] [8] [9] [10] [11] [12] [13] [14] [15] [16] [17] [18] [19] [20] [21] [22] [23]. The first studies that investigated this type of correlation were conducted between 1960 and 1970 but only in recent years, thanks to the work carried out by the authors, it was possible to understand that all potentially destructive seismic activity is always preceded by an increase the density of the solar ion flux. This work will present the results of a study conducted on the Ecuadorian M7.5 earthquake recorded On February 22, 2019 at 10:17:23 UTC (**Fig. 1**).

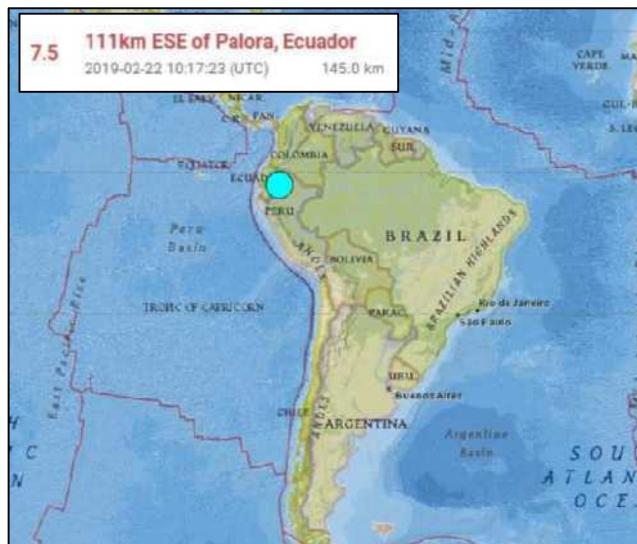


Fig. 1 – Seismic epicenter of the Ecuadorean M7.5 earthquake recorded on February 22, 2019. The map above shows the seismic epicenter of the Ecuadorean M7.5 earthquake recorded on February 22, 2019. Credits: USGS, Radio Emissions Project.

Data analysis

Between February 19, 2019 at 10:00 UTC and February 23, 2019 at 24:00 UTC, the DSCOVR Satellite (located in Lagrangian orbit L1) detected a solar wind proton density increase whose maximum peak was recorded on February 20, 2019 at 20:02 UTC (**Fig. 2**). 72 hours after the start of the proton increase (and 38 hours after the maximum peak) the Ecuadorean M7.5 earthquake was recorded. (**Fig. 2**).

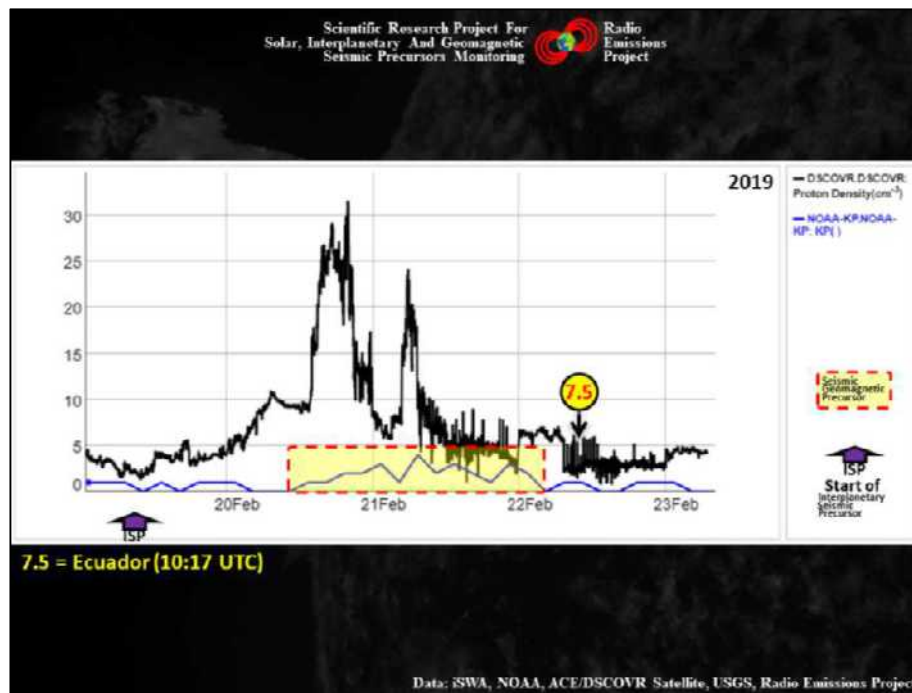


Fig. 2 – Variation in solar ion flux and Earth's geomagnetic activity related to the M7.5 Ecuadorian earthquake recorded on February 22, 2019. The graph above shows the time marker of the Ecuadorian M6.7 earthquake recorded on February 22, 2019 at 10:17 UTC (black vertical arrow). Analyzing the data in the graph it is evident that the Ecuadorian earthquake was preceded by a solar wind proton density increase (Interplanetary Seismic Precursor; black curve) and by an increase of Kp Index (Seismic Geomagnetic Precursor; blue curve highlighted by the yellow area). The purple arrow indicates the start of solar wind proton density increase. Credits: iSWA, USGS, Radio Emissions Project.

The graph visible in **Fig. 2** condenses the data relating to solar wind proton density increase and those on Earth's geomagnetic activity. From the integration of the data, it is evident that the proton increase has generated a geomagnetic perturbation: phenomena of an electromagnetic nature that preceded the Ecuadorian seismic event. Geomagnetic activity reached its maximum value on February 21, 2019 at 07:30 UTC: Kp Index = 4 (**Fig. 3**).

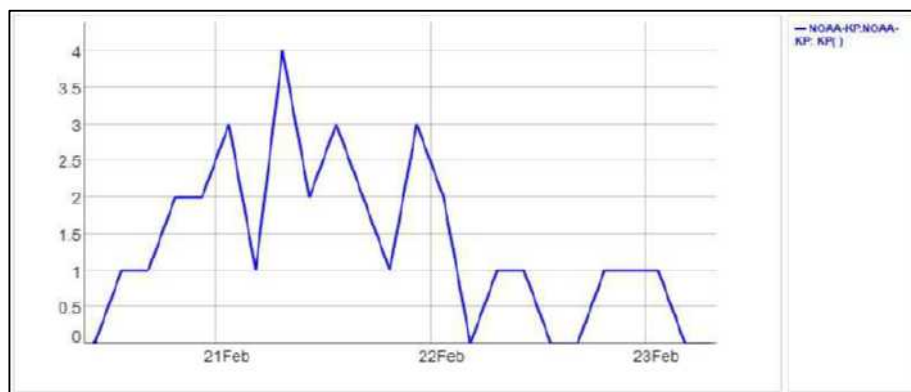


Fig. 3 – Earth's geomagnetic activity related to M7.5 Ecuadorian earthquake recorded on February 22, 2019. The graph above shows the modulation of Kp Index in the hours preceding the Ecuadorian earthquake recorded on February 22, 2019 at 10:17 UTC. Credits: iSWA, USGS, Radio Emissions Project.

Confirmations on the correlation between Earth's geomagnetic activity and M6+ global seismic activity have been obtained by the authors in many cases: [2] [3] [5] [10] [12] [14] [17] [19] [23]. Since the intensity of the geomagnetic variation depends substantially on the density and the velocity of the solar ion flux reaching the Earth's magnetosphere, not always the potentially destructive seismic activity is correlated to geomagnetic storms of class G1-G5: the authors observed that also increases more modest of Kp Index may be related to the M6+ seismic activity, just like in the case of the Ecuadorian M7.5 earthquake. (**Fig. 2** and **4**)

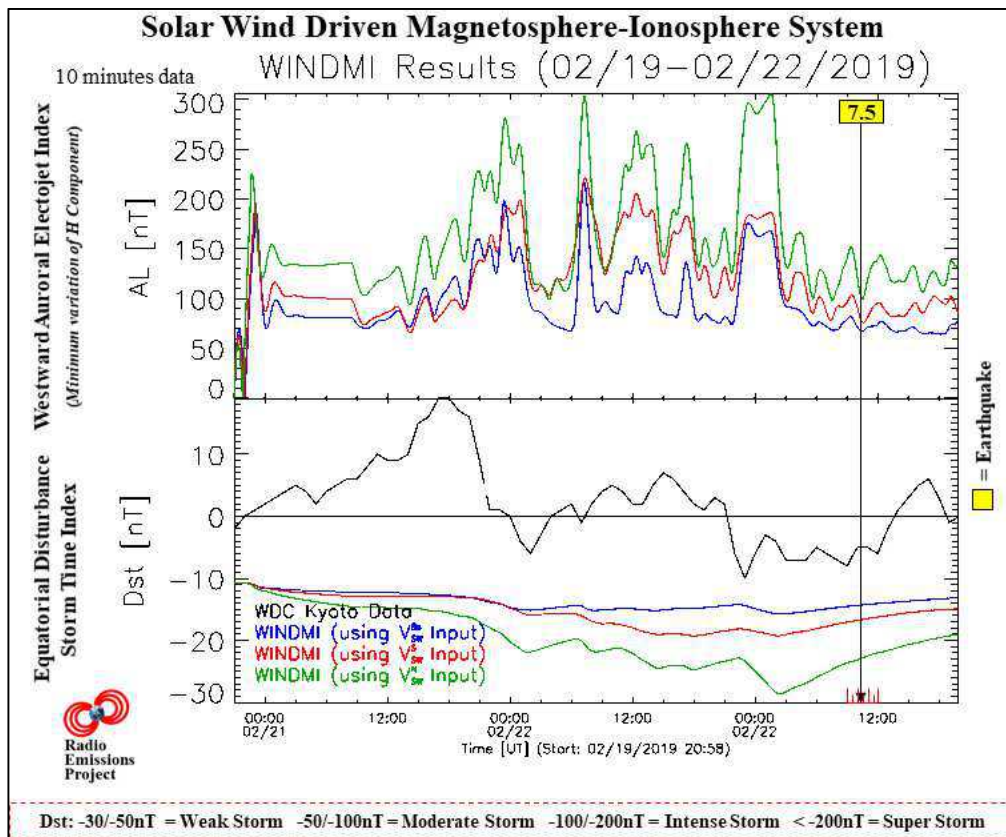


Fig. 4 – Low-dimensional model of the energy transfer from the solar wind through the magnetosphere and into the ionosphere (WINDMI). The picture shows the variation of the AL-Index (at top) and the DST-Index (at bottom) in the hours that preceded the Ecuadorean M6.7 earthquake recorded on February 22, 2019 (the time marker of the earthquake is indicated by a vertical black line). The DST-Index is a direct measure of the Earth’s geomagnetic horizontal (H) component variation due to the equatorial ring current, while the AL-Index (Auroral Lower) is at all times, the minimum value of the variation of the geomagnetic H component of the geomagnetic field recorded by observers of reference and provides a quantitative measure of global Westward Auroral Electrojet (WEJ) produced by increased of ionospheric currents therein present. Model developed by the Institute for Fusion Studies, Department of Physics, University of Texas at Austin. Credits: iSWA, USGS, Radio Emissions Project.

The graph in **Fig. 4** confirms what has just been stated: a geomagnetic perturbation measured through the “H” component of the geomagnetic field (AL Index, which reached 300nT) preceded the Ecuadorian earthquake by about 48 hours, while the DST Index almost reached the degree of “weak geomagnetic storm” about 8 hours before the earthquake. The variations in the density of the ion flux of the interplanetary medium and the variations in the Earth’s geomagnetic field that precede potentially destructive earthquakes are phenomena of an electromagnetic nature that can be classified within the so-called “seismic precursors of the electromagnetic type” according to the classification developed by the authors in 2013 (**Fig. 5**) [1] [19] [23]. This classification is the result of years of solar activity and natural electromagnetic background monitoring, and currently represents the only electromagnetic model capable of supporting both the theory of microfractures (electromagnetic emission generated as a result of tectonic stress - piezoelectricity) [1] [23], and the correlations observed between seismic activity and space weather (geomagnetic radio emissions) [22]. According to this new classification, pre-seismic radio emissions can be divided into two main families:

1. “Local” seismic precursors.
2. “Non local” seismic precursors.

The first are represented by local electromagnetic emissions, generated in the earthquake preparation area following the accumulation of tectonic stress (through the phenomenon of piezoelectricity); while the latter are generated by solar electromagnetic activity, i.e. that visible on the photosphere, chromosphere and in the solar corona (solar flare, sunspots, coronal hole, coronal mass ejection or CME, magnetic loops) responsible for the increase in the speed and density of the solar ion flux [19] [23].

New classification of pre-seismic radio emissions

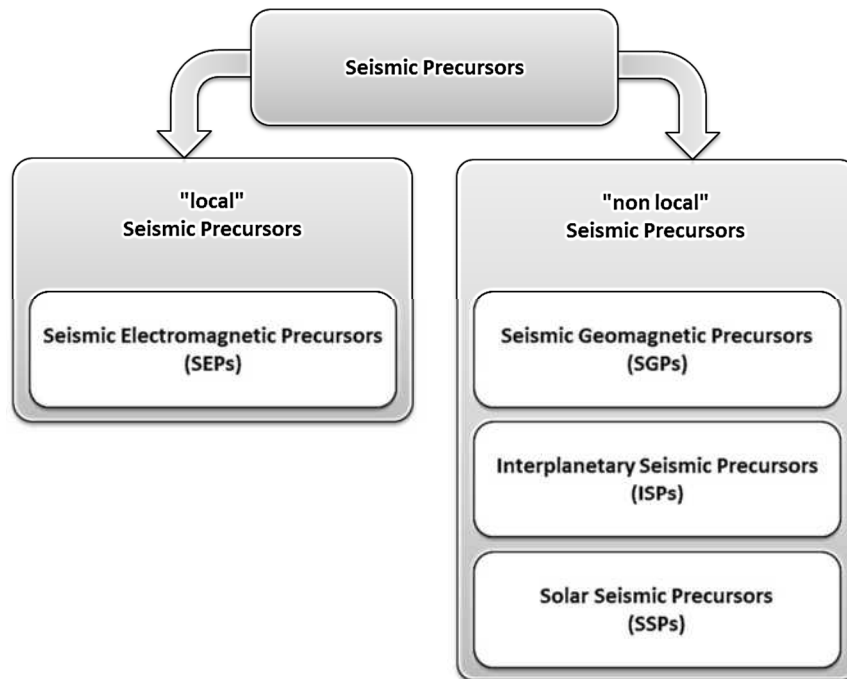


Fig. 5 – New classification of pre-seismic radio emissions. Above it is visible the new classification of pre-seismic radio emissions created by the authors following the studies conducted on environmental electromagnetic monitoring and on seismic activity monitoring starting from 2012. Credits: Radio Emissions Project.

Conclusions

The potentially destructive seismic activity is closely related to solar activity and, consequently, to the Earth's geomagnetic activity. This is the conclusion the authors came to after ten years of observing. What remains to be done is to expand the current electromagnetic monitoring network created by the authors (Radio Emissions Project network) and implemented with Radio Direction Finding (RDF) technology that allows to perform a crustal diagnosis thanks to the identification of pre-seismic radiofrequency through the triangulation technique. According to the authors, this is currently the best way forward for the scientific community to develop a better seismic forecasting method than the current one. [24-39].

Credits

- [1] G. Cataldi, D. Cataldi, V. Straser. (2013). Variations Of Terrestrial Geomagnetic Activity Correlated To M6+ Global Seismic Activity. EGU (European Geosciences Union) 2013, General Assembly, Seismology Section (SM3.1), Earthquake precursors, bio-anomalies prior to earthquakes and prediction, Geophysical Research Abstracts, Vol. 15. EGU2013-2617, Vienna, Austria. Harvard-Smithsonian Center for Astrophysics, High Energy Astrophysics Division, SAO/NASA Astrophysics Data System.
- [2] G. Cataldi, D. Cataldi and V. Straser. (2014). Earth's magnetic field anomalies that precede the M6+ global seismic activity. European Geosciences Union (EGU) General Assembly 2014, Geophysical Research Abstract, Vol. 16, EGU2014-1068, Vienna, Austria. Natural Hazard Section (NH4.3), Electromagnetic phenomena and connections with seismo-tectonic activity, Harvard-Smithsonian Center for Astrophysics, High Energy Astrophysics Division, SAO/NASA Astrophysics Data System.
- [3] D. Cataldi, G. Cataldi and V. Straser. (2014). Variations of the Electromagnetic field that preceded the Peruvian M7.0 earthquake occurred on September 25, 2013. European Geosciences Union (EGU) General

Assembly 2014, Geophysical Research Abstract, Vol. 16, EGU2014-1075, Natural Hazard Section (NH4.3), Electro-magnetic phenomena and connections with seismo-tectonic activity, Vienna, Austria. Harvard-Smithsonian Center for Astrophysics, High Energy Astrophysics Division, SAO/NASA Astrophysics Data System.

- [4] T. Rabeh, G. Cataldi, V. Straser. (2014). Possibility of coupling the magnetosphere–ionosphere during the time of earthquakes. European Geosciences Union (EGU) General Assembly 2014, Geophysical Research Abstract, Vol. 16, EGU2014-1067, Vienna, Austria. Natural Hazard Section (NH4.3), Electro-magnetic phenomena and connections with seismo-tectonic activity. Harvard-Smithsonian Center for Astrophysics, High Energy Astrophysics Division, SAO/NASA Astrophysics Data System.
- [5] V. Straser, G. Cataldi. (2014). Solar wind proton density increase and geomagnetic background anomalies before strong M6+ earthquakes. Space Research Institute of Moscow, Russian Academy of Sciences, MSS-14. 2014. Moscow, Russia. pp280-286.
- [6] V. Straser, G. Cataldi. (2015). Solar wind ionic variation associated with earthquakes greater than magnitude M6.0. *New Concepts in Global Tectonics Journal*, V. 3, No. 2, June 2015, Australia. P.140-154.
- [7] G. Cataldi, D. Cataldi, V. Straser. (2015). Solar wind proton density variations that preceded the M6+ earthquakes occurring on a global scale between 17 and 20 April 2014. European Geosciences Union (EGU) General Assembly 2015, Vienna, Austria. Natural Hazard Section (NH5.1), Sea & Ocean Hazard - Tsunami, Geophysical Research Abstract, Vol. 17, EGU2015-4157-2, Harvard-Smithsonian Center for Astrophysics, High Energy Astrophysics Division, SAO/NASA Astrophysics Data System.
- [8] G. Cataldi, D. Cataldi, V. Straser. (2015). Solar wind ion density variations that preceded the M6+ earthquakes occurring on a global scale between 3 and 15 September 2013. European Geosciences Union (EGU) General Assembly 2015, Geophysical Research Abstract, Vol. 17, EGU2015-4581, Vienna, Austria. Natural Hazard Section (NH5.1), Sea & Ocean Hazard - Tsunami, Harvard-Smithsonian Center for Astrophysics, High Energy Astrophysics Division, SAO/NASA Astrophysics Data System.
- [9] G. Cataldi, D. Cataldi, V. Straser. (2015). Solar wind proton density variations that preceded the M6,1 earthquake occurred in New Caledonia on November 10, 2014. European Geosciences Union (EGU) General Assembly 2015, Geophysical Research Abstract, Vol. 17, EGU2015-4167, Vienna, Austria. Natural Hazard Section (NH5.1), Sea & Ocean Hazard - Tsunami, Harvard-Smithsonian Center for Astrophysics, High Energy Astrophysics Division, SAO/NASA Astrophysics Data System.
- [10] V. Straser, G. Cataldi, D. Cataldi. (2015). Solar wind ionic and geomagnetic variations preceding the M8.3 Chile Earthquake. *New Concepts in Global Tectonics Journal*, V. 3, No. 3, September 2015, Australia. P.394-399.
- [11] G. Cataldi, D. Cataldi, V. Straser. (2016). Solar activity correlated to the M7.0 Japan earthquake occurred on April 15, 2016. *New Concepts in Global Tectonics Journal*, V. 4, No. 2, pp202-208, June 2016.
- [12] G. Cataldi, D. Cataldi, V. Straser. (2016). Tsunami related to solar and geomagnetic activity. European Geosciences Union (EGU) General Assembly 2016, Natural Hazard Section (NH5.6), Complex modeling of earthquake, landslide, and volcano tsunami sources. Geophysical Research Abstract, Vol. 18, EGU2016-9626, Vienna, Austria. Harvard-Smithsonian Center for Astrophysics, High Energy Astrophysics Division, SAO/NASA Astrophysics Data System.
- [13] G. Cataldi, D. Cataldi, V. Straser. (2017). SELF-VLF electromagnetic signals and solar wind proton density variations that preceded the M6.2 Central Italy earthquake on August 24, 2016. *International Journal of Modern Research in Electrical and Electronic Engineering*, Vol. 1, No. 1, 1-15. DOI: 10.20448/journal.526/2017.1.1/526.1.1.15. Harvard-Smithsonian Center for Astrophysics, High Energy Astrophysics Division, SAO/NASA Astrophysics Data System.

- [14] G. Cataldi, D. Cataldi, V. Straser. (2017). Solar and Geomagnetic Activity Variations Correlated to Italian M6+ Earthquakes Occurred in 2016. European Geosciences Union (EGU), General Assembly 2017. Geophysical Research Abstracts Vol. 19, EGU2017-3681, 2017. Seismology (SM1.2)/Natural Hazards (NH4.7)/Tectonics & Structural Geology (TS5.5) The 2016 Central Italy Seismic sequence: overview of data analyses and source models. Harvard-Smithsonian Center for Astrophysics, High Energy Astrophysics Division, SAO/NASA Astrophysics Data System.
- [15] G. Cataldi, D. Cataldi, V. Straser. (2017). Solar wind proton density increase that preceded Central Italy earthquakes occurred between 26 and 30 October 2016. European Geosciences Union (EGU), General Assembly 2017. Geophysical Research Abstracts Vol. 19, EGU2017-3774, 2017. Seismology (SM1.2)/Natural Hazards (NH4.7)/Tectonics & Structural Geology (TS5.5) The 2016 Central Italy Seismic sequence: overview of data analyses and source models. Harvard-Smithsonian Center for Astrophysics, High Energy Astrophysics Division, SAO/NASA Astrophysics Data System.
- [16] V. Straser, G. Cataldi, D. Cataldi. (2017). Solar and electromagnetic signal before Mexican Earthquake M8.1, September 2017. *New Concepts in Global Tectonics Journal*, V. 5, No. 4, December 2017. pp600-609.
- [17] G. Cataldi, D. Cataldi, V. Straser. (2017). Solar and Geomagnetic Activity Variations Correlated to Italian M6+ Earthquakes Occurred in 2016. EGU General Assembly 2017. EGU2017-3681, Vol. 19.
- [18] G. Cataldi, D. Cataldi, V. Straser. (2019). Solar wind ionic density variations related to M6+ global seismic activity between 2012 and 2018. European Geosciences Union (EGU) General Assembly 2019, Short-term Earthquake Forecast (StEF) and multi-parametric time-Dependent Assessment of Seismic Hazard (t-DASH) (NH4.3/AS4.62/EMRP2.40/ESSI1.7/Gi2.13/SM3.9), General Contribution on Earthquakes, Earth Structure, Seismology (SM1.1), Geophysical Research Abstract, Vol. 21, EGU2019-3067, 2019, Vienna, Austria. Harvard-Smithsonian Center for Astrophysics, High Energy Astrophysics Division, SAO/NASA Astrophysics Data System.
- [19] G. Cataldi. (2020). *Precursori Sismici – Monitoraggio Elettromagnetico*. Kindle-Amazon, ISBN: 9798664537970. ASIN Code: B08CPDBGX9.
- [20] G. Cataldi, D. Cataldi, V. Straser. (2019). Wolf Number Related To M6+ Global Seismic Activity. *New Concepts in Global Tectonics Journal*, Volume 7, Number 3, December 2019, pp. 178-186.
- [21] V. Straser, G. Cataldi, D. Cataldi. (2020). The Space Weather Related to the M7+ Seismic Activity Recorded on a Global Scale between 28 January and 25 March 2020. *Acta Scientific Agriculture* 4.12 (2020): 55-62.
- [22] G. Cataldi, V. Straser, D. Cataldi. (2020). Space Weather related to potentially destructive seismic activity recorded on a global scale. *New Concepts in Global Tectonics Journal*. Vol.8, No.3, pp.233-253, December 2020. ISSN 2202-0039.
- [23] G. Cataldi. (2021). *Radio Emissions Project – A new approach to seismic prediction*. Kindle-Amazon, ISBN: 9798709593411.
- [24] V. Straser, D. Cataldi, G. Cataldi. (2021). Radio Direction Finding, A New Method For The Investigation Of Preseismic Phenomena. The Case Of Japan. *International Journal Of Engineering Sciences & Research Technology (IJESRT)*. ISSN: 2277-9655, CODEN: IJESS7. 10(2): February, 2021, p.10-18. <https://doi.org/10.29121/ijesrt.v10.i2.2021>.
- [25] V. Straser, D. Cataldi, G. Cataldi, G. G. Giuliani. (2021). Pre-Seismic Signals Recorded By The Italian RDF Network Before The Occurrence Of Some Earthquakes In Northern Italy. *International Journal of Software & Hardware Research in Engineering (IJSHRE)*, ISSN-2347-4890, Volume 9, Issue 1, pp63-76. January 2021.

- [26] V. Straser, D. Cataldi, G. Cataldi, G. G. Giuliani, J. R. Wright. (2020). Effects Of Hurricane Laura On The New Madrid Fault Area - Results Of Electromagnetic Monitoring Through The RDF Network - Radio Direction Finding - And Arkansas Electromagnetic Monitoring Station. *New Concepts in Global Tectonics Journal*. Vol.8, No.3, pp.187-218, December 2020. ISSN 2202-0039.
- [27] D. Cataldi, V. Straser, G. Cataldi, G. G. Giuliani, Z. Z. Adibin. (2020). Registration of Pre-Seismic Radio Signals Related To The Russian And Jamaican Earthquakes With The RDF System Developed By The Radio Emissions Project. *International Advance Journal of Engineering Research (IAJER)*, Volume 3, Issue 9 (September – 2020), PP 01-30; ISSN 2360-819X.
- [28] T. Rabe, D. Cataldi, Z. Z. Adibin, G. Cataldi, V. Straser. (2020). International study Italy-Malaysia pre-seismic signals recorded by RDF – Radio Direction Finding monitoring network, before earthquakes: Mw 6.3, occurred at 111 km SW of Puerto Madero in Mexico and Mw 6.3, occurred at 267 km NW of Ozernovskiy in Russia, November 20, 2019. *New Concept in Geoplasma Tectonics*. Vol. 8, No. 2, pp.105-118. August 2020.
- [29] V. Straser, D. Cataldi, G. Cataldi. (2020). Radio Direction Finding (RDF) - Geomagnetic monitoring study of the Japanese area related to pre-seismic electromagnetic signals. *New Concepts in Geoplasma Tectonics Journal*. Vol. 8, No. 2, August 2020. pp119-141.
- [30] V. Straser, G. Cataldi, D. Cataldi. (2020). Radio direction finding for short-term crustal diagnosis and pre-seismic signals. The case of the Colonna earthquake, Rome (Italy). *European Journal of Advances in Engineering and Technology*, 2020, 7(7):46-59.
- [31] F. Di Stefano, G. Giuliani, D. Ouzounov, D. Cataldi, C. Fidani, A. D'Errico, G. Fioravanti. (2020). Support for preventions and preparedness of the strait of Messina-Reggio Calabria – An earthquake forecasting project. *Attidella Accademia Peloritana dei Pericolanti Classe di Scienze Fisiche, Matematiche e Naturali*. May 4, 2020.
- [32] D. Cataldi, G. G. Giuliani, V. Straser, G. Cataldi. (2020). Radio signals and changes of flow of Radon gas (Rn222) which led the seismic sequence and the earthquake of magnitude Mw 4.4 that has been recorded in central Italy (Balsorano, L'Aquila) on November 7, 2019. *An international journal for New Concepts in Geoplasma Tectonics*, Volume 8, Number 1, May 2020, pp. 32-42.
- [33] V. Straser, G. G. Giuliani, D. Cataldi, G. Cataldi. (2020). Multi-parametric investigation of pre-seismic origin phenomena through the use of RDF technology (Radio Direction Finding) and the monitoring of Radon gas stream (RN222). *An international journal for New Concepts in Geoplasma Tectonics*, Volume 8, Number 1, May 2020, pp. 11-27.
- [34] V. Straser, G. Cataldi, D. Cataldi. (2019). *Namazu's Tail – RDF: a new perspective for the study of seismic precursors of Japan*. Lulu Editore, 2019.
- [35] V. Straser, D. Cataldi, G. Cataldi. (2019). Electromagnetic monitoring of the New Madrid fault us area with the RDF system - Radio Direction Finding of the radio emissions project. *New Concepts in Global Tectonics Journal*, V7 N1, March 2019. pp43-62.
- [36] V. Straser, D. Cataldi, G. Cataldi. (2019). Radio Direction Finding (RDF) - Geomagnetic Monitoring Study of the Himalaya Area in Search of Pre-Seismic Electromagnetic Signals. *Asian Review of Environmental and Earth Sciences*, v. 6, n. 1, p. 16-27, 14 jun. 2019.
- [37] D. Cataldi, G. Cataldi, V. Straser. (2019). Radio Direction Finding (RDF) - Pre-seismic signals recorded before the earthquake in central Italy on 1/1/2019 west of (AQ). *European Geosciences Union (EGU) General Assembly 2019, Seismology (SM1.1) General Contributions on Earthquakes, Earth Structure, Seismology, Geophysical Research Abstract*, Vol. 21, EGU2019-3124, 2019, Vienna, Austria. Harvard-Smithsonian Center for Astrophysics, High Energy Astrophysics Division, SAO/NASA Astrophysics Data System.

- [38] V. Straser, D. Cataldi, G. Cataldi. (2019). Registration of Pre-Seismic Signals Related to the Mediterranean Area with the RDF System Developed by the Radio Emissions Project. International Journal of Engineering Science Invention (IJESI), www.ijesi.org. Volume 8 Issue 03 Series. March 2019. PP 26-35. ISSN (Online): 2319 – 6734, ISSN (Print): 2319 – 6726.2019.
- [39] V. Straser, D. Cataldi, G. Cataldi. (2018). Radio Direction Finding System, a new perspective for global crust diagnosis. New Concepts in Global Tectonics Journal, V. 6, No. 2, June 2018. pp203-211.

Solar activity and geomagnetic activity related to M6+ global seismic activity recorded on March 20, 2021

Cataldi Gabriele¹, Daniele Cataldi¹⁻², Valentino Straser³

- (1) Radio Emissions Project, Rome, Italy – ltpaobserverproject@gmail.com
 (2) Fondazione Permanente G. Giuliani, L'Aquila, Italy – danielle77c@gmail.com
 (3) Department of Science and Environment UPKL, Brussels – Valentino.straser@gmail.com

Abstract

On March 20, 2021, two potentially destructive earthquakes were recorded on our planet: Macquarie Island M6.1 earthquake, recorded at 05:19:31 UTC at a depth of 10 km; Japan M7.0 earthquake recorded at 09:09:45 UTC at a depth of 54 km. These two earthquakes were recorded after a solar wind proton density increase which subsequently generated a geomagnetic perturbation that reached the degree G1 (NOAA G Scale). This type of correlation was observed by the authors for the first time since 2011, while from January 1, 2012 to date it was possible to see that all potentially destructive seismic events that are recorded on a global scale are always preceded by a solar wind proton density increase which can subsequently produce a perturbation of the Earth's geomagnetic activity.

Keywords: solar activity, Earth's geomagnetic activity, seismic precursor, earthquake prevision, proton density increase.

Introduction

On March 20, 2021, two potentially destructive seismic events have been recorded on our planet (**Fig.1**):

- 1) Macquarie Island M6.1 earthquake, recorded at 05:19:31 UTC at a depth of 10 km;
- 2) Japan M7.0 earthquake recorded at 09:09:45 UTC at a depth of 54 km.

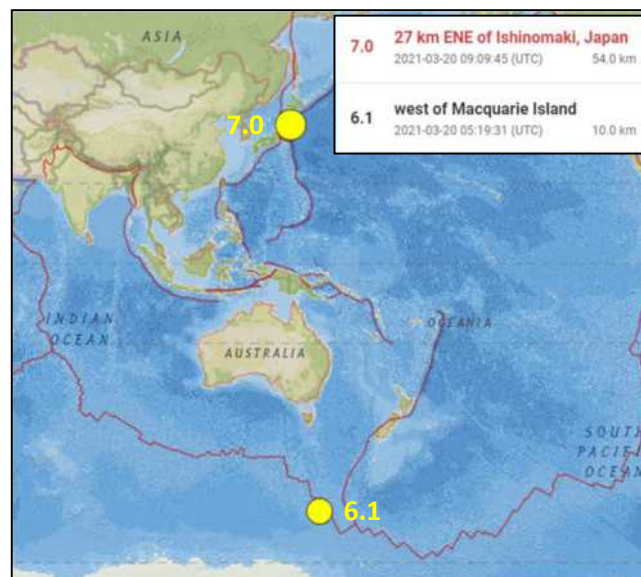


Fig. 1 – Seismic epicenters of M6+ earthquakes recorded on March 20, 2021.

Credits: USGS

The studies conducted by the authors from 2012 to today have shown that all the potentially destructive seismic activity that is recorded on our planet (M6+ global seismic activity) is always preceded by an increase in the solar ion flux [4] [5] [7- 24] namely by a solar wind proton density increase (Interplanetary Seismic Precursor or ISP) which can produce important geomagnetic perturbations [1-3] [5] [6] [11] [13-15] [18] [20] [24] (Seismic Geomagnetic Precursor or SGP). This important result has been confirmed for

every single potentially destructive seismic event: a unique scientific achievement in the history of research dedicated to seismic prediction but which is not yet widely discussed within the international scientific community. In this paper the authors will present the results of this type of correlation obtained with respect to the M6+ seismic events recorded on a global scale on March 20, 2021.

Data analysis

The authors constantly monitor the conditions of space weather and geomagnetic activity to understand when a resumption of M6+ global seismic activity is expected. On March 18, 2021 at 22:46 UTC the DSCOVR Satellite (in Lagrangian orbit L1) started detecting a solar wind proton density increase (**Fig. 2**) which reached its maximum level (63.47 p/cm³) on March 20, 2021 at 03:58 UTC. At 04:10 UTC this increase quickly decreased and two seismic events of strong intensity were recorded within a few hours:

- 1) Macquarie Island M6.1 earthquake, recorded at 05:19:31 UTC at a depth of 10 km;
- 2) Japan M7.0 earthquake recorded at 09:09:45 UTC at a depth of 54 km.

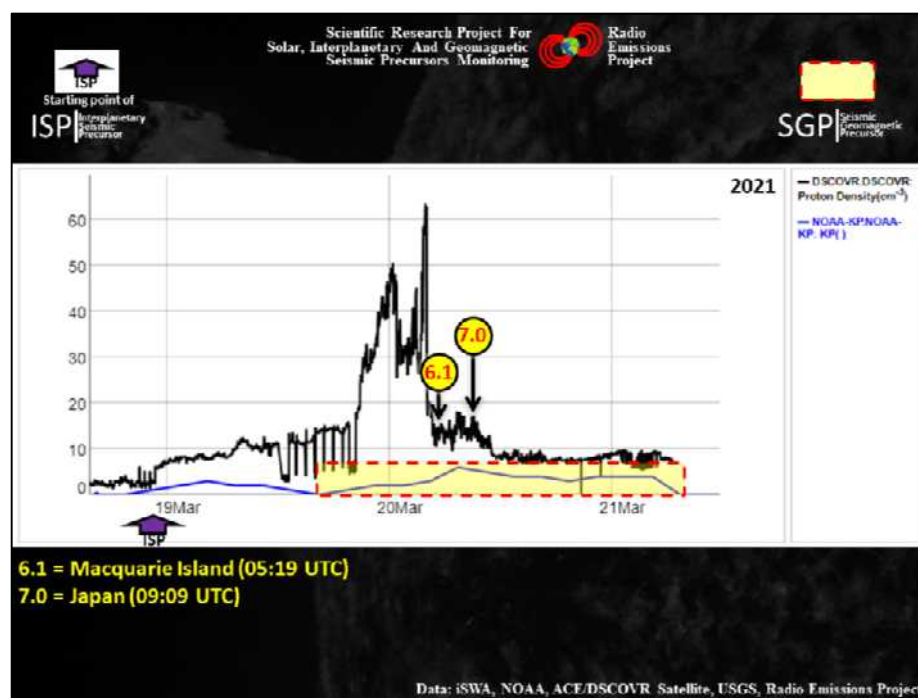


Fig. 2 – Electromagnetic seismic precursors related to the M6+ earthquake. The graph above shows the variation curve relating to the solar wind proton density increase (black line) and the variation curve of the geomagnetic activity (Kp Index; blue line) recorded between 18 and 21 March 2021. The area yellow highlights the geomagnetic increase (Seismic Geomagnetic Precursor or SGP) that preceded the M6+ global seismic activity that have been recorded on March 21, 2021. The solar wind proton density increase started on 18 March 2021 at ... UTC (see purple arrow) and represents the Interplanetary Seismic Precursor (ISP) related to the M6+ earthquakes. Credits: USGS, iSWA, Radio Emissions Project.

Observing **Fig. 2** it is evident that the proton increase (Interplanetary Seismic Precursor or ISP) produced an increase in geomagnetic activity (**Fig. 2** and **3**) which preceded, in turn, the two M6+ seismic events (Seismic Geomagnetic Precursor or SGP). From a predictive point of view, therefore, we are faced with two phenomena of an electromagnetic nature (one of which is the consequence of the other) which can be monitored with enormous ease and which give us a certain time indication (on average within 108 hours) about when a resumption of M6+ global seismic activity can be expected. This seismic forecasting method is not able to identify the epicentral areas of potentially destructive earthquakes but it gives us the certainty that a resumption of M6+ seismic activity will take place on a global scale. Considering that this mechanism has been observed for every potentially destructive seismic event occurring from January 1, 2021 to date, the authors believe that this is an unprecedented scientific achievement and, as such, should find adequate recognition within the international scientific community



Fig. 3 – Kp Index related to M6+ global seismic activity recorded on March 20, 2021. The graph above shows the Kp Index curve recorded between 18 and 21 March 2021: it is clear that the M6+ global seismic activity earthquake was preceded by a geomagnetic increase that reached the degree of 6 (geomagnetic storm of G1 degree; NOAA G Scale), as indicated by the dashed red line. Credits: iSWA.

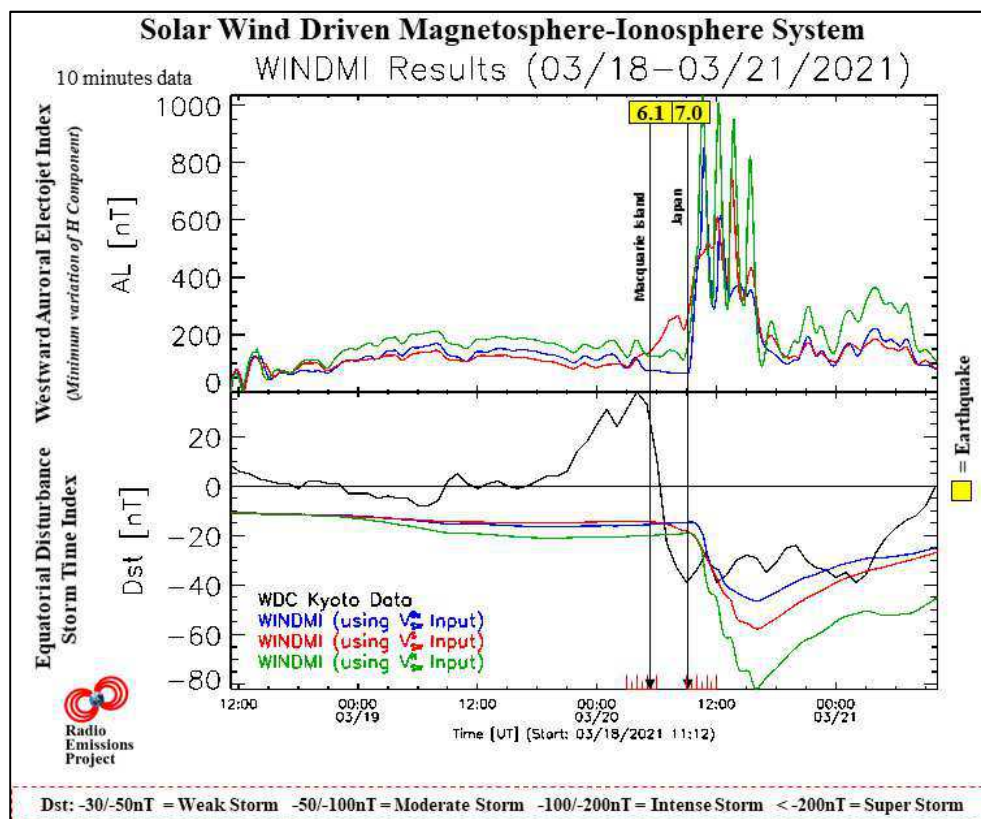


Fig. 4 – Low-dimensional model of the energy transfer from the solar wind through the magnetosphere and into the ionosphere (WINDMI). The picture shows the variation of the AL-Index (at top) and the DST-Index (at bottom) in the hours that preceded the M6+ global seismic activity recorded on March 20, 2021 (the time marker of the earthquake is indicated by a vertical black line). The DST-Index is a direct measure of the Earth's geomagnetic horizontal (H) component variation due to the equatorial ring current, while the AL-Index (Auroral Lower) is at all times, the minimum value of the variation of the geomagnetic H component of the geomagnetic field recorded by observers of reference and provides a quantitative measure of global Westward Auroral Electrojet (WEJ) produced by increased of ionospheric currents therein present. Model developed by the Institute for Fusion Studies, Department of Physics, University of Texas at Austin. Credits: iSWA, USGS, Radio Emissions Project.

Other interesting data come from the analysis of the “Low-dimensional model of the energy transfer from the solar wind through the magnetosphere and into the ionosphere (WINDMI)” (Fig. 4). Observing the graphs of Fig. 4 it is possible to understand that the two earthquakes were preceded by an increment of DST Index and AL Index: two indices used to have an indication of the entity of the geomagnetic perturbations induced by solar activity, i.e. by the solar ion flux. This data confirms that the two earthquakes were preceded by an

increase in the Earth's geomagnetic activity produced as a result of the coupling between solar activity (solar ion flux) and the Earth's magnetosphere, as shown in **fig. 2**. In fact, it was no coincidence that the two M6+ seismic events were recorded shortly before and shortly after the geomagnetic increase of G1 class (NOAA G Scale) (**Fig. 3**).

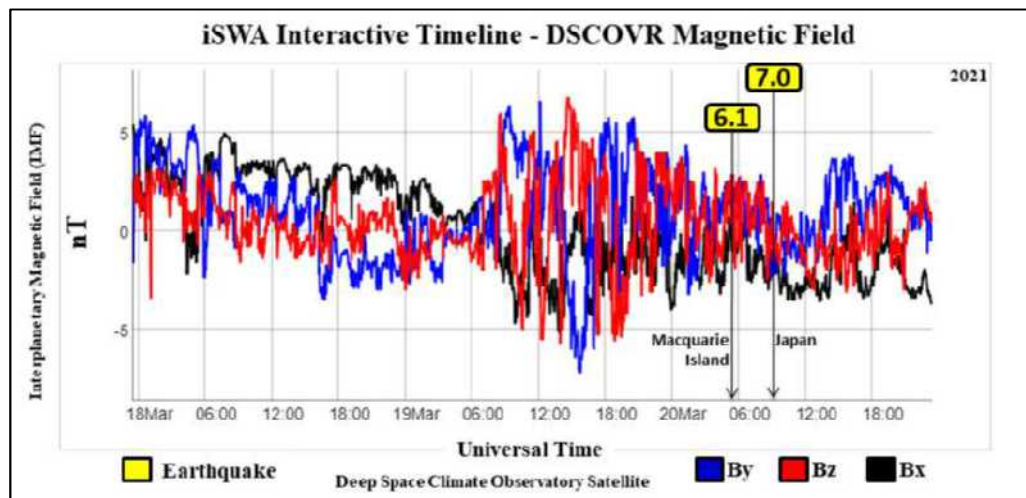


Fig. 5 – Solar wind magnetic field perturbation correlated to South Sandwich Islands region M6.0 earthquake. The chart above shows the variation of the interplanetary magnetic field (IMF) recorded through the Deep Space Climate Observatory (DSCOVR) Satellite in orbit at L1 Lagrange point. The recording was done on 3 axes (By, Bx, Bz). Analyzing the variation curves it is evident that the M6.0 earthquake occurred in South Sandwich Islands region on March 14, 2021 has been preceded by a perturbation of the interplanetary magnetic field (IMF) whose greater intensity was recorded between 02:30 UTC and 06:00 UTC of March 13, 2021. The long black vertical arrow represents the temporal markers of South Sandwich Islands region M6.0 earthquake recorded on March 14, 2021 at 12:05 UTC. Credits: iSWA, USGS, Radio Emissions Project.

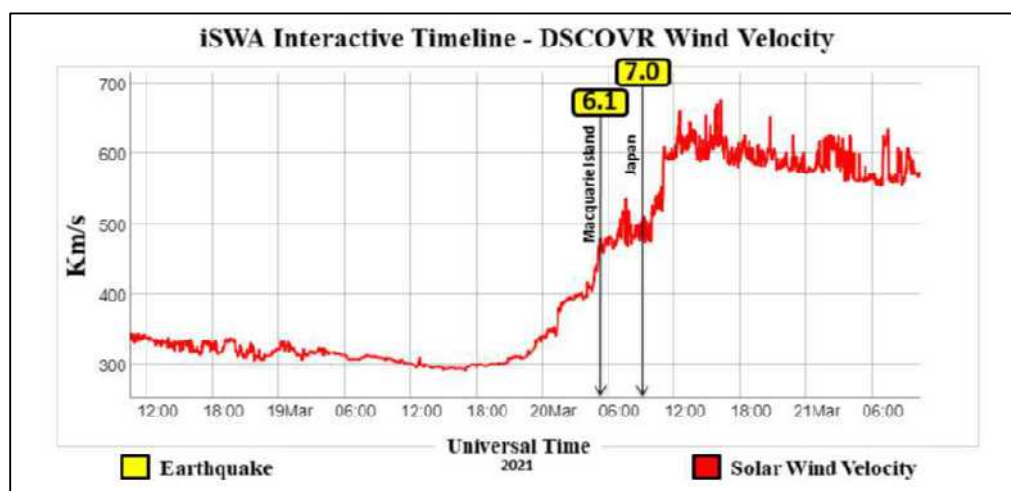


Fig. 6 – Solar wind velocity correlated to M6+ global seismic activity recorded on March 20, 2021. The graph shows the variation of solar wind velocity recorded between 18 and 21 March 2021 by Deep Space Climate Observatory (DSCOVR) Satellite, in orbit at L1 Lagrange point. Analyzing the variation curve it is possible to understand that the M6+ earthquakes was preceded by an increase of the solar wind speed. The black vertical arrow shows the temporal marker of the M6+ earthquakes occurred on March 20, 2021. Credits: iSWA, USGS, Radio Emissions Project.

Fig. 5 and 6 confirm what has been stated so far. Very interesting is the perturbation (Interplanetary Seismic Precursor or ISP) of Interplanetary Magnetic Field (IMF) highlighted many hours before the two M6+ seismic events recorded on March 20, 2021: 24 hours before Macquarie Island earthquake and 28 hours before Japanese earthquake. Also in this case, the speed of the solar wind has undergone an increase correlated to the M6+ seismic activity: the two seismic events analyzed in this work were recorded during a rapid increase in the solar ion flux which reached ~670 km/s 8 hours after the Japanese earthquake. This type

of correlation was observed for the first time by the authors in 2011 and allowed to focus attention on the density of the solar ion flux [4] [5] [7-24].

Conclusions

Thanks to the enormous work that the authors have been carrying out since 2012, the conclusions should be taken for granted, however it should be reiterated that the M6+ global seismic activity is closely related to the solar activity and, more precisely, to the solar wind proton density increases that can subsequently determine of the important perturbations of the Earth's geomagnetic field. The authors were able to verify that every single M6+ seismic event is always preceded by solar wind proton density increase and this allows to establish with certainty when on Earth it is possible to expect a resumption of global M6+ seismic activity. What has been ascertained represents in all respects an important scientific achievement which, according to the authors, should be counted among the most important scientific discoveries of the century as it could (today) be used as a tool capable of predicting (with an average forewarning of 108 hours) when a resumption of M6+ seismic activity occurs on Earth. This tool has been tested by the authors for more than nine years and, unlike other methods, has always proved reliable.

Credits

- [1] G. Cataldi, D. Cataldi, V. Straser. (2013). Variations Of Terrestrial Geomagnetic Activity Correlated To M6+ Global Seismic Activity. EGU (European Geosciences Union) 2013, General Assembly, Seismology Section (SM3.1), Earthquake precursors, bio-anomalies prior to earthquakes and prediction, Geophysical Research Abstracts, Vol. 15. EGU2013-2617, Vienna, Austria. Harvard-Smithsonian Center for Astrophysics, High Energy Astrophysics Division, SAO/NASA Astrophysics Data System.
- [2] G. Cataldi, D. Cataldi and V. Straser. (2014). Earth's magnetic field anomalies that precede the M6+ global seismic activity. European Geosciences Union (EGU) General Assembly 2014, Geophysical Research Abstract, Vol. 16, EGU2014-1068, Vienna, Austria. Natural Hazard Section (NH4.3), Electromagnetic phenomena and connections with seismo-tectonic activity, Harvard-Smithsonian Center for Astrophysics, High Energy Astrophysics Division, SAO/NASA Astrophysics Data System.
- [3] D. Cataldi, G. Cataldi and V. Straser. (2014). Variations of the Electromagnetic field that preceded the Peruvian M7.0 earthquake occurred on September 25, 2013. European Geosciences Union (EGU) General Assembly 2014, Geophysical Research Abstract, Vol. 16, EGU2014-1075, Natural Hazard Section (NH4.3), Electro-magnetic phenomena and connections with seismo-tectonic activity, Vienna, Austria. Harvard-Smithsonian Center for Astrophysics, High Energy Astrophysics Division, SAO/NASA Astrophysics Data System.
- [4] T. Rabeh, G. Cataldi, V. Straser. (2014). Possibility of coupling the magnetosphere-ionosphere during the time of earthquakes. European Geosciences Union (EGU) General Assembly 2014, Geophysical Research Abstract, Vol. 16, EGU2014-1067, Vienna, Austria. Natural Hazard Section (NH4.3), Electromagnetic phenomena and connections with seismo-tectonic activity. Harvard-Smithsonian Center for Astrophysics, High Energy Astrophysics Division, SAO/NASA Astrophysics Data System.
- [5] V. Straser, G. Cataldi. (2014). Solar wind proton density increase and geomagnetic background anomalies before strong M6+ earthquakes. Space Research Institute of Moscow, Russian Academy of Sciences, MSS-14. 2014. Moscow, Russia. pp280-286.
- [6] V. Straser, G. Cataldi, D. Cataldi. (2015). Radio-anomalies: tool for earthquakes and tsunami forecasts. European Geosciences Union (EGU) General Assembly 2015, Natural Hazard Section (NH5.1), Sea & Ocean Hazard - Tsunami, Geophysical Research Abstract, Vol. 17, Vienna, Austria. Harvard-Smithsonian Center for Astrophysics, High Energy Astrophysics Division, SAO/NASA Astrophysics Data System.

- [7] V. Straser, G. Cataldi. (2015). Solar wind ionic variation associated with earthquakes greater than magnitude M6.0. *New Concepts in Global Tectonics Journal*, V. 3, No. 2, June 2015, Australia. P.140-154.
- [8] G. Cataldi, D. Cataldi, V. Straser. (2015). Solar wind proton density variations that preceded the M6+ earthquakes occurring on a global scale between 17 and 20 April 2014. European Geosciences Union (EGU) General Assembly 2015, Vienna, Austria. Natural Hazard Section (NH5.1), Sea & Ocean Hazard - Tsunami, Geophysical Research Abstract, Vol. 17, EGU2015-4157-2, Harvard-Smithsonian Center for Astrophysics, High Energy Astrophysics Division, SAO/NASA Astrophysics Data System.
- [9] G. Cataldi, D. Cataldi, V. Straser. (2015). Solar wind ion density variations that preceded the M6+ earthquakes occurring on a global scale between 3 and 15 September 2013. European Geosciences Union (EGU) General Assembly 2015, Geophysical Research Abstract, Vol. 17, EGU2015-4581, Vienna, Austria. Natural Hazard Section (NH5.1), Sea & Ocean Hazard - Tsunami, Harvard-Smithsonian Center for Astrophysics, High Energy Astrophysics Division, SAO/NASA Astrophysics Data System.
- [10] G. Cataldi, D. Cataldi, V. Straser. (2015). Solar wind proton density variations that preceded the M6.1 earthquake occurred in New Caledonia on November 10, 2014. European Geosciences Union (EGU) General Assembly 2015, Geophysical Research Abstract, Vol. 17, EGU2015-4167, Vienna, Austria. Natural Hazard Section (NH5.1), Sea & Ocean Hazard - Tsunami, Harvard-Smithsonian Center for Astrophysics, High Energy Astrophysics Division, SAO/NASA Astrophysics Data System.
- [11] V. Straser, G. Cataldi, D. Cataldi. (2015). Solar wind ionic and geomagnetic variations preceding the M8.3 Chile Earthquake. *New Concepts in Global Tectonics Journal*, V. 3, No. 3, September 2015, Australia. P.394-399.
- [12] G. Cataldi, D. Cataldi, V. Straser. (2016). Solar activity correlated to the M7.0 Japan earthquake occurred on April 15, 2016. *New Concepts in Global Tectonics Journal*, V. 4, No. 2, pp202-208, June 2016.
- [13] G. Cataldi, D. Cataldi, V. Straser. (2016). Tsunami related to solar and geomagnetic activity. European Geosciences Union (EGU) General Assembly 2016, Natural Hazard Section (NH5.6), Complex modeling of earthquake, landslide, and volcano tsunami sources. Geophysical Research Abstract, Vol. 18, EGU2016-9626, Vienna, Austria. Harvard-Smithsonian Center for Astrophysics, High Energy Astrophysics Division, SAO/NASA Astrophysics Data System.
- [14] G. Cataldi, D. Cataldi, V. Straser. (2017). SELF-VLF electromagnetic signals and solar wind proton density variations that preceded the M6.2 Central Italy earthquake on August 24, 2016. *International Journal of Modern Research in Electrical and Electronic Engineering*, Vol. 1, No. 1, 1-15. DOI: 10.20448/journal.526/2017.1.1/526.1.1.15. Harvard-Smithsonian Center for Astrophysics, High Energy Astrophysics Division, SAO/NASA Astrophysics Data System.
- [15] G. Cataldi, D. Cataldi, V. Straser. (2017). Solar and Geomagnetic Activity Variations Correlated to Italian M6+ Earthquakes Occurred in 2016. European Geosciences Union (EGU), General Assembly 2017. Geophysical Research Abstracts Vol. 19, EGU2017-3681, 2017. Seismology (SM1.2)/Natural Hazards (NH4.7)/Tectonics & Structural Geology (TS5.5) The 2016 Central Italy Seismic sequence: overview of data analyses and source models. Harvard-Smithsonian Center for Astrophysics, High Energy Astrophysics Division, SAO/NASA Astrophysics Data System.
- [16] G. Cataldi, D. Cataldi, V. Straser. (2017). Solar wind proton density increase that preceded Central Italy earthquakes occurred between 26 and 30 October 2016. European Geosciences Union (EGU), General Assembly 2017. Geophysical Research Abstracts Vol. 19, EGU2017-3774, 2017. Seismology (SM1.2)/Natural Hazards (NH4.7)/Tectonics & Structural Geology (TS5.5) The 2016 Central Italy Seismic sequence: overview of data analyses and source models. Harvard-Smithsonian Center for Astrophysics, High Energy Astrophysics Division, SAO/NASA Astrophysics Data System.

- [17] V. Straser, G. Cataldi, D. Cataldi. (2017). Solar and electromagnetic signal before Mexican Earthquake M8.1, September 2017. *New Concepts in Global Tectonics Journal*, V. 5, No. 4, December 2017, pp. 600-609.
- [18] G. Cataldi, D. Cataldi, V. Straser. (2017). Solar and Geomagnetic Activity Variations Correlated to Italian M6+ Earthquakes Occurred in 2016. *EGU General Assembly 2017*. EGU2017-3681, Vol. 19.
- [19] G. Cataldi, D. Cataldi, V. Straser. (2019). Solar wind ionic density variations related to M6+ global seismic activity between 2012 and 2018. *European Geosciences Union (EGU) General Assembly 2019, Short-term Earthquake Forecast (StEF) and multi-parametric time-Dependent Assessment of Seismic Hazard (t-DASH) (NH4.3/AS4.62/EMRP2.40/ESSI1.7/Gi2.13/SM3.9)*, General Contribution on Earthquakes, Earth Structure, Seismology (SM1.1), *Geophysical Research Abstract*, Vol. 21, EGU2019-3067, 2019, Vienna, Austria. Harvard-Smithsonian Center for Astrophysics, High Energy Astrophysics Division, SAO/NASA Astrophysics Data System.
- [20] G. Cataldi. (2020). *Precursori Sismici – Monitoraggio Elettromagnetico*. Kindle-Amazon, ISBN: 9798664537970. ASIN Code: B08CPDBGX9.
- [21] G. Cataldi, D. Cataldi, V. Straser. (2019). Wolf Number Related To M6+ Global Seismic Activity. *New Concepts in Global Tectonics Journal*, Volume 7, Number 3, December 2019, pp. 178-186.
- [22] V. Straser, G. Cataldi, D. Cataldi. (2020). The Space Weather Related to the M7+ Seismic Activity Recorded on a Global Scale between 28 January and 25 March 2020. *Acta Scientific Agriculture* 4.12 (2020): 55-62.
- [23] G. Cataldi, V. Straser, D. Cataldi. (2020). Space Weather related to potentially destructive seismic activity recorded on a global scale. *New Concepts in Global Tectonics Journal*. Vol.8, No.3, pp. 233-253, December 2020. ISSN 2202-0039.
- [24] G. Cataldi. (2021). *Radio Emissions Project – A new approach to seismic prediction*. Kindle-Amazon, ISBN: 9798709593411.

Space weather and geomagnetic activity related to M6+ global seismic activity recorded on 3-4 March 2021

Gabriele Cataldi¹, Daniele Cataldi¹⁻², Valentino Straser³

- (1) Radio Emissions Project (I). ltpaobserverproject@gmail.com
 (2) Fondazione Permanente G. Giuliani - Onlus (I). danielle77c@hotmail.it
 (3) Department of Science and Environment UPKL Brussel (B). valentino.straser@gmail.com

Abstract

On 3-4 March 2021, seven M6+ seismic events were recorded on our planet: 1) Greece M6.3 earthquake, recorded on March 3, 2021 at 10:16 UTC; 2) New Zealand M7.3 earthquake, recorded on March 4, 2021 at 13:27 UTC; 3) Vanuatu M6.1 earthquake, recorded on March 4, 2021 at 16:53 UTC; 4) Kermadec Islands M7.4 earthquake, recorded on March 4, 2021 at 17:41 UTC 5) New Zealand 8.1 earthquake, recorded on March 4, 2021 at 19:28 UTC; 6) Kermadec Islands M6.1 earthquake, recorded on March 4, 2021 at 20:25 UTC; 7) Kermadec Islands M6.2 earthquake, recorded on March 4, 2021 at 23:12. The peculiarity that unites these potentially destructive earthquakes was the fact that they were recorded during a solar wind proton density increase that started on March 28, 2021 at 00:00 UTC and ended on March 5, 2021 at 00:00 UTC which caused a series of geomagnetic perturbations.

Keywords: proton density increase, seismic precursors, solar activity, geomagnetic activity, electromagnetic precursors.

Introduction

Seven M6+ seismic events were recorded on our planet between 3 and 4 March 2021 (**Fig. 1**):

- 1) Greece M6.3 earthquake, recorded on March 3, 2021 at 10:16 UTC (depth = 10 km);
- 2) New Zealand M7.3 earthquake, recorded on March 4, 2021 at 13:27 UTC (depth = 20.8 km);
- 3) Vanuatu M6.1 earthquake, recorded on March 4, 2021 at 16:53 UTC (depth = 172.1 km);
- 4) Kermadec Islands M7.4 earthquake, recorded on March 4, 2021 at 17:41 UTC (depth = 55.6 km);
- 5) New Zealand 8.1 earthquake, recorded on March 4, 2021 at 19:28 UTC (depth = 19.4 km);
- 6) Kermadec Islands M6.1 earthquake, recorded on March 4, 2021 at 20:25 UTC (depth = 10 km);
- 7) Kermadec Islands M6.2 earthquake, recorded on March 4, 2021 at 23:12 (depth = 10 km).

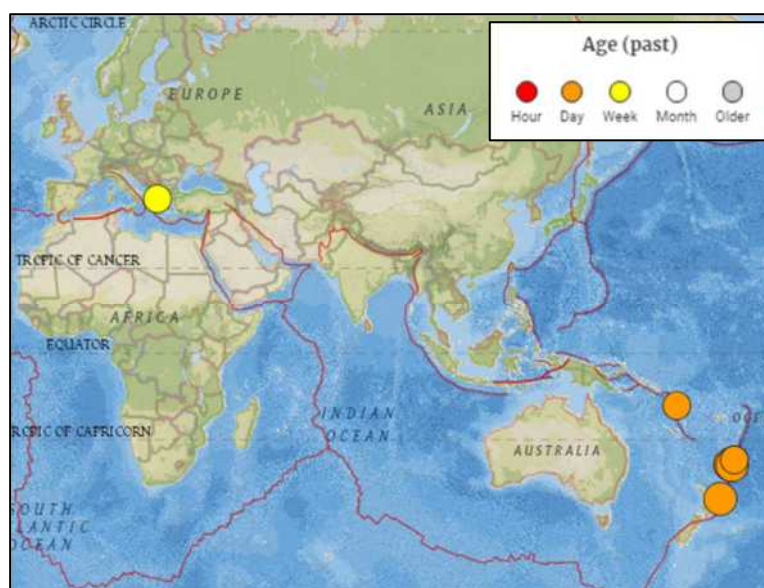


Fig. 1 – Epicenter of the M6+ seismic events recorded between 3 and 4 March 2021. The image above shows the map of the M6+ earthquake epicenter recorded between 3 and 4 March 2021. Credits: USGS, Radio Emissions Project.

Six of the seven earthquakes were recorded on March 4, 2021; while only one was recorded on March 3, 2021: it is a rare concentration of destructive seismic events of which very few precedents are known that occurred over the last ten years. In this paper, the authors will present the results of a correlation study that showed that these seven potentially destructive seismic events were preceded by a solar wind proton density increase and two increases in the Earth's geomagnetic activity. This type of correlation was observed by the authors since 2011 [1-24].

Data analysis

This work served to demonstrate that the potentially destructive seismic activity that is recorded on our planet is always preceded by an increase in solar activity which determines an increase in the Earth's geomagnetic activity [1-24]. To confirm this trend, the authors analyzed the characteristics of the solar ion flux in the hours and days preceding the seven M6+ seismic events recorded between 3 to 4 March 2021: the results of this analysis can be seen in Fig. 2.

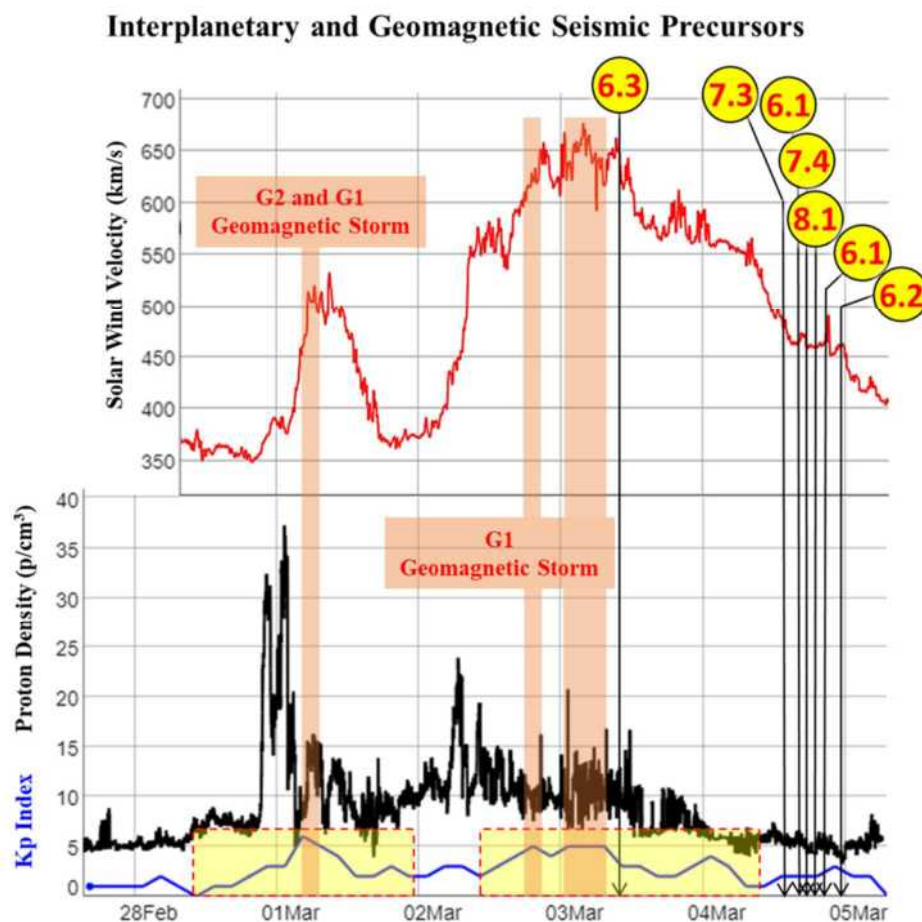


Fig. 2 – Interplanetary and Geomagnetic Seismic Precursors related to M6+ earthquake recorded between 3 and 4 March 2021. The graph above shows the classic correlation that exists between potentially destructive seismic events that are recorded on a global scale and solar and geomagnetic activity. The upper part of the graph (red curve; expression of the increase in solar activity) refers to the change in the speed of the solar wind recorded between February 28, 2021 and March 5, 2021. The lower part of the graph highlights the variation of solar wind proton density increase (black curve; expression of the increase in solar activity, started on February 28, 2021 at 00:00 UTC) and the variation of Kp Index (blue curve; expression of geomagnetic activity). The vertical black arrows represent the temporal markers of potentially destructive seismic events related to solar increase and geomagnetic increase: the increases in geomagnetic activity have been highlighted through the yellow and orange areas. The latter represents the time frame in which a geomagnetic storm of class G2 and G1 (NOAA G Scale) was recorded on our planet, corresponding to a Kp Index of 6 and 5. Credits: iSWA, USGS, Radio Emissions Project.

Thanks to the data provided by DSCOVR Satellite (placed in Lagrangian orbit L1), on February 28, 2021, at 00:00 UTC a solar wind proton density increase began to manifest itself which ended five days later, and exactly on March 5, 2021 at 00:00 UTC. Over this period of time it has undergone several fluctuations (Fig. 2):

1. on February 28, 2021 at 22:23 UTC the proton flow has reached a first peak of intensity (32.27 p/cm^3);
2. on March 1, 2021 at 01:24 UTC the proton flow has reached a second peak of intensity (37.23 p/cm^3);
3. on March 2, 2021 at 06:47 UTC the proton flux has reached the third peak of intensity (23.84 p/cm^3).

From a geomagnetic point of view, however, thanks to data provided by the National Oceanic and Atmospheric Administration (NOAA) it was possible to observe two increases in terrestrial geomagnetic activity which are superimposed on the general proton increase recorded between February 28, 2021 and March 5, 2021 (**Fig. 2**):

1. the first, reached a Kp Index of 6 on March 1, 2021 at 04:30 UTC (geomagnetic storm of class G2) and was recorded a few hours after the maximum proton increase peak (the second of the three increases; March 1, 2021 at 01:24 UTC);
2. the second, reached a Kp Index of 5 between March 2, 2021 at 19:30 UTC and March 3, 2021 at 07:30 UTC (geomagnetic storm of class G1) and was recorded more than 12 hours after the third proton increment.

Exactly after the second geomagnetic increase of class G1 the seismic sequence of the seven potentially destructive earthquakes analyzed in this work began. The two intense geomagnetic increases that have rightly been superimposed on a series of solar wind proton density increases (secondary) have resulted in a typical global seismic trigger pattern related to solar activity [5] [7-12] [14-24]. The solar wind proton density increases, since they are phenomena of an electromagnetic nature related to M6+ global seismic activity have been classified by the authors as “Interplanetary Seismic Precursors” or ISPs; the same is true for geomagnetic increases produced as a result of one or more ISPs: the authors have classified these geomagnetic perturbations as “Seismic Geomagnetic Precursors” or SGPs. The first draft of this classification was made by the authors during 2012 [1].

Conclusions

The M6+ seismic sequence recorded between 3 and 4 March 2021 was correlated to a series of electromagnetic phenomena of a solar nature (ISPs) and, subsequently, of a geomagnetic nature (SGPs) that the authors observed for the first time in 2010-2011. In this work they were presented only the data of a small part of the correlation study (which is still in progress) and which allowed the authors to correlate all M6+ seismic events occurring on a global scale to variations of solar wind proton density increases. This type of analysis will allow in the future to create a seismic forecasting method based solely on the monitoring of solar activity (and on the effects it has on the Earth’s geomagnetic field) and on environmental electromagnetic monitoring [20] [24].

Credits

- [1] G. Cataldi, D. Cataldi, V. Straser. (2013). Variations Of Terrestrial Geomagnetic Activity Correlated To M6+ Global Seismic Activity. EGU (European Geosciences Union) 2013, General Assembly, Seismology Section (SM3.1), Earthquake precursors, bio-anomalies prior to earthquakes and prediction, Geophysical Research Abstracts, Vol. 15. EGU2013-2617, Vienna, Austria. Harvard-Smithsonian Center for Astrophysics, High Energy Astrophysics Division, SAO/NASA Astrophysics Data System.
- [2] G. Cataldi, D. Cataldi and V. Straser. (2014). Earth’s magnetic field anomalies that precede the M6+ global seismic activity. European Geosciences Union (EGU) General Assembly 2014, Geophysical Research Abstract, Vol. 16, EGU2014-1068, Vienna, Austria. Natural Hazard Section (NH4.3), Electromagnetic phenomena and connections with seismo-tectonic activity, Harvard-Smithsonian Center for Astrophysics, High Energy Astrophysics Division, SAO/NASA Astrophysics Data System.
- [3] D. Cataldi, G. Cataldi and V. Straser. (2014). Variations of the Electromagnetic field that preceded the Peruvian M7.0 earthquake occurred on September 25, 2013. European Geosciences Union (EGU)

General Assembly 2014, Geophysical Research Abstract, Vol. 16, EGU2014-1075, Natural Hazard Section (NH4.3), Electro-magnetic phenomena and connections with seismo-tectonic activity, Vienna, Austria. Harvard-Smithsonian Center for Astrophysics, High Energy Astrophysics Division, SAO/NASA Astrophysics Data System.

- [4] T. Rabe, G. Cataldi, V. Straser. (2014). Possibility of coupling the magnetosphere–ionosphere during the time of earthquakes. European Geosciences Union (EGU) General Assembly 2014, Geophysical Research Abstract, Vol. 16, EGU2014-1067, Vienna, Austria. Natural Hazard Section (NH4.3), Electro-magnetic phenomena and connections with seismo-tectonic activity. Harvard-Smithsonian Center for Astrophysics, High Energy Astrophysics Division, SAO/NASA Astrophysics Data System.
- [5] V. Straser, G. Cataldi. (2014). Solar wind proton density increase and geomagnetic background anomalies before strong M6+ earthquakes. Space Research Institute of Moscow, Russian Academy of Sciences, MSS-14. 2014. Moscow, Russia. pp280-286.
- [6] V. Straser, G. Cataldi, D. Cataldi. (2015). Radio-anomalies: tool for earthquakes and tsunami forecasts. European Geosciences Union (EGU) General Assembly 2015, Natural Hazard Section (NH5.1), Sea & Ocean Hazard - Tsunami, Geophysical Research Abstract, Vol. 17, Vienna, Austria. Harvard-Smithsonian Center for Astrophysics, High Energy Astrophysics Division, SAO/NASA Astrophysics Data System.
- [7] V. Straser, G. Cataldi. (2015). Solar wind ionic variation associated with earthquakes greater than magnitude M6.0. *New Concepts in Global Tectonics Journal*, V. 3, No. 2, June 2015, Australia. P.140-154.
- [8] G. Cataldi, D. Cataldi, V. Straser. (2015). Solar wind proton density variations that preceded the M6+ earthquakes occurring on a global scale between 17 and 20 April 2014. European Geosciences Union (EGU) General Assembly 2015, Vienna, Austria. Natural Hazard Section (NH5.1), Sea & Ocean Hazard - Tsunami, Geophysical Research Abstract, Vol. 17, EGU2015-4157-2, Harvard-Smithsonian Center for Astrophysics, High Energy Astrophysics Division, SAO/NASA Astrophysics Data System.
- [9] G. Cataldi, D. Cataldi, V. Straser. (2015). Solar wind ion density variations that preceded the M6+ earthquakes occurring on a global scale between 3 and 15 September 2013. European Geosciences Union (EGU) General Assembly 2015, Geophysical Research Abstract, Vol. 17, EGU2015-4581, Vienna, Austria. Natural Hazard Section (NH5.1), Sea & Ocean Hazard - Tsunami, Harvard-Smithsonian Center for Astrophysics, High Energy Astrophysics Division, SAO/NASA Astrophysics Data System.
- [10] G. Cataldi, D. Cataldi, V. Straser. (2015). Solar wind proton density variations that preceded the M6.1 earthquake occurred in New Caledonia on November 10, 2014. European Geosciences Union (EGU) General Assembly 2015, Geophysical Research Abstract, Vol. 17, EGU2015-4167, Vienna, Austria. Natural Hazard Section (NH5.1), Sea & Ocean Hazard - Tsunami, Harvard-Smithsonian Center for Astrophysics, High Energy Astrophysics Division, SAO/NASA Astrophysics Data System.
- [11] V. Straser, G. Cataldi, D. Cataldi. (2015). Solar wind ionic and geomagnetic variations preceding the Md8.3 Chile Earthquake. *New Concepts in Global Tectonics Journal*, V. 3, No. 3, September 2015, Australia. P.394-399.
- [12] G. Cataldi, D. Cataldi, V. Straser. (2016). Solar activity correlated to the M7.0 Japan earthquake occurred on April 15, 2016. *New Concepts in Global Tectonics Journal*, V. 4, No. 2, pp202-208, June 2016.
- [13] G. Cataldi, D. Cataldi, V. Straser. (2016). Tsunami related to solar and geomagnetic activity. European Geosciences Union (EGU) General Assembly 2016, Natural Hazard Section (NH5.6), Complex modeling of earthquake, landslide, and volcano tsunami sources. Geophysical Research Abstract, Vol.

18, EGU2016-9626, Vienna, Austria. Harvard-Smithsonian Center for Astrophysics, High Energy Astrophysics Division, SAO/NASA Astrophysics Data System.

- [14] G. Cataldi, D. Cataldi, V. Straser. (2017). SELF-VLF electromagnetic signals and solar wind proton density variations that preceded the M6.2 Central Italy earthquake on August 24, 2016. *International Journal of Modern Research in Electrical and Electronic Engineering*, Vol. 1, No. 1, 1-15. DOI: 10.20448/journal.526/2017.1.1/526.1.1.15. Harvard-Smithsonian Center for Astrophysics, High Energy Astrophysics Division, SAO/NASA Astrophysics Data System.
- [15] G. Cataldi, D. Cataldi, V. Straser. (2017). Solar and Geomagnetic Activity Variations Correlated to Italian M6+ Earthquakes Occurred in 2016. *European Geosciences Union (EGU), General Assembly 2017. Geophysical Research Abstracts Vol. 19, EGU2017-3681, 2017. Seismology (SM1.2)/Natural Hazards (NH4.7)/Tectonics & Structural Geology (TS5.5) The 2016 Central Italy Seismic sequence: overview of data analyses and source models.* Harvard-Smithsonian Center for Astrophysics, High Energy Astrophysics Division, SAO/NASA Astrophysics Data System.
- [16] G. Cataldi, D. Cataldi, V. Straser. (2017). Solar wind proton density increase that preceded Central Italy earthquakes occurred between 26 and 30 October 2016. *European Geosciences Union (EGU), General Assembly 2017. Geophysical Research Abstracts Vol. 19, EGU2017-3774, 2017. Seismology (SM1.2)/Natural Hazards (NH4.7)/Tectonics & Structural Geology (TS5.5) The 2016 Central Italy Seismic sequence: overview of data analyses and source models.* Harvard-Smithsonian Center for Astrophysics, High Energy Astrophysics Division, SAO/NASA Astrophysics Data System.
- [17] V. Straser, G. Cataldi, D. Cataldi. (2017). Solar and electromagnetic signal before Mexican Earthquake M8.1, September 2017. *New Concepts in Global Tectonics Journal*, V. 5, No. 4, December 2017, pp. 600-609.
- [18] G. Cataldi, D. Cataldi, V. Straser. (2017). Solar and Geomagnetic Activity Variations Correlated to Italian M6+Earthquakes Occurred in 2016. *EGU General Assembly 2017. EGU2017-3681, Vol. 19.*
- [19] G. Cataldi, D. Cataldi, V. Straser. (2019). Solar wind ionic density variations related to M6+ global seismic activity between 2012 and 2018. *European Geosciences Union (EGU) General Assembly 2019, Short-term Earthquake Forecast (StEF) and multy-parametric time-Dependent Assessment of Seismic Hazard (t-DASH) (NH4.3/AS4.62/EMRP2.40/ESSI1.7/Gi2.13/SM3.9), General Contribution on Earthquakes, Earth Structure, Seismology (SM1.1), Geophysical Research Abstract, Vol. 21, EGU2019-3067, 2019, Vienna, Austria.* Harvard-Smithsonian Center for Astrophysics, High Energy Astrophysics Division, SAO/NASA Astrophysics Data System.
- [20] G. Cataldi. (2020). *Precursori Sismici – Monitoraggio Elettromagnetico.* Kindle-Amazon, ISBN: 9798664537970. ASIN Code: B08CPDBGX9.
- [21] G. Cataldi, D. Cataldi, V. Straser. (2019). Wolf Number Related To M6+ Global Seismic Activity. *New Concepts in Global Tectonics Journal*, Volume 7, Number 3, December 2019, pp. 178-186.
- [22] V. Straser, G. Cataldi, D. Cataldi. (2020). The Space Weather Related to the M7+ Seismic Activity Recorded on a Global Scale between 28 January and 25 March 2020. *Acta Scientific Agriculture* 4.12 (2020): 55-62.
- [23] G. Cataldi, V. Straser, D. Cataldi. (2020). Space Weather related to potentially destructive seismic activity recorded on a global scale. *New Concepts in Global Tectonics Journal*. Vol.8, No.3, pp. 233-253, December 2020. ISSN 2202-0039.
- [24] G. Cataldi. (2021). *Radio Emissions Project – A new approach to seismic prediction.* Kindle-Amazon, ISBN: 9798709593411.

Solar activity and geomagnetic activity related to M6.0 South Sandwich Islands region earthquake recorded on March 14, 2021

Cataldi Gabriele¹, Daniele Cataldi¹⁻², Valentino Straser³

- (1) Radio Emissions Project, Rome, Italy – ltpaobserverproject@gmail.com
- (2) Fondazione Permanente G. Giuliani, L'Aquila, Italy – danielle77c@gmail.com
- (3) Department of Science and Environment UPKL, Brussels – Valentino.straser@gmail.com

Abstract

On March 14, 2021, at 12:05:13 UTC, an M6.0 earthquake was recorded in the South region of the Sandwich Islands. The analysis of the modulation of the solar ion flux and of the Earth's geomagnetic activity showed that the M6.0 earthquake was preceded by a solar wind proton density increase and by an increase in the Earth's geomagnetic field. This type of correlation was observed for the first time by the authors in 2011 [20] [23] and currently has allowed the development of a new seismic forecasting method that is able to provide (with an average advance of 108.4 hours) when it is possible to expect a resumption of M6+ seismic activity on a global scale [24].

Keywords: solar activity, Earth's geomagnetic activity, seismic precursor, earthquake prevision, proton increase.

Introduction

On March 14, 2021, at 12:05:13 UTC, an M6.0 earthquake was recorded in the South region of the Sandwich Islands and at a depth of 10 km (**Fig. 1**). This strong seismic event was recorded after an increase in solar activity and terrestrial geomagnetic activity, as well as all potentially destructive seismic events recorded between January 1, 2012 to date [20] [23] [24]. The authors, thanks to the studies conducted on the modulation of the solar ion flux and thanks to the monitoring of the Earth's geomagnetic activity, were able to prove at the end of 2012 [1] the existence of an electromagnetic seismic precursor that always precedes potentially destructive earthquakes which are recorded on a global scale. This seismic precursor is represented by solar wind proton density increases (Interplanetary Seismic Precursors or ISPs) which can also generate increases in terrestrial geomagnetic activity (Seismic Geomagnetic Precursors or SGPs) [2-6] [11-15] [17] [18] [21-23]. In this work, the authors will present data relating to solar activity and terrestrial geomagnetic activity that have been related to the M6.0 earthquake recorded in the South region of the Sandwich Islands on March 14, 2021.

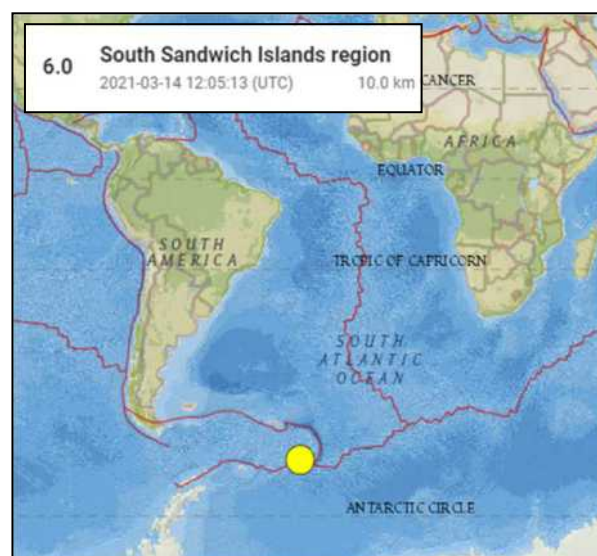


Fig. 1 – Seismic epicenter of the M6.0 earthquake recorded in the South Sandwich Islands region on March 14, 2021.

Credits: USGS

Data analysis

The confirmation of a theory in the scientific field is an extraordinary event that requires a lot of significant data. The authors, through the monitoring of solar activity and terrestrial geomagnetic activity, have managed in a few years to scientifically validate what at first seemed to be simply a series of events that repeated themselves according to a certain frequency and this suggested that they had to be connected. To confirm that every single destructive seismic event that occurs on a global scale is always preceded by a solar wind proton density increase, it was necessary to analyze the entire M6+ seismic activity that occurs on a global scale in relation to the conditions of space weather and in relation to the effects that this has on the Earth's geomagnetic field [23]. As happened for all potentially destructive seismic events recorded on Earth, also the M6.0 earthquake recorded in the South Sandwich Islands region on March 14, 2021 at 12:05 UTC was preceded by a solar wind proton density increase (Fig. 2) which subsequently produced a degree 5 increase in the Earth's geomagnetic activity (Fig. 3).

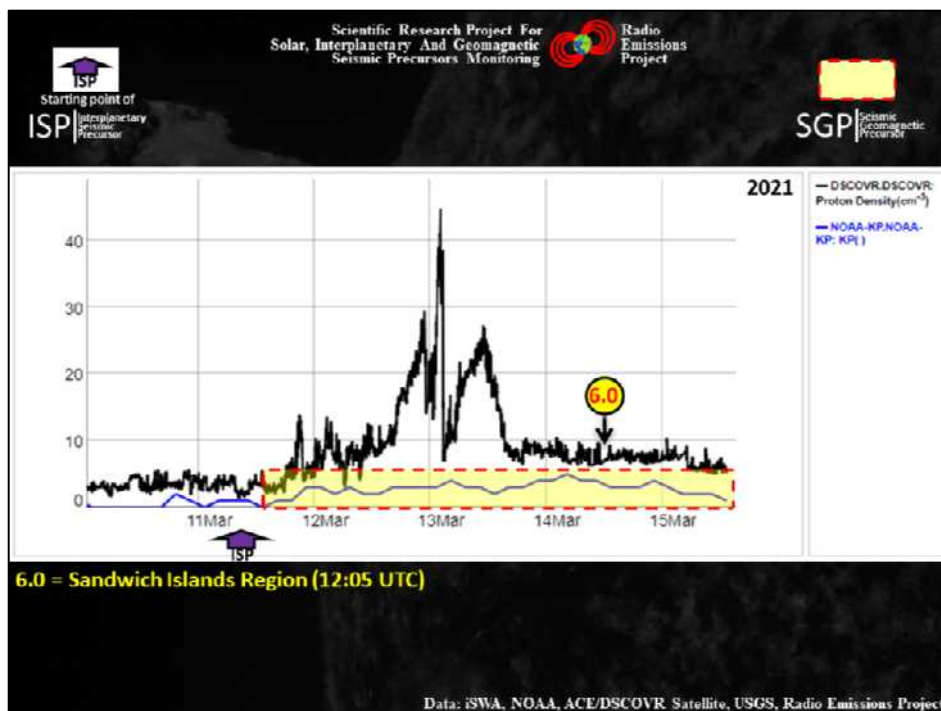


Fig. 2 – Electromagnetic seismic precursors related to the M6.0 earthquake. The graph above shows the variation curve relating to the solar wind proton density increase (black line) and the variation curve of the geomagnetic activity (Kp Index; blue line) recorded between 10 and 15 March 2021. The area yellow highlights the geomagnetic increase (Seismic Geomagnetic Precursor or SGP) that preceded the M6.0 seismic event recorded in the South Sandwich Islands region on March 14, 2021 at 12:05 UTC. The solar wind proton density increase started on 11 March 2021 at 08:50 UTC (see purple arrow) and represents the Interplanetary Seismic Precursor (ISP) related to the M6.0 earthquake. Credits: USGS, iSWA, Radio Emissions Project.

The M6.0 South Sandwich Islands region earthquake was the potentially destructive seismic event #1205 recorded after an increase in solar activity from January 1, 2012. The start of the proton increase preceded the M6.0 earthquake by 68 hours, while the peak of maximum density was recorded on March 13, 2021 at 02:21 UTC. The increase in Earth's geomagnetic activity (Kp Index) instead began on 11 March 2021 at 13:30 UTC.

By analyzing the modulation of the Earth's geomagnetic activity it was possible to observe the effects of the impact that this solar wind proton density increase had on the terrestrial magnetosphere (Fig. 4): Fig. 4 highlights that the seismic event M6.0 was preceded by an increase in the geomagnetic field measured on the vector component H (AL Index); while the DST Index shows that the earthquake was preceded by a geomagnetic storm of a weak degree which after a few hours became of moderate degree. Both of these electromagnetic phenomena can be considered geomagnetic seismic precursors (Seismic Geomagnetic Precursors or SGPs) [20] [23] [24].

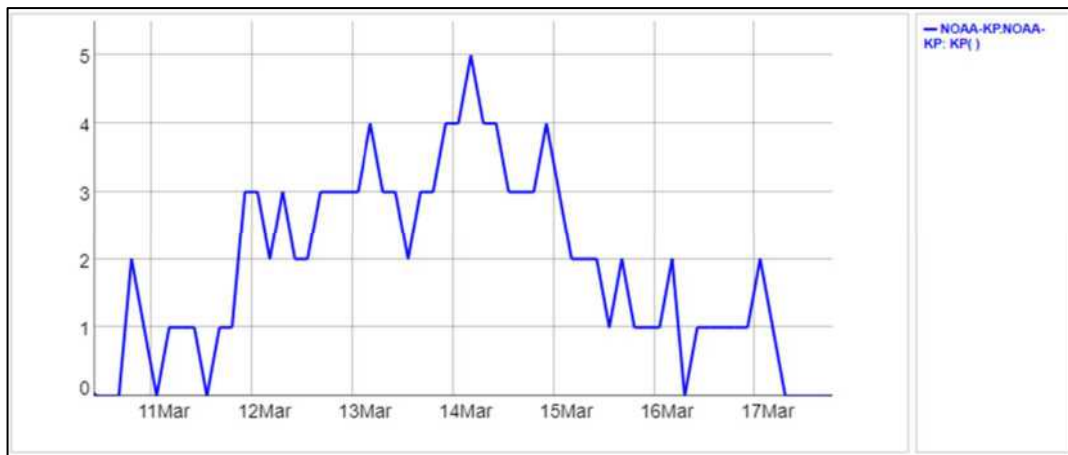


Fig. 3 – Kp Index related to M6.0 earthquake recorded on March 14, 2021. The graph above shows the Kp Index curve recorded between 10 and 17 March 2021: it is clear that the M6.0 earthquake was preceded by a geomagnetic increase that reached the degree of 5. Credits: iSWA.

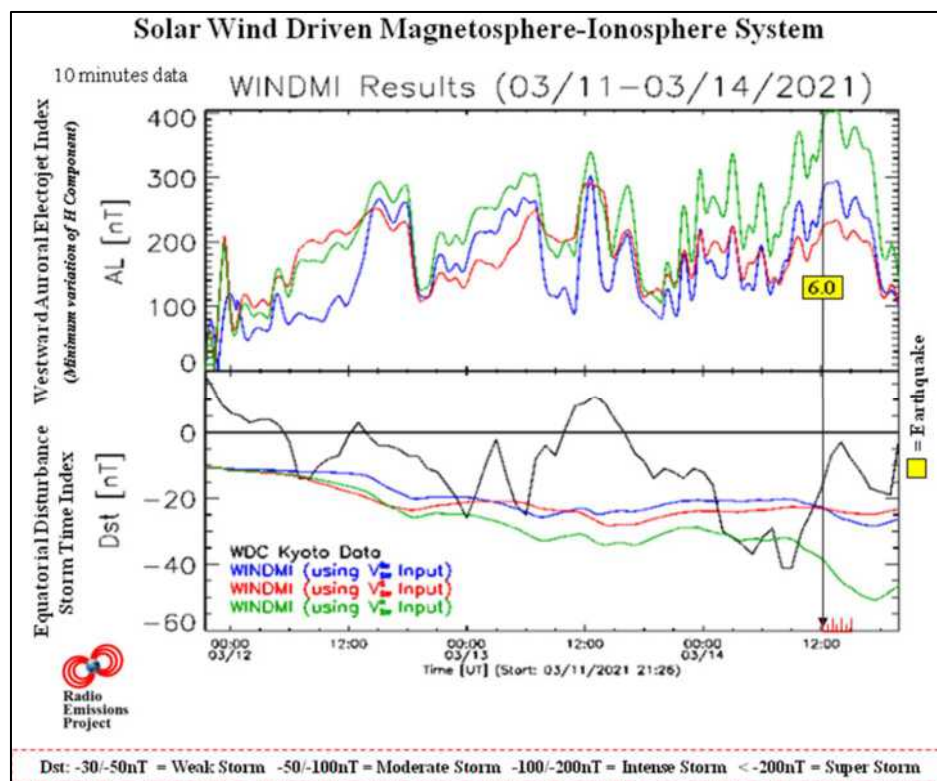


Fig. 4 – Low-dimensional model of the energy transfer from the solar wind through the magnetosphere and into the ionosphere (WINDMI). The picture shows the variation of the AL-Index (at top) and the DST-Index (at bottom) in the hours that preceded the M6.0 South Sandwich Islands region earthquake occurred on March 14, 2021 (the time marker of the earthquake is indicated by a vertical black line). The DST-Index is a direct measure of the Earth's geomagnetic horizontal (H) component variation due to the equatorial ring current, while the AL-Index (Auroral Lower) is at all times, the minimum value of the variation of the geomagnetic H component of the geomagnetic field recorded by observers of reference and provides a quantitative measure of global Westward Auroral Electrojet (WEJ) produced by increased of ionospheric currents therein present. Model developed by the Institute for Fusion Studies, Department of Physics, University of Texas at Austin. Credits: iSWA, USGS, Radio Emissions Project.

To confirm this type of correlation it is possible to observe Fig. 5 and 6: within Fig. 5 another type of Interplanetary Seismic Precursor is visible, represented by a perturbation of Interplanetary Magnetic Field (IMF): the potentially destructive seismic event was recorded after a vast disruption of IMF that began on March 12, 2021 at 12:00 UTC and ended few hours before the quake. In addition, the M6.0 earthquake occurred during a slight change in the IMF. This type of correlation was first observed by the authors between 2010 and 2011.

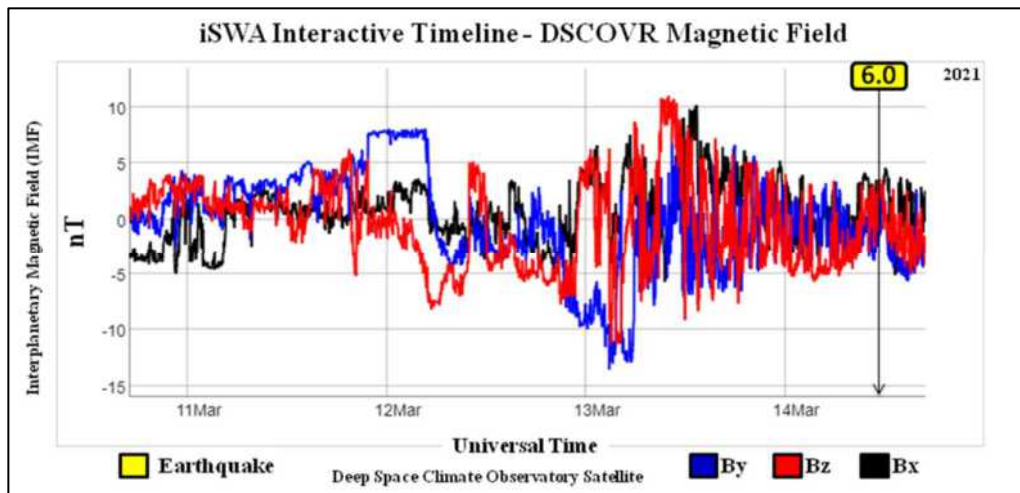


Fig. 5 – Solar wind magnetic field perturbation correlated to South Sandwich Islands region M6.0 earthquake. The chart above shows the variation of the interplanetary magnetic field (IMF) recorded through the Deep Space Climate Observatory (DSCOVR) Satellite in orbit at L1 Lagrange point. The recording was done on 3 axes (By, Bx, Bz). Analyzing the variation curves it is evident that the M6.0 earthquake occurred in South Sandwich Islands region on March 14, 2021 has been preceded by a perturbation of the interplanetary magnetic field (IMF) whose greater intensity was recorded between 02:30 UTC and 06:00 UTC of March 13, 2021. The long black vertical arrow represents the temporal markers of South Sandwich Islands region M6.0 earthquake recorded on March 14, 2021 at 12:05 UTC. Credits: iSWA, USGS, Radio Emissions Project.

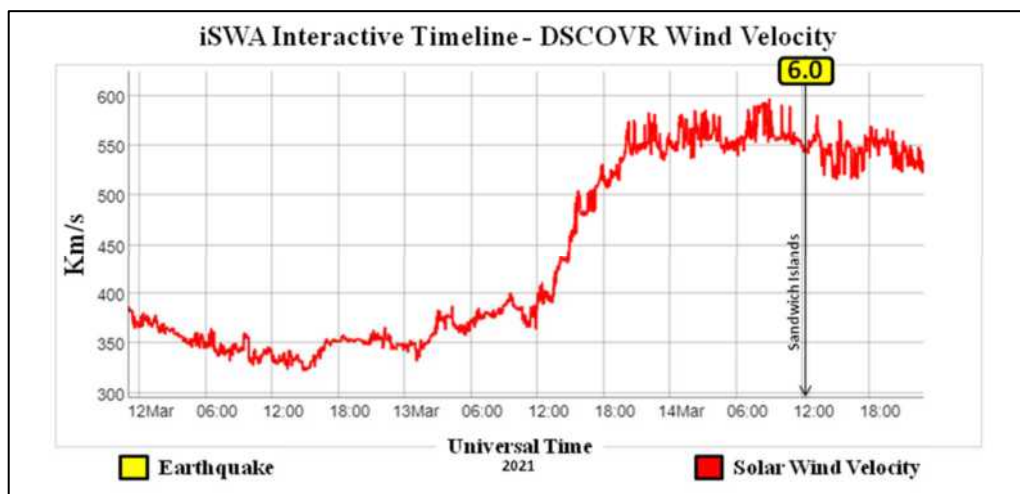


Fig. 6 – Solar wind velocity correlated to M6.0 earthquake. The graph shows the variation of solar wind velocity recorded between 12 and 14 March 2021 by Deep Space Climate Observatory (DSCOVR) Satellite, in orbit at L1 Lagrange point. Analyzing the variation curve it is possible to understand that the M6.5 South Sandwich Islands region earthquake was preceded by an increase of the solar wind speed. The black vertical arrow shows the temporal marker of the M6.0 earthquake occurred on March 14, 2021. Credits: iSWA, USGS, Radio Emissions Project.

Analyzing the curve of **Fig. 6**, however, we observe that the M6.0 earthquake recorded in the South Sandwich Islands region on March 14, 2021 was preceded by an increase in the solar wind speed which almost reached 600km/s a few hours earlier of the earthquake. The increase started on March 12, 2021 at 15:00 UTC. Also in this case we are faced with an “Interplanetary Seismic Precursor” or ISP.

Through the data that the authors presented in this work, it is evident that the M6.0 earthquake recorded in the South Sandwich Islands region was preceded by a series of clearly evident electromagnetic phenomena of a solar and geomagnetic nature that can be constantly monitored via the internet thanks to data provided by iSWA (iNTEGRATED SPACE WEATHER ANALYSIS SYSTEM). These electromagnetic phenomena occur according to a very precise modulation as they are the expression of solar activity and the impact it has on the earth’s magnetosphere [20] [23] [24].

Conclusions

The analysis of solar activity and the consequent geomagnetic activity of the Earth shows a close correlation between the density of the solar ion flux, the Earth's geomagnetic activity and the M6+ global seismic activity which is recorded on a global scale. We are therefore faced with a series of phenomena that are able to indicate when on a global scale it is possible to expect a resumption of potentially destructive seismic activity: this is the result of a study initiated by the authors in 2012 and which still continues. today confirming each time the close correlation that exists between the solar wind proton density increase and the M6+ seismic activity. Today, through this type of analysis it is possible to understand a few days in advance when it is possible to expect a resumption of potentially destructive seismic activity on a global scale.

Credits

- [1] G. Cataldi, D. Cataldi, V. Straser. (2013). Variations Of Terrestrial Geomagnetic Activity Correlated To M6+ Global Seismic Activity. EGU (European Geosciences Union) 2013, General Assembly, Seismology Section (SM3.1), Earthquake precursors, bio-anomalies prior to earthquakes and prediction, Geophysical Research Abstracts, Vol. 15. EGU2013-2617, Vienna, Austria. Harvard-Smithsonian Center for Astrophysics, High Energy Astrophysics Division, SAO/NASA Astrophysics Data System.
- [2] G. Cataldi, D. Cataldi and V. Straser. (2014). Earth's magnetic field anomalies that precede the M6+ global seismic activity. European Geosciences Union (EGU) General Assembly 2014, Geophysical Research Abstract, Vol. 16, EGU2014-1068, Vienna, Austria. Natural Hazard Section (NH4.3), Electro-magnetic phenomena and connections with seismo-tectonic activity, Harvard-Smithsonian Center for Astrophysics, High Energy Astrophysics Division, SAO/NASA Astrophysics Data System.
- [3] D. Cataldi, G. Cataldi and V. Straser. (2014). Variations of the Electromagnetic field that preceded the Peruvian M7.0 earthquake occurred on September 25, 2013. European Geosciences Union (EGU) General Assembly 2014, Geophysical Research Abstract, Vol. 16, EGU2014-1075, Natural Hazard Section (NH4.3), Electro-magnetic phenomena and connections with seismo-tectonic activity, Vienna, Austria. Harvard-Smithsonian Center for Astrophysics, High Energy Astrophysics Division, SAO/NASA Astrophysics Data System.
- [4] T. Rabeh, G. Cataldi, V. Straser. (2014). Possibility of coupling the magnetosphere-ionosphere during the time of earthquakes. European Geosciences Union (EGU) General Assembly 2014, Geophysical Research Abstract, Vol. 16, EGU2014-1067, Vienna, Austria. Natural Hazard Section (NH4.3), Electro-magnetic phenomena and connections with seismo-tectonic activity. Harvard-Smithsonian Center for Astrophysics, High Energy Astrophysics Division, SAO/NASA Astrophysics Data System.
- [5] V. Straser, G. Cataldi. (2014). Solar wind proton density increase and geomagnetic background anomalies before strong M6+ earthquakes. Space Research Institute of Moscow, Russian Academy of Sciences, MSS-14. 2014. Moscow, Russia. pp280-286.
- [6] V. Straser, G. Cataldi, D. Cataldi. (2015). Radio-anomalies: tool for earthquakes and tsunami forecasts. European Geosciences Union (EGU) General Assembly 2015, Natural Hazard Section (NH5.1), Sea & Ocean Hazard - Tsunami, Geophysical Research Abstract, Vol. 17, Vienna, Austria. Harvard-Smithsonian Center for Astrophysics, High Energy Astrophysics Division, SAO/NASA Astrophysics Data System.
- [7] V. Straser, G. Cataldi. (2015). Solar wind ionic variation associated with earthquakes greater than magnitude M6.0. New Concepts in Global Tectonics Journal, V. 3, No. 2, June 2015, Australia. P.140-154.
- [8] G. Cataldi, D. Cataldi, V. Straser. (2015). Solar wind proton density variations that preceded the M6+ earthquakes occurring on a global scale between 17 and 20 April 2014. European Geosciences Union (EGU) General Assembly 2015, Vienna, Austria. Natural Hazard Section (NH5.1), Sea & Ocean

Hazard - Tsunami, Geophysical Research Abstract, Vol. 17, EGU2015-4157-2, Harvard-Smithsonian Center for Astrophysics, High Energy Astrophysics Division, SAO/NASA Astrophysics Data System.

- [9] G. Cataldi, D. Cataldi, V. Straser. (2015). Solar wind ion density variations that preceded the M6+ earthquakes occurring on a global scale between 3 and 15 September 2013. European Geosciences Union (EGU) General Assembly 2015, Geophysical Research Abstract, Vol. 17, EGU2015-4581, Vienna, Austria. Natural Hazard Section (NH5.1), Sea & Ocean Hazard - Tsunami, Harvard-Smithsonian Center for Astrophysics, High Energy Astrophysics Division, SAO/NASA Astrophysics Data System.
- [10] G. Cataldi, D. Cataldi, V. Straser. (2015). Solar wind proton density variations that preceded the M6,1 earthquake occurred in New Caledonia on November 10, 2014. European Geosciences Union (EGU) General Assembly 2015, Geophysical Research Abstract, Vol. 17, EGU2015-4167, Vienna, Austria. Natural Hazard Section (NH5.1), Sea & Ocean Hazard - Tsunami, Harvard-Smithsonian Center for Astrophysics, High Energy Astrophysics Division, SAO/NASA Astrophysics Data System.
- [11] V. Straser, G. Cataldi, D. Cataldi. (2015). Solar wind ionic and geomagnetic variations preceding the Md8.3 Chile Earthquake. *New Concepts in Global Tectonics Journal*, V. 3, No. 3, September 2015, Australia. P.394-399.
- [12] G. Cataldi, D. Cataldi, V. Straser. (2016). Solar activity correlated to the M7.0 Japan earthquake occurred on April 15, 2016. *New Concepts in Global Tectonics Journal*, V. 4, No. 2, pp202-208, June 2016.
- [13] G. Cataldi, D. Cataldi, V. Straser. (2016). Tsunami related to solar and geomagnetic activity. European Geosciences Union (EGU) General Assembly 2016, Natural Hazard Section (NH5.6), Complex modeling of earthquake, landslide, and volcano tsunami sources. Geophysical Research Abstract, Vol. 18, EGU2016-9626, Vienna, Austria. Harvard-Smithsonian Center for Astrophysics, High Energy Astrophysics Division, SAO/NASA Astrophysics Data System.
- [14] G. Cataldi, D. Cataldi, V. Straser. (2017). SELF-VLF electromagnetic signals and solar wind proton density variations that preceded the M6.2 Central Italy earthquake on August 24, 2016. *International Journal of Modern Research in Electrical and Electronic Engineering*, Vol. 1, No. 1, 1-15. DOI: 10.20448/journal.526/2017.1.1/526.1.1.15. Harvard-Smithsonian Center for Astrophysics, High Energy Astrophysics Division, SAO/NASA Astrophysics Data System.
- [15] G. Cataldi, D. Cataldi, V. Straser. (2017). Solar and Geomagnetic Activity Variations Correlated to Italian M6+ Earthquakes Occurred in 2016. European Geosciences Union (EGU), General Assembly 2017. Geophysical Research Abstracts Vol. 19, EGU2017-3681, 2017. Seismology (SM1.2)/Natural Hazards (NH4.7)/Tectonics & Structural Geology (TS5.5) The 2016 Central Italy Seismic sequence: overview of data analyses and source models. Harvard-Smithsonian Center for Astrophysics, High Energy Astrophysics Division, SAO/NASA Astrophysics Data System.
- [16] G. Cataldi, D. Cataldi, V. Straser. (2017). Solar wind proton density increase that preceded Central Italy earthquakes occurred between 26 and 30 October 2016. European Geosciences Union (EGU), General Assembly 2017. Geophysical Research Abstracts Vol. 19, EGU2017-3774, 2017. Seismology (SM1.2)/Natural Hazards (NH4.7)/Tectonics & Structural Geology (TS5.5) The 2016 Central Italy Seismic sequence: overview of data analyses and source models. Harvard-Smithsonian Center for Astrophysics, High Energy Astrophysics Division, SAO/NASA Astrophysics Data System.
- [17] V. Straser, G. Cataldi, D. Cataldi. (2017). Solar and electromagnetic signal before Mexican Earthquake M8.1, September 2017. *New Concepts in Global Tectonics Journal*, V. 5, No. 4, December 2017, pp. 600-609.
- [18] G. Cataldi, D. Cataldi, V. Straser. (2017). Solar and Geomagnetic Activity Variations Correlated to Italian M6+Earthquakes Occurred in 2016. EGU General Assembly 2017. EGU2017-3681, Vol. 19.

- [19] G. Cataldi, D. Cataldi, V. Straser. (2019). Solar wind ionic density variations related to M6+ global seismic activity between 2012 and 2018. European Geosciences Union (EGU) General Assembly 2019, Short-term Earthquake Forecast (StEF) and multy-parametric time-Dependent Assessment of Seismic Hazard (t-DASH) (NH4.3/AS4.62/EMRP2.40/ESSI1.7/Gi2.13/SM3.9), General Contribution on Earthquakes, Earth Structure, Seismology (SM1.1), Geophysical Research Abstract, Vol. 21, EGU2019-3067, 2019, Vienna, Austria. Harvard-Smithsonian Center for Astrophysics, High Energy Astrophysics Division, SAO/NASA Astrophysics Data System.
- [20] G. Cataldi. (2020). Precursori Sismici – Monitoraggio Elettromagnetico. Kindle-Amazon, ISBN: 9798664537970. ASIN Code: B08CPDBGX9.
- [21] G. Cataldi, D. Cataldi, V. Straser. (2019). Wolf Number Related To M6+ Global Seismic Activity. New Concepts in Global Tectonics Journal, Volume 7, Number 3, December 2019, pp. 178-186.
- [22] V. Straser, G. Cataldi, D. Cataldi. (2020). The Space Weather Related to the M7+ Seismic Activity Recorded on a Global Scale between 28 January and 25 March 2020. Acta Scientific Agriculture 4.12 (2020): 55-62.
- [23] G. Cataldi, V. Straser, D. Cataldi. (2020). Space Weather related to potentially destructive seismic activity recorded on a global scale. New Concepts in Global Tectonics Journal. Vol.8, No.3, pp. 233-253, December 2020. ISSN 2202-0039.
- [24] G. Cataldi. (2021). Radio Emissions Project – A new approach to seismic prediction. Kindle-Amazon, ISBN: 9798709593411.

Space weather and geomagnetic activity related to the Vanuatu M6.3 earthquake recorded on March 20, 2019

Gabriele Cataldi¹, Daniele Cataldi¹⁻², Valentino Straser³

- (1) Radio Emissions Project (I). ltpaobserverproject@gmail.com
- (2) Fondazione Permanente G. Giuliani - Onlus (I). danielle77c@hotmail.it
- (3) Department of Science and Environment UPKL Brussel (B). valentino.straser@gmail.com

Abstract

On March 20, 2019 at 15:23:58 UTC, an M6.3 earthquake was recorded in Vanuatu at a depth of 119 km. The analysis of solar activity and terrestrial geomagnetic activity allowed the authors to verify that the M6.3 Vanuatu earthquake was preceded by an increase in solar activity (solar wind proton density increase; Interplanetary Seismic Precursor) and in terrestrial geomagnetic activity (Seismic Geomagnetic Precursor). This type of correlation was first observed by the authors in 2011 and is currently related to all potentially destructive seismic events recorded on a global scale from January 1, 2012 to date.

Keywords: proton density increase, seismic precursors, solar activity, geomagnetic activity.

Introduction

The eastern edge of the Australian plate is one of the most seismically active areas in the world due to the high convergence rates between the Australian and Pacific plates. In this tectonic context, on March 20, 2019 at 15:23:58 UTC, an M6.3 earthquake was recorded in Vanuatu (**Fig. 1**).

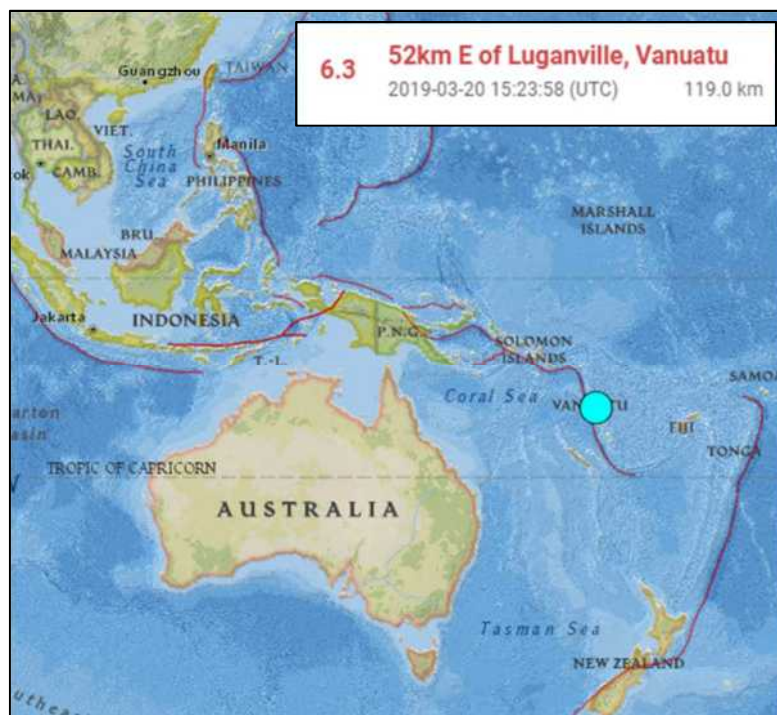


Fig. 1 – Epicenter of the M6.3 Vanuatu earthquake. The image above shows the map of the M6.3 Vanuatu earthquake epicenter recorded on March 20, 2019 at 15:23:58 UTC and at a depth of 119 km. Credits: USGS, Radio Emissions Project.

The monitoring of solar activity and terrestrial geomagnetic activity allowed the authors to verify that the potentially destructive seismic activity that is recorded on a global scale is always preceded by a solar wind proton density increase and, due to the impact that has the solar wind on the Earth's magnetosphere, also by a consequent increase in the Earth's geomagnetic activity [1-24]. In this work, the results of the close

correlation that the authors found between the M6.3 earthquake and solar and geomagnetic activity will be presented.

Data analysis

Analyzing the data on the modulation of the solar ion flux density provided by DSCOVR Satellite (located in the Lagrangian point L1) between 17 and 21 March 2019, the authors found that the Vanuatu M6.3 earthquake was preceded by a major solar wind proton density increase which started on March 17, 2019 at 11:30 and ended on March 21, 2019 at 12:00 UTC: the solar wind proton density increase preceded the Vanuatu M6.3 seismic event by approximately 76 hours. The maximum increment of protonic density was recorded on March 19, 2019 at 08:23 UTC, and preceded the seismic event by 17 hours (**Fig. 2**).

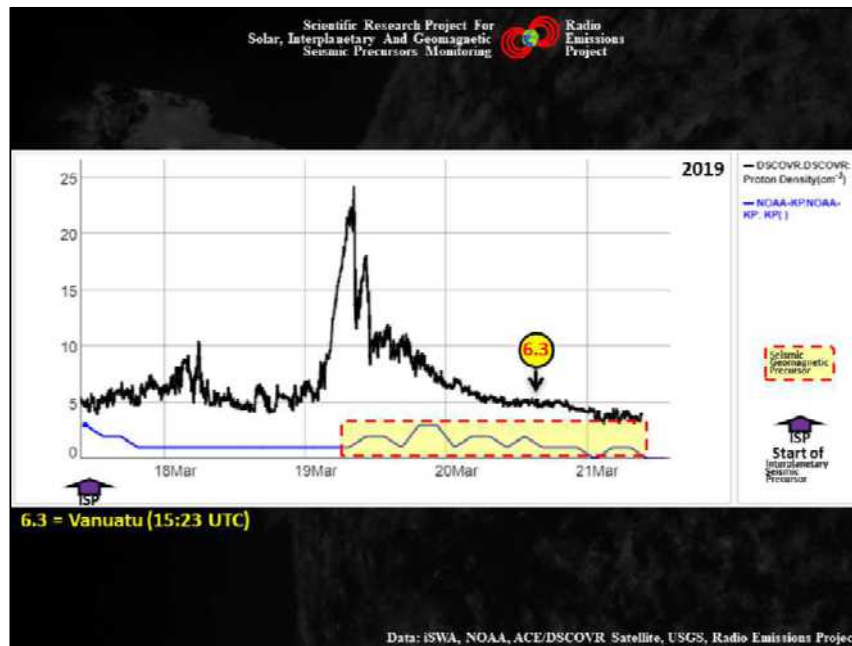


Fig. 2 – Interplanetary and Geomagnetic Seismic Precursors related to Vanuatu M6.3 earthquake. The graph above shows the variation curves of the solar wind proton density (black curve) and the geomagnetic activity (blue curve, highlighted by the yellow area) on which the time marker of Vanuatu M6.3 earthquake (recorded on March 20, 2019 at 15:23 UTC) has been superimposed. Credits: USGS, Radio Emissions Project.

The beginning of the proton increase was identified by detecting the lower level of proton density present on the variation curve: this can correspond to the basal level present in the interplanetary medium during solar quiet, or it can correspond to the variation line present between two close increases and therefore, it may also not correspond to the actual basal level. The studies conducted by the authors also highlighted that the time interval that separates the seismic event from the starting point of proton density increase can undergo variations in relation to the type of measurement that is taken as a reference: the measurement in p/cm^3 generally determines time intervals earlier than the measurement in $p/(cm^2\text{-sec}\text{-ster}\text{-MeV})$. Furthermore, other differences can be determined by taking as reference a certain fraction of protons energy respect that other [20]. The average time interval (which separates the solar wind proton density starting point and the seismic event) calculated by analyzing the seismic activity and the solar activity that occurred between January 1, 2012 and March 4, 2021 is equal to 108.8 hours: the average was calculated by analyzing 1193 M6+ seismic events that occurred in the same period.

Other important results were obtained by analyzing the Earth's geomagnetic activity that preceded the M6.3 earthquake (**Fig. 3**): confirming the solar wind proton density increase, the Vanuatu M6.3 earthquake was preceded by an evident increase in intensity of the Earth's magnetic field measured on the vector component "H" which touched 330nT; while a second increase in Earth's geomagnetic activity accompanied the M6.3 earthquake. The main geomagnetic increase preceded the Vanuatu M6.3 earthquake by about 30 hours.

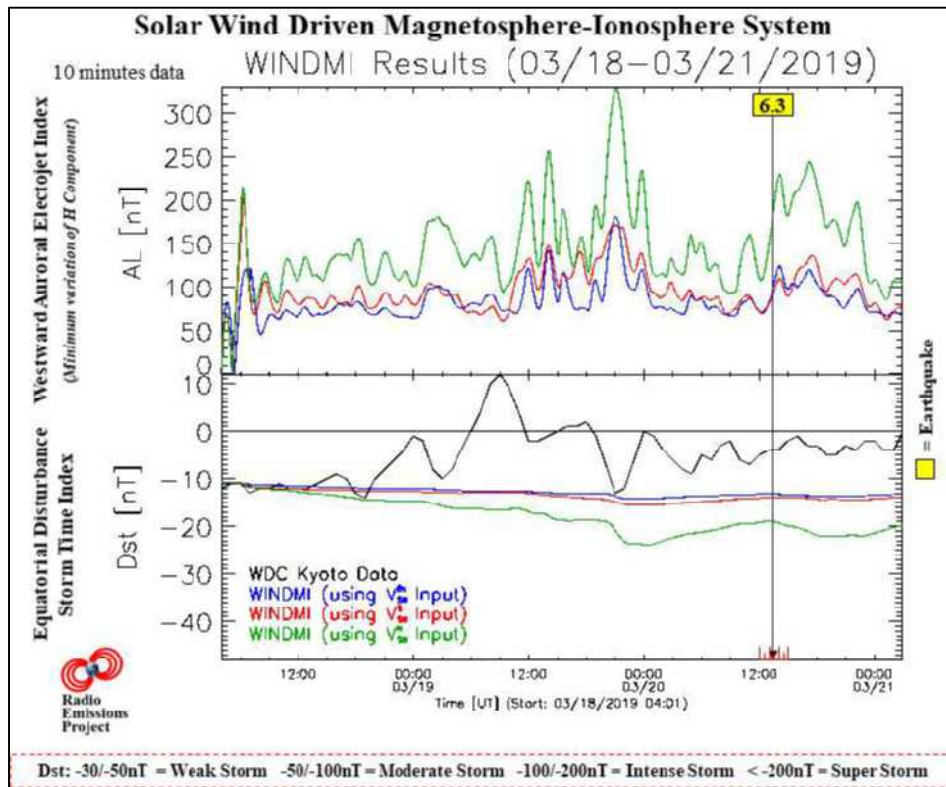


Fig. 3 – Low-dimensional model of the energy transfer from the solar wind through the magnetosphere and into the ionosphere (WINDMI). The picture shows the variation of the AL-Index (at top) and the DST-Index (at bottom) in the hours that preceded the Vanuatu M6.3 earthquake occurred on March 20, 2019 (the time marker of the earthquake is indicated by a vertical black line). The DST-Index is a direct measure of the Earth’s geomagnetic horizontal (H) component variation due to the equatorial ring current, while the AL-Index (Auroral Lower) is at all times, the minimum value of the variation of the geomagnetic H component of the geomagnetic field recorded by observers of reference and provides a quantitative measure of global Westward Auroral Electrojet (WEJ) produced by increased of ionospheric currents therein present. Model developed by the Institute for Fusion Studies, Department of Physics, University of Texas at Austin. Credits: iSWA, USGS, Radio Emissions Project.

In addition, the curve relating to the DST Index showed a slight decline about 17 hours before the seismic event M6.3 confirming the presence of a pre-seismic geomagnetic perturbation.

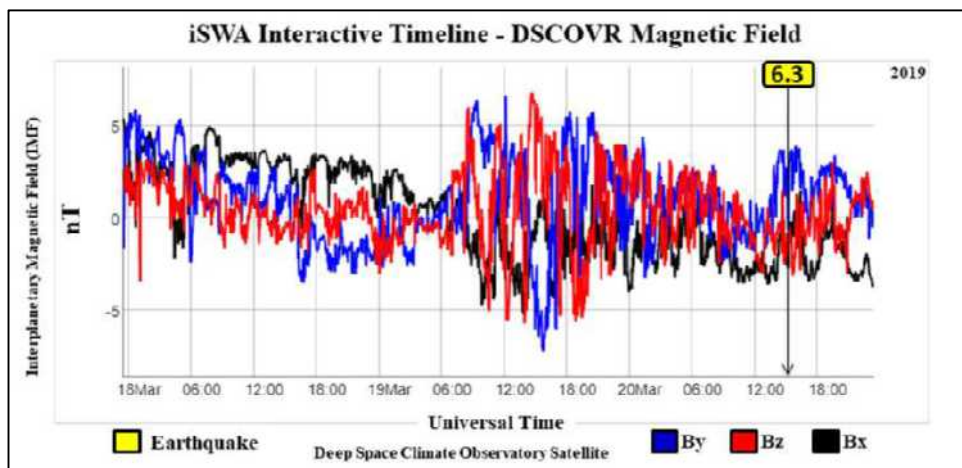


Fig. 4 – Interplanetary Magnetic Field (IMF) related to M7.1 Japan earthquake. The graph above shows a disturbance of Interplanetary Magnetic Field (IMF) which preceded the Vanuatu M6.3 earthquake recorded on March 20, 2019 (black vertical arrow) by almost 33 hours. Credits: iSWA, USGS, Radio Emissions Project.

Further confirmation of the observed correlation between the variation of the solar ion flux density and the M6.3 seismic event can be observed by the variation of Interplanetary Magnetic Field (**Fig. 4**): the potentially destructive earthquake was preceded by a perturbation of Interplanetary Magnetic Field which

occurred about 33 hours before the earthquake; while a second and slight increase accompanied the seismic event.

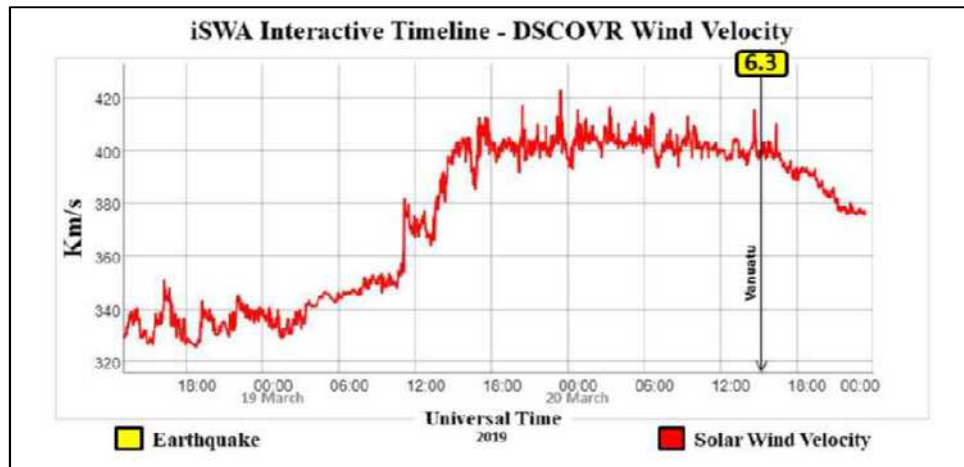


Fig. 5 – Solar wind velocity related to Vanuatu M6.3 earthquake. The graph above shows a rapid increase in the speed of the solar wind that preceded the Vanuatu M6.3 earthquake recorded on March 20, 2019 (black vertical arrow). Credits: iSWA, USGS, Radio Emissions Project.

A perturbation of Interplanetary Magnetic Field (IMF) is usually associated with an increase in the speed of the solar wind: the electrically charged particles that compose it, having a greater speed, determine a greater magnetic field in interplanetary space. Thanks to this electromagnetic mechanism, it is also possible to correlate potentially destructive seismic activity at solar wind velocity increase (**Fig. 5**), but this does not always happen. An increase in solar wind speed preceded the Vanuatu M6.3 earthquake by approximately 36 hours (**Fig. 5**).

Conclusions

Over the last ten years, the authors were able to identify a “certain” earthquake precursor that is able to predict when a resumption of M6+ global seismic activity is expected on our planet: we are talking about the increases in the proton density of the solar wind. The correlation data that have been presented in this work regarding the M6.3 earthquake recorded in Vanuatu in 2019 are only a very small part of the data related to the 1193 M6+ seismic events recorded on a global scale between January 1, 2012 and March 4, 2021 (corresponding to 100% of the M6+ seismic events recorded on a global scale in the same period): seismic events that were preceded by a solar wind proton density increase [5] [7] [8] [9] [10] [11] [12] [14] [15] [16] [17] [18] [19] [20] [21] [22] [23] [24].

Credits

- [1] G. Cataldi, D. Cataldi, V. Straser. (2013). Variations Of Terrestrial Geomagnetic Activity Correlated To M6+ Global Seismic Activity. EGU (European Geosciences Union) 2013, General Assembly, Seismology Section (SM3.1), Earthquake precursors, bio-anomalies prior to earthquakes and prediction, Geophysical Research Abstracts, Vol. 15. EGU2013-2617, Vienna, Austria. Harvard-Smithsonian Center for Astrophysics, High Energy Astrophysics Division, SAO/NASA Astrophysics Data System.
- [2] G. Cataldi, D. Cataldi and V. Straser. (2014). Earth’s magnetic field anomalies that precede the M6+ global seismic activity. European Geosciences Union (EGU) General Assembly 2014, Geophysical Research Abstract, Vol. 16, EGU2014-1068, Vienna, Austria. Natural Hazard Section (NH4.3), Electromagnetic phenomena and connections with seismo-tectonic activity, Harvard-Smithsonian Center for Astrophysics, High Energy Astrophysics Division, SAO/NASA Astrophysics Data System.
- [3] D. Cataldi, G. Cataldi and V. Straser. (2014). Variations of the Electromagnetic field that preceded the Peruvian M7.0 earthquake occurred on September 25, 2013. European Geosciences Union (EGU)

General Assembly 2014, Geophysical Research Abstract, Vol. 16, EGU2014-1075, Natural Hazard Section (NH4.3), Electro-magnetic phenomena and connections with seismo-tectonic activity, Vienna, Austria. Harvard-Smithsonian Center for Astrophysics, High Energy Astrophysics Division, SAO/NASA Astrophysics Data System.

- [4] T. Rabeh, G. Cataldi, V. Straser. (2014). Possibility of coupling the magnetosphere–ionosphere during the time of earthquakes. European Geosciences Union (EGU) General Assembly 2014, Geophysical Research Abstract, Vol. 16, EGU2014-1067, Vienna, Austria. Natural Hazard Section (NH4.3), Electro-magnetic phenomena and connections with seismo-tectonic activity. Harvard-Smithsonian Center for Astrophysics, High Energy Astrophysics Division, SAO/NASA Astrophysics Data System.
- [5] V. Straser, G. Cataldi. (2014). Solar wind proton density increase and geomagnetic background anomalies before strong M6+ earthquakes. Space Research Institute of Moscow, Russian Academy of Sciences, MSS-14. 2014. Moscow, Russia. pp280-286.
- [6] V. Straser, G. Cataldi, D. Cataldi. (2015). Radio-anomalies: tool for earthquakes and tsunami forecasts. European Geosciences Union (EGU) General Assembly 2015, Natural Hazard Section (NH5.1), Sea & Ocean Hazard - Tsunami, Geophysical Research Abstract, Vol. 17, Vienna, Austria. Harvard-Smithsonian Center for Astrophysics, High Energy Astrophysics Division, SAO/NASA Astrophysics Data System.
- [7] V. Straser, G. Cataldi. (2015). Solar wind ionic variation associated with earthquakes greater than magnitude M6.0. *New Concepts in Global Tectonics Journal*, V. 3, No. 2, June 2015, Australia. P.140-154.
- [8] G. Cataldi, D. Cataldi, V. Straser. (2015). Solar wind proton density variations that preceded the M6+ earthquakes occurring on a global scale between 17 and 20 April 2014. European Geosciences Union (EGU) General Assembly 2015, Vienna, Austria. Natural Hazard Section (NH5.1), Sea & Ocean Hazard - Tsunami, Geophysical Research Abstract, Vol. 17, EGU2015-4157-2, Harvard-Smithsonian Center for Astrophysics, High Energy Astrophysics Division, SAO/NASA Astrophysics Data System.
- [9] G. Cataldi, D. Cataldi, V. Straser. (2015). Solar wind ion density variations that preceded the M6+ earthquakes occurring on a global scale between 3 and 15 September 2013. European Geosciences Union (EGU) General Assembly 2015, Geophysical Research Abstract, Vol. 17, EGU2015-4581, Vienna, Austria. Natural Hazard Section (NH5.1), Sea & Ocean Hazard - Tsunami, Harvard-Smithsonian Center for Astrophysics, High Energy Astrophysics Division, SAO/NASA Astrophysics Data System.
- [10] G. Cataldi, D. Cataldi, V. Straser. (2015). Solar wind proton density variations that preceded the M6.1 earthquake occurred in New Caledonia on November 10, 2014. European Geosciences Union (EGU) General Assembly 2015, Geophysical Research Abstract, Vol. 17, EGU2015-4167, Vienna, Austria. Natural Hazard Section (NH5.1), Sea & Ocean Hazard - Tsunami, Harvard-Smithsonian Center for Astrophysics, High Energy Astrophysics Division, SAO/NASA Astrophysics Data System.
- [11] V. Straser, G. Cataldi, D. Cataldi. (2015). Solar wind ionic and geomagnetic variations preceding the Md8.3 Chile Earthquake. *New Concepts in Global Tectonics Journal*, V. 3, No. 3, September 2015, Australia. P.394-399.
- [12] G. Cataldi, D. Cataldi, V. Straser. (2016). Solar activity correlated to the M7.0 Japan earthquake occurred on April 15, 2016. *New Concepts in Global Tectonics Journal*, V. 4, No. 2, pp202-208, June 2016.
- [13] G. Cataldi, D. Cataldi, V. Straser. (2016). Tsunami related to solar and geomagnetic activity. European Geosciences Union (EGU) General Assembly 2016, Natural Hazard Section (NH5.6), Complex modeling of earthquake, landslide, and volcano tsunami sources. Geophysical Research Abstract, Vol.

18, EGU2016-9626, Vienna, Austria. Harvard-Smithsonian Center for Astrophysics, High Energy Astrophysics Division, SAO/NASA Astrophysics Data System.

- [14] G. Cataldi, D. Cataldi, V. Straser. (2017). SELF-VLF electromagnetic signals and solar wind proton density variations that preceded the M6.2 Central Italy earthquake on August 24, 2016. *International Journal of Modern Research in Electrical and Electronic Engineering*, Vol. 1, No. 1, 1-15. DOI: 10.20448/journal.526/2017.1.1/526.1.1.15. Harvard-Smithsonian Center for Astrophysics, High Energy Astrophysics Division, SAO/NASA Astrophysics Data System.
- [15] G. Cataldi, D. Cataldi, V. Straser. (2017). Solar and Geomagnetic Activity Variations Correlated to Italian M6+ Earthquakes Occurred in 2016. *European Geosciences Union (EGU), General Assembly 2017. Geophysical Research Abstracts Vol. 19, EGU2017-3681, 2017. Seismology (SM1.2)/Natural Hazards (NH4.7)/Tectonics & Structural Geology (TS5.5) The 2016 Central Italy Seismic sequence: overview of data analyses and source models.* Harvard-Smithsonian Center for Astrophysics, High Energy Astrophysics Division, SAO/NASA Astrophysics Data System.
- [16] G. Cataldi, D. Cataldi, V. Straser. (2017). Solar wind proton density increase that preceded Central Italy earthquakes occurred between 26 and 30 October 2016. *European Geosciences Union (EGU), General Assembly 2017. Geophysical Research Abstracts Vol. 19, EGU2017-3774, 2017. Seismology (SM1.2)/Natural Hazards (NH4.7)/Tectonics & Structural Geology (TS5.5) The 2016 Central Italy Seismic sequence: overview of data analyses and source models.* Harvard-Smithsonian Center for Astrophysics, High Energy Astrophysics Division, SAO/NASA Astrophysics Data System.
- [17] V. Straser, G. Cataldi, D. Cataldi. (2017). Solar and electromagnetic signal before Mexican Earthquake M8.1, September 2017. *New Concepts in Global Tectonics Journal*, V. 5, No. 4, December 2017, pp. 600-609.
- [18] G. Cataldi, D. Cataldi, V. Straser. (2017). Solar and Geomagnetic Activity Variations Correlated to Italian M6+Earthquakes Occurred in 2016. *EGU General Assembly 2017. EGU2017-3681, Vol. 19.*
- [19] G. Cataldi, D. Cataldi, V. Straser. (2019). Solar wind ionic density variations related to M6+ global seismic activity between 2012 and 2018. *European Geosciences Union (EGU) General Assembly 2019, Short-term Earthquake Forecast (StEF) and multy-parametric time-Dependent Assessment of Seismic Hazard (t-DASH) (NH4.3/AS4.62/EMRP2.40/ESSI1.7/Gi2.13/SM3.9), General Contribution on Earthquakes, Earth Structure, Seismology (SM1.1), Geophysical Research Abstract, Vol. 21, EGU2019-3067, 2019, Vienna, Austria.* Harvard-Smithsonian Center for Astrophysics, High Energy Astrophysics Division, SAO/NASA Astrophysics Data System.
- [20] G. Cataldi. (2020). *Precursori Sismici – Monitoraggio Elettromagnetico.* Kindle-Amazon, ISBN: 9798664537970. ASIN Code: B08CPDBGX9.
- [21] G. Cataldi, D. Cataldi, V. Straser. (2019). Wolf Number Related To M6+ Global Seismic Activity. *New Concepts in Global Tectonics Journal*, Volume 7, Number 3, December 2019, pp. 178-186.
- [22] V. Straser, G. Cataldi, D. Cataldi. (2020). The Space Weather Related to the M7+ Seismic Activity Recorded on a Global Scale between 28 January and 25 March 2020. *Acta Scientific Agriculture* 4.12 (2020): 55-62.
- [23] G. Cataldi, V. Straser, D. Cataldi. (2020). Space Weather related to potentially destructive seismic activity recorded on a global scale. *New Concepts in Global Tectonics Journal*. Vol.8, No.3, pp. 233-253, December 2020. ISSN 2202-0039.
- [24] G. Cataldi. (2021). *Radio Emissions Project – A new approach to seismic prediction.* Kindle-Amazon, ISBN: 9798709593411.

Possible quake-related, pre-seismic impulses near 10 and 15 Hz that were not recorded by a 1 Hz seismometer.

John Ricken Wright

Emeritus Professor of Chemistry, Southeastern Oklahoma State University, Durant, Oklahoma

Email: cotterobservatory403@gmail.com

ABSTRACT

Fourier Transformation of the FM time domain signals coming from a Lehman seismometer creates a bipolar spectrum of frequencies between 0.5 and 30 Hz and thus completely separates the intended (1.0 Hz) resonant signal from the parasitic frequencies. The highest frequency parasitic resonance, found at + and - 15.7 Hz relative to the seismic baseline, was strong enough that it amounted to a short period seismometer channel. During the distinctly seismoelectromagnetic (SEM) event near Bardwell KY on 2017-03-19, both before and after the 3.2 magnitude earthquake at 14:25:12 UTC, the 15.7 Hz channel picked up seismic impulses similar to the ELF outbursts, which also showed a staggered relationship with some of the ELF signals, thus indicating possible intimate connectivity. There was also some minimal pre-quake seismic activity at the 10.1 Hz parasitic frequency. The 15.7 Hz seismic impulses began at least 28 minutes before the earthquake, while the ELF outbursts at 20.3 Hz began approximately 11 minutes before the quake. The 10.1 Hz seismic impulses began within five minutes of the oncoming quake's p-wave. These short period seismic signals have not been recorded before or since the Bardwell SEM event, thus should be considered as possible earthquake precursor signals. The peculiar strobing recorded during the Bardwell event was also unique and has not been observed before or since.

Key Words and Phrases

Seismoelectromagnetic (SEM) event, short period seismometry, New Madrid Seismic Zone, slow quakes, ELF, strobing, pre-quake signals, intraplate earthquake.

Introduction

Multivariable seismometry, as conceived [1], envisioned comparing *at least* two variables, one *always* being a seismic signal, and another one, coded as frequency or amplitude, on a frequency versus time versus intensity recording. In fact, possibly as many as five or six other signals, sufficiently dispersed in frequency, could fit into such a recording. The method is not proposed as a means for detecting oncoming earthquakes (not at this point), but rather, as a research tool for studying the relationships between earthquakes and possible pre-quake phenomena, including correlations among the various pre-quake variables under consideration.

When the prototype instrument detected pre-rupture, Schumann resonance-like outbursts associated with a small (3.2 magnitude) New Madrid Seismic Zone earthquake on 2019-03-19, there were *two* variables in addition to the seismic one: e.g., electric field changes, recorded as vertical discontinuities of the seismic baseline along the frequency axis, and

the recorded series of ELF outbursts very near the third Schumann resonance frequency. The latter were detected using the overland wiring and less than linear transformers of the power grid as, respectively, antennas and heterodyne mixers of an ELF radio receiver. The detected ELF outbursts near 20.3 Hz were recorded as sum and difference frequencies relative to the higher harmonics of the U.S. power grid's 60 Hz operating frequency, for example, 2160 or 2220 Hz. The recordings *usually* plot the latter harmonic reference frequencies, and they are a kind of baseline. All three variables proved to be of value for interpreting the data from the seismoelectromagnetic event in 2017 [1] near Bardwell KY.

Some of the information in the original paper [1] has not been fully analyzed, and it is about variables probably worth including in the recordings. It is well-known that Fourier transformation of the time domain signals from a Lehman-type mass balance finds not only the intended frequency, in this case 1.0 Hz, but also several parasitic frequencies [2]. The 15.7 Hz resonance became of interest because it detected seismic impulses, similar to the ELF outbursts, that were not seen in the 1.0 Hz part of the seismic recording. Some of the ELF and 15.7 Hz seismic signals could be intimately related.

Experimental Methods

The intended resonant frequency of the prototype instrument is 1.0 Hz, and its bipolar, Fourier transform spectrum of stronger parasitic resonances includes 3.0, 7.6, 10.1 and 15.7 Hz [2]; The resonance at 3.0 Hz was found to be a transverse vibration of the instrument's spring, but the sources of the other modes are still uncertain. Details of the instrument, its controls and a simple interface to a computer are found in [1]. Fourier transform analysis has other advantages, especially going to a 2D display; it spreads the noise out and thus improves the signal to noise ratio.

The 15.7 Hz recordings of interest are in Figs. 1 - 3, and their signal gain had been increased *after* an instrument adjustment. This had the effect of suppressing the 60 Hz harmonic at 2160 Hz while enhancing the four parasitic seismic frequencies of Fig. 2.

Seismic signals show up as sum and difference pairs, thus are found symmetrically above and below the seismic baseline. They are created in the FM modulator of the seismic instrument, i.e., the CD4046BE integrated circuit [1; see pages 218 to 220]. Electromagnetic signals in the ELF (3 to 30 Hz) and sub-ELF (0.5 to 3 Hz) range also show up as sum and difference pairs, but are symmetrically above and below the higher harmonics of 60 Hz, such as 2160 Hz. These heterodyne products are created in the stepdown transformers of the American power grid.

Results and Discussion

The parasitic resonances at + and - 15.7 Hz detected seismic impulses well-before the rupture event. In Fig. 1 a sequence of three modest seismic impulses at the 15.7 Hz parasitic frequency (circled dark blue) began about 28 minutes before the actual earthquake. Two more seismic impulses also happened at the 15.7 Hz parasitic frequency about two minutes before the quake's p-wave (Fig. 2), and another weak impulse at that frequency followed the quake by about 12 minutes (Fig. 3).

There is also a weak, noise-like line of lesser impulses paralleling the seismic baseline, i.e., displaced by + and - 15.7 Hz from that baseline and thus following the baseline's thermal undulations. The line of impulses is more noticeable around the second circled impulse of Fig. 1 and the one modest impulse of Fig. 3; these might be an example of the *stick-slip phenomenon* [3]. The signals were absent on days before and after the day of the earthquake; in fact, I have only noticed them in the time frame of the 2017-03-19 (Bardwell) event. There is thus good reason to suspect that they are associated with that earthquake.

The red rectangles (Fig. 2) enclose an extended, Type 2 ELF signal, symmetrical about 2160 Hz. Such ELF signals may also derive from the *stick-slip phenomenon*.

Similar seismic signals were not observed along the + or - 1.0 Hz pair near the seismic baseline, or the + or - 3.0 Hz or + or - 7.6 Hz pairs, but weak outbursts at 10.1 Hz did occur more than four minutes before the seismic rupture signal arrived. A Type 2 ELF emission, enclosed in the red rectangles in Fig. 2, started about five minutes before the arriving p-wave [See Ref. 1, at the bottom of p227]. The weak 10.1 Hz features are enclosed in dark blue rectangles in Fig. 2. The vertical, aqua green line in Fig. 2, i.e., the p-wave, marks the arrival of the signal from the quake's seismic rupture [4].

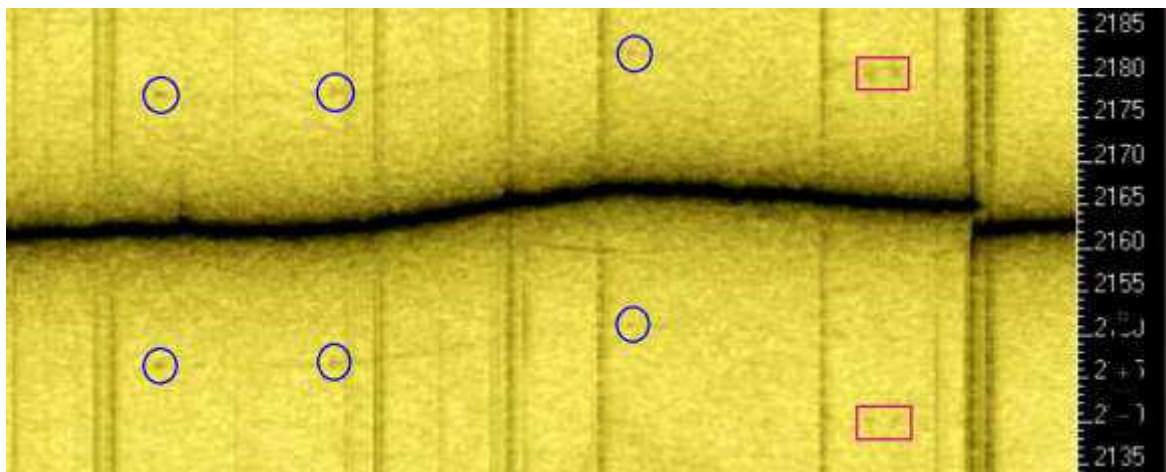


**Fig. 1 - Preceding the earthquake. Tilt the laptop display away from your eyes for better contrast).
Red rectangles enclose ELF emissions. Blue circles enclose seismic events.**

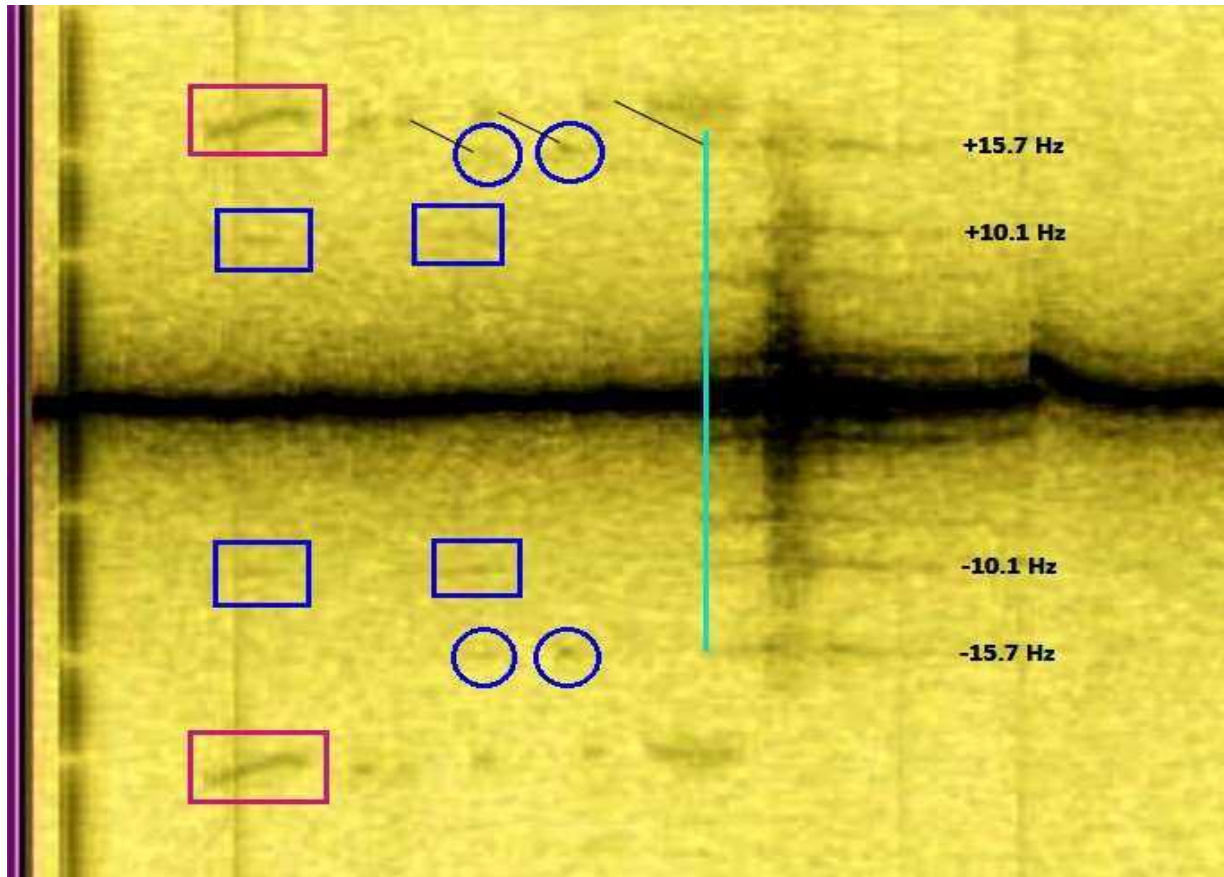


Fig. 2 - Just Before the Seismic Rupture. The thin, black diagonal tie lines show possible intimate connectivities of ELF outbursts and +15.7 Hz seismic impulses. The tie lines are not exactly parallel because the 2160 Hz signal carrier wanders a little in frequency. Figs. 1 - 3 are contrast enhanced recordings of the New Madrid 2017-03-19 14:25:12 UTC event. The 2160 Hz harmonic of 60 Hz is suppressed in these recordings. Usually it is shown.

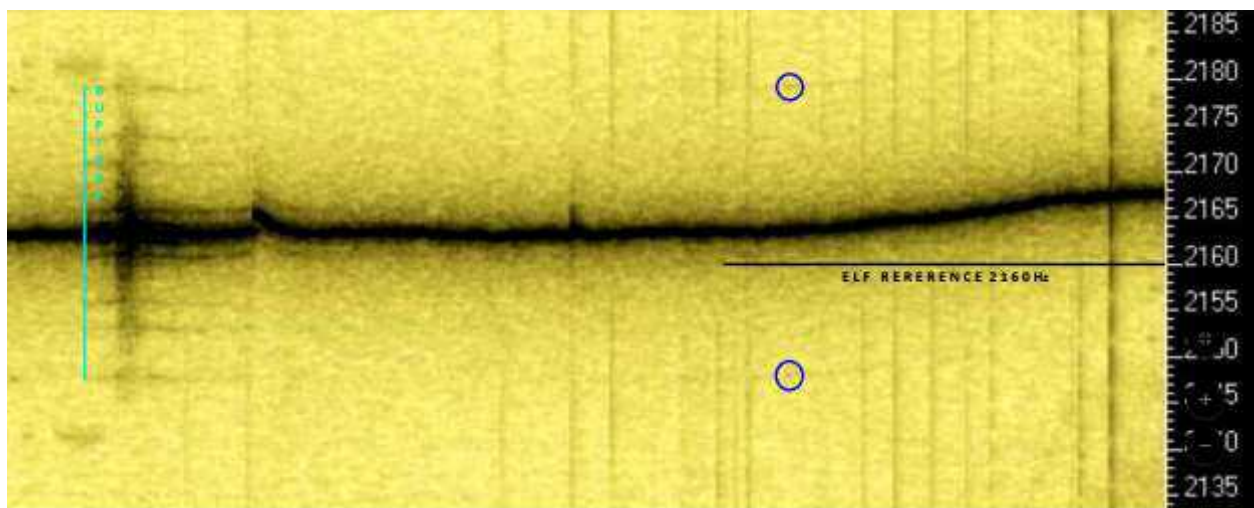


Fig. 3 - After the Earthquake

What is the best way to characterize the various signals that *precede* the onset of a seismic rupture [4]? The pre-seismic events might be closely related to those seismic phenomena classified as “slow earthquakes” [5a and 5b]. The Type 2 ELF outbursts actually look like a “scooting” process. The unusual 3.6 magnitude New Madrid Zone quake of 2020-08-30 02:34:43 UTC [6], which was possibly dominated by a low frequency wave

component (and followed closely by a Type 2 ELF emission), also suggests that slow-moving events happen in the New Madrid Zone. Slow movement in plate subduction zones brought about the concept of “slow earthquakes;” but is there any reason why less frequent slow events can’t happen in seismically active, intraplate regions like Lake Baikal or the New Madrid Seismic Zone?

There were no special damping or filtering provisions for the resonances at 10.1 and 15.7 Hz, which would soften any brief impulses. Owing to the burden of Fourier transform processing, the instrument’s frame time (cycling time) is almost 3 seconds, which is not a lot smaller than the measured 4.2 to 8.6 second duration of the impulses coming from the 15.7 Hz channel. This property also applies to the lesser impulses arranged in lines paralleling the seismic baseline; the lines appear and fade in a wave-like manner, being visible for about 10 minutes. Again, that describes slow waves that start and stop.

The Cotter recordings are fairly weak signals, but if they actually did originate from the quake’s location, moving the instrument to the Bardwell area would have resulted in a large improvement in signal strength. Short period seismometers and geophones are typically located near active seismic zones, preferably within a ~30 km range [7], and the Cotter instrument was about 311 km from the quake’s epicenter (near Bardwell KY). The author does not have access to CERI’s digital recordings archive of the New Madrid Seismic Zone, but it might be interesting to apply a Fourier Transform analysis to the data from any very short period seismometers or geophones near Bardwell KY on 2017-03-19 around 14:25:12 UTC.

Conclusions

1. The parasitic resonances of seismic instruments are generally thought of as nuisances, properties that need to be eliminated or at least minimized, but here is a case where, owing to spectroscopic dispersion, they can become useful. It would not be difficult to add an *intentional*, more sensitive resonator at, for example, 20 Hz.
2. The resonances near 10 and 15 Hz are probably worth monitoring on a trial basis, and they are already compatible with the existing instrument. Adding or removing sensors is one of the provisions of the multivariable seismometer.
3. Very short period detection of seismic phenomena between 10 and 20 Hz ought to be improved simply by moving the seismometer closer to the earthquake zone; short period instruments with resonant frequencies near the audible threshold, which is about 20 Hz, are *insensitive to distant earthquakes*. [The prototype instrument at Cotter AR was one of the few that detected a swarm of upper magnitude 1 isostatic adjustment earthquakes caused by flooding of the Bull Shoals Reservoir (June, 2017), and their detection at ~30 km was almost entirely by means of the 10.1 and 15.7 Hz parasitic resonances.]
4. “The **stick-slip phenomenon**, also known as the **slip-stick phenomenon** or simply **stick-slip**, is the spontaneous jerking motion that can occur while two objects are sliding over each other [3].” It is a possible explanation for *both* the 15.7 Hz seismic wave impulses and the Types 1 and 2 ELF signals [1], *i.e.*, coming from sticking-caused, sudden high pressures that produce seismic waves and eventually, strong electric currents able to reach the Earth-Ionosphere cavity.

Professor Freund's lab experiments with igneous rocks put under stress show that with sufficient pressure, **electric charges are separated**. The negative charges remain where they originated, while the positive charges (as holes) diffuse rapidly outward and are potentially able to reach the lithosphere/atmosphere interface through mafic dykes and trigger the Schumann resonance phenomenon. Anticipated effects are thus electric and magnetic field discontinuities, electromagnetic emissions [8a] and the earthquake light phenomenon [8b]. Intuitively, seismic impulses should show up first, then as the forces build further, impulses strong enough to separate electric charges would lead to ELF outbursts, consistent with the data. Type 3 ELF outbursts [1] may derive from an avalanche of electric currents that follow a seismic rupture. The aqua-green line in Fig. 2 points to a Type 3 signal.

5. The quake-related ELF signals near the Schumann Resonant Frequencies, while of considerable interest, do not occur during most earthquakes, one possible reason being that the electrical conductivity between a particular quake's focus and the Earth-Ionosphere cavity is very low [9] in those cases. If the cavity *is* electrically connected, the resulting Schumann resonances are inherently **global phenomena**, detectable nearly everywhere on Earth except at the standing wave node lines. I favor putting wires down deep boreholes in seismic areas.

6. The vertical strobos observed before and after the seismo-electromagnetic event near Bardwell KY on 2017-03-19, **especially their fading out near the seismic baseline**, might count as a warning signal from the New Madrid Seismic Zone. Nothing exactly like that has been recorded by the Cotter instrument, before or since, and the reason is currently obscure. The seismic baseline's line-shape is Lorentzian, but a contrast effect from its "wings" isn't an adequate explanation. Strobos usually indicate out-of-band impulses. The quake was a small one at Magnitude 3.2, but its focus, directly beneath the Mississippi River, was near a suspected location of a major earthquake of the 1811-1812 time period [10].

7. The three diagonal 15.7 Hz seismic/20.3 Hz ELF relationships in Fig. 2 may show intimate connectivity, i.e., **if** ELF signals arrive virtually instantaneously while seismic signals are delayed by their travel times from the earthquake's focus. But there could be some delay between current generated at a quake's focus and its arrival at Earth's surface.

References Cited

1. Wright, J.R. (2020) "A Multivariable, Two-Dimensional Plot of Electromagnetic, Electric Field and Seismic Information for the Characterization of Earthquake Precursors." *Open Journal of Geology*, **10**, pp 213-234. https://www.researchgate.net/publication/339951533_A_Multivariable_Two-Dimensional_Plot_of_Electromagnetic_Electric_Field_and_Seismic_Information_for_the_Characterization_of_Earthquake_Precursors
2. Ackerley, N. (2014) "Principles of Broadband Seismometry." In: Beer, M., Kougioumtzoglou, I., Patelli, E., Au IK. (eds) *Encyclopedia of Earthquake Engineering*. Springer, Berlin, Heidelberg. https://doi.org/10.1007/978-3-642-36197-5_172-1

[Parasitic Resonances are usually problematic, a spurious source of noise to be removed by magnetic levitation or given a higher resonant frequency, but in the case of Fourier Transform spectroscopy the parasitic frequencies become sidebands of the seismic baseline, i.e., separate, potentially unique information channels.]

3. From Wikipedia, “The Stick-Slip Phenomenon” Go to: https://en.wikipedia.org/wiki/Stick-slip_phenomenon

4. From Wikipedia, “The definition of a Seismic Rupture:”

https://en.wikipedia.org/wiki/Earthquake_rupture#:~:text=An%20earthquake%20rupture%20is%20the,slip%20on%20an%20existing%20fault.

5.a. Ide, S., Beroza, G. C., Shelly, D. R. & Uchide, T., (2007), “A scaling law for slow earthquakes,” *Nature - Letters*, **447**, pp 76-79 doi:10.1038/nature05780

https://www.researchgate.net/publication/6354452_A_scaling_law_for_slow_earthquakes ; and 5.b. Ide, S., (2016),

“Characteristics of slow earthquakes in the very low frequency band: Application to the Cascadia subduction zone,” *JGR Solid Earth*, **121**, Issue 8, pp 5942-5952.

<https://agupubs.onlinelibrary.wiley.com/doi/pdfdirect/10.1002/2016JB013085>

6. Straser, V., Cataldi, D., Cataldi, G., Giuliani, G. G., and Wright, J. R., (December 2020), Effects of Hurricane Laura on the New Madrid Fault Area, Results of Electromagnetic Monitoring Through the RDF Network - Radio Direction-Finding and [an] Arkansas Electromagnetic Monitoring Station, *New Concepts in Global Tectonics Journal*, **8**, No.3, pp 187 to 218.

https://www.academia.edu/44806011/Effects_Of_Hurricane_Laura_On_The_New_Madrid_Fault_Area_Results_Of_Electromagnetic_Monitoring_Through_The_RDF_Network_Radio_Direction_Finding_And_Arkansas_Electromagnetic_Monitoring_Station

7. PROSPECTS FOR LOW FREQUENCY SEISMOMETRY, A REPORT OF THE IRIS BROADBAND SEISMOMETER WORKSHOP, Held March 24-26, 2004, Granlibakken, California, Edited by Ingate, S. & J. Berger, J., Source:

http://ds.iris.edu/stations/seisWorkshop04/iris_sensor_ws_9.19.05.pdf See table 1 on page 4.

8.a. Freund, F. (2002), “Charge Generation and Propagation in Igneous Rocks.” *Journal of Geodynamics*, **33**, 543-570.

https://www.quakefinder.com/research/EQTdata/Freund%20paper%20Sept_2004.pdf

[https://doi.org/10.1016/S0264-3707\(02\)00015-7](https://doi.org/10.1016/S0264-3707(02)00015-7)

8.b. Thériault, R., France St-Laurent, F., Freund, F. T., Derr, J. S. (January 2014), “Prevalence of Earthquake Lights Associated with Rift Environments,” *Seismological Research Letters*, **85** (1): 159–178.

<https://doi.org/10.1785/0220130059>

9. Gürer, A., Bayrak, M., (2007), “Relation between electrical resistivity and earthquake generation in the crust of West Anatolia, Turkey,” *Tectonophysics*, **445**, Issues 1–2, pp 49-65 <https://doi.org/10.1016/j.tecto.2007.06.009> Gürer and Bayrak note that “...most of the large crustal earthquakes occurred in and around the areas of the highest electrical resistivity in the upper crust, although rare small magnitude earthquakes are observed in some parts of the conductive lower crust in West Anatolian extensional terrain. The high-resistivity zones may represent rocks that are probably mechanically strong enough to permit sufficient stress to accumulate for earthquakes to occur...” [Similarly, the Schumann Resonance-like emissions tend to accompany smaller earthquakes, not the larger ones. Gürer and Bayrak also noted that “...some recent studies state that the generation of a large earthquake is not only a pure mechanical process, but is closely related to fluid existence, meaning brines, etc.].”

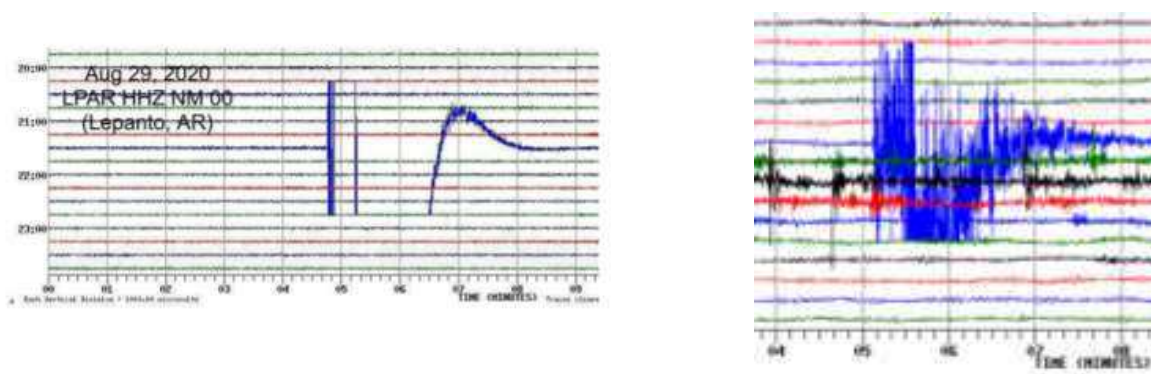
10. Tavakoli, B., Pezeshk, S. and Cox, R.T. (2010), “Seismicity of the New Madrid Seismic Zone Derived from a Deep-Seated Strike-Slip Fault.” *Bulletin of the Seismological Society of America*, **100**, pp 1646-1658. See Fig. 6 on page 1653: https://www.researchgate.net/publication/250075120_Seismicity_of_the_New_Madrid_Seismic_Zone_Derived_from_a_Deep-Seated_Strike-Slip_Fault .

11.a. Goto, H., Kaneko, Y., Young, J., Avery H., and Damiano, L. (2019), “Extreme Accelerations During Earthquakes Caused by Elastic Flapping Effect,” *Scientific Reports*, **9**, Article number: 1117. <https://doi.org/10.1038/s41598-018-37716-y> ; 11.b. Lentas, K. (March 2018), “Towards routine determination of focal mechanisms obtained from first motion *P*-wave arrivals,” *Geophysical Journal International*, **212**, Issue 3, pp 1665–1686. <https://doi.org/10.1093/gji/ggx503>

Supplementary Material

The very distorted seismic wave produced by the Magnitude 3.6 New Madrid Seismic Zone event of 2020-08-30 02:34:43 UTC might be a first motion effect, but the distortion was so strong (see references [11] for comparison) that it might have a long wave component from a slow event. This event is also notable for a Type 2 ELF emission at ~15 Hz that followed the quake by only 7 minutes [6]. This small quake was near the site of an 1843, magnitude ~6.0 earthquake, thus also very near a subsidence lake (St. Francis Lake) caused by the 1843 event. Is the unusual seismic signal possibly related to standing waves on that lake (a seiche) or elastic effects [11]? A seiche is not a slow earthquake, but if that is what happened during 2020-08-30 UTC NMSZ event, it does not detract from the possibility that drawn out sequences of quake-related ELF emissions, both preceding and following seismic rupture, are slow quake phenomena.

LPAR, the seismic instrument near Lepanto Arkansas, was closest to the 2020 quake, only a few km distant from the quake’s epicenter (see the left hand seismic image, below). FCAR’s recording (to the right) was from almost halfway across the state of Arkansas and also shows a highly distorted waveform. These recordings are courtesy of the University of Memphis/CERI website at: <https://www.memphis.edu/ceri/seismic/heli.php> .



This paper is dedicated to my mother, who had many talents. She was especially good with oil painting art.

ABOUT THE NCGT JOURNAL

The NCGT Newsletter, the predecessor of the NCGT Journal, was begun as a result of discussions at the symposium “Alternative Theories to Plate Tectonics” held at the 30th International Geological Congress in Beijing in August 1996. The name is taken from an earlier symposium held in association with the 28th International Geological Congress in Washington, D. C. in 1989. The first issue of the NCGT Newsletter was December 1996. The NCGT Newsletter changed its name in 2013 to the NCGT Journal.

Aims of the NCGT Journal include:

1. Providing an international forum for the open exchange of new ideas and approaches in the fields of geology, geophysics, solar and planetary physics, cosmology, climatology, oceanography, electric universe, and other fields that affect or are closely related to physical processes occurring on Earth from its core to the top of its atmosphere.
2. Forming an organizational focus for creative ideas not fitting readily within the scope of dominant tectonic models.
3. Forming the basis for the reproduction and publication of such work, especially where there has been censorship or discrimination.

Submission of content

Manuscripts, letters, articles and notes should be submitted as Microsoft Word documents, Margins, top 2.54cm, 1 inch, bottom, left and right 1.27 cm, 1/2 inch. Times New Roman font. Drawings and images should be uncompressed png, tiff, format, No Jpegs. No PDF's will be accepted. A minimal number of styles are accepted. Language should be US English. No page or section breaks are permitted. All images are to be presented as individual graphic files and no images are to be embedded in the text. Tables should be submitted as Microsoft Excel work sheets and will be added to the page as images (png) rather than active tables that potentially create problems with column sizes etc.

I use Microsoft Word to edit the text and either Microsoft publisher or Affinity Publisher to layout the journal pages when text frames and image frames are used. Word is a writing/editing word processor, Publisher and Affinity Publisher are specific desktop publishing applications where layout is paramount.